Institutionen för Vattenbyggnad
Chalmers University of Technology

Department of Hydraulics
Chalmers University of Technology

Dynamic Characteristics of Floating Breakwaters

by

Aurora Xiaomeng Lei

Submitted to the School of Civil Engineering, Chalmers University of Technology in partial fulfillment of the requirements for the degree of Doctor of Philosophy.

Opponent: Professor Odd Faltinsen, Marin Hydrodynamikk, NTH, Trondheim, Norge

ACKNOWLEDGEMENTS

Göteborg, March 1996

Aurora Xiaomeng Lei

TABLE OF CONTENTS

Appended Papers

Paper A

Paper B

1 INTRODUCTION

1.1 Background

Along with the development of coastal engineering, various types of breakwaters have been built. The main purposes of breakwaters are to provide harbour protection against waves, to stabilise beaches against erosion due to large wave action, and to provide for temporary wave protection for installations in or under the water surface.

Breakwaters may cause waves to break, they may just reflect waves, they may dissipate wave energy through turbulence and friction, or they may exert some combination of these, depending on their construction, the wave characteristics, and the condition of the sea floor. According to their structure, they can be classified in two groups: bottom mounted breakwaters (fixed breakwaters) and floating breakwaters.

Examples of bottom mounted breakwaters include two types, the first of which is made up of rubble-mound breakwaters and artificial stone breakwaters. Rubble-mound breakwaters are composed of rock pieces graded, from inner core to outer face, from fine to large. A typical section is shown in Fig. 1.1. On the faces of artificial stone breakwaters, concrete blocks are used as armour on the outer slopes. For this type of breakwater a part of the incident wave energy is dissipated by waves breaking in front of or on the face; the dissipation depends upon face slope and porosity, the depth of water at the toe of the breakwater, the wave height, and the wave steepness.
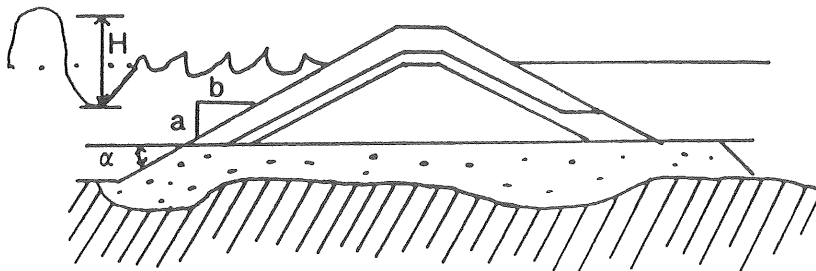
Fig. 1.1   A typical section of Rubble-mound breakwater

1

Vertical breakwaters are another type of bottom mounted breakwater. Vertical breakwaters are mostly constructed of caissons, that is large rectangular or circular concrete boxes, composed of walls and internal diaphragms to give strength, and filled with sand or gravel to give weight, see Fig. 1.2. It is also common practice to use sheet piling driven in circular patterns and filled with sand for stability. A vertical breakwater reflects the waves. Energy is only dissipated if the steepness of the combined incident and reflected wave becomes high.
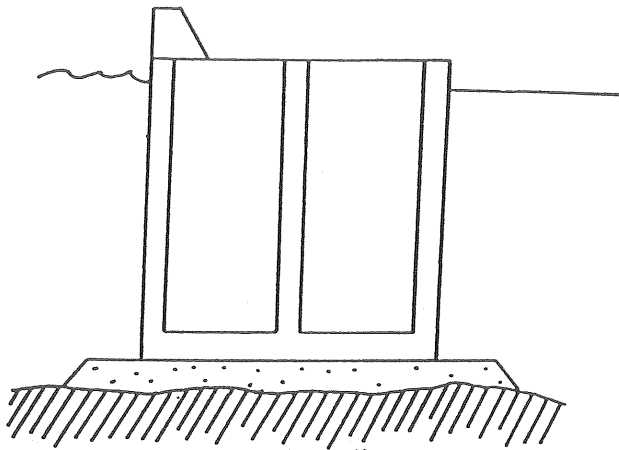
Fig. 1.2   Section of vertical breakwater

Floating breakwaters form the second of the two major groups of breakwaters. There are many different types in this group. Their effect is to either reflect or dissipate the incident wave energy. These breakwaters are designed with the motivation of improving the wave attenuation and the stability of the structures. Floating breakwaters can be subdivided into four general categories according to their construction, as shown in Fig. 1.3

- (i)   Box type breakwater (solid rectangle and barge);
- (ii)   Pontoon type breakwater (twin pontoon, open compartment, A-frame etc.);
- (iii) Mat breakwater.
- (iv)   Tethered-float breakwater;

Floating breakwaters have some advantageous features in practical use, for example floating breakwaters can be used where bottom-mounted breakwaters are not feasible because of soft bottom, deep water, or

2
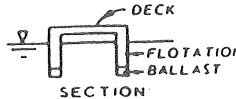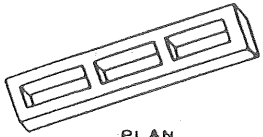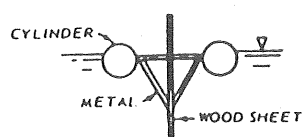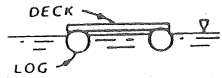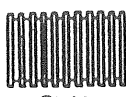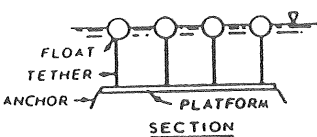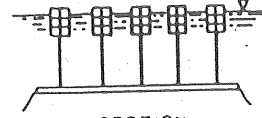
TYPE	VIEW	REMARKS
BOX		
SOLID RECTANGLE		REINFORCED CONCRETE UNITS ARE THE MOST COMMON TYPE.
BARGE	SECTION	STANDARD BARGE SIZES ON INLAND WATERWAYS ARE 195' X 35' X 12' AND 175' X 26 X 11'. INCLINED BARGES (ONE END SUBMERGED) HAVE BEEN TESTED.
PONTOON		
TWIN PONTOON	DECK / FLOTATION / BALLAST / SECTION	CATAMARAN SHAPE
OPEN COMPARTMENT	PLAN	ALSO CALLED ALASKA TYPE
A FRAME	CYLINDER / METAL / WOOD SHEET / SECTION	
TWIN LOG	DECK / LOG / SECTION	DECK IS OPEN WOOD FRAME.
MAT		
TIRE MAT	SECTION	SCRAP TIRES STRUNG ON POLE FRAMEWORK OR BOUND TOGETHER WITH CHAIN OR BELTING. FOAM FLOTATION IS USUALLY NEEDED
LOG MAT	PLAN	LOG RAFT CHAINED OR CABLED TOGETHER.
TETHERED FLOAT		
SPHERE	FLOAT / TETHER / ANCHOR / PLATFORM / SECTION	FLOATS PLACED IN ROWS.
TIRE	SECTION	ARRANGEMENT SIMILAR TO SPHERES STEEL DRUMS WITH BALLASTS CAN BE USED IN LIEU OF TIRES

Fig. 1.3 Various types of floating breakwaters
(McCartney, 1985)

3

problems with sand and silt transport. The cost of traditional fixed breakwaters increases significantly with water depth, so that floating breakwaters are an attractive option in deep water. Floating breakwaters allow better water quality because they permit water circulation underneath the structures, which reduces environmental problems. Floating breakwaters can also be relocated to new positions or rearranged in an alternative layout. However, floating breakwaters do not provide the complete wave protection offered by fixed breakwaters. Part of the incident energy is transmitted past the floating breakwater structures, and this is more pronounced for long (and usually high) waves; therefore the usefulness of these structures has been assumed to be limited to attenuation of short-period waves. For long-period wave reduction, massive structures could still be required.

An example of this was an installation for Town Quay in Reykjavik Harbour, Iceland, by the Swedish company, SF Marina System AB. In February 1992, the breakwaters of barge type were subjected to wind and wave conditions similar to the predicted 1 in 50 year return period wave condition for the Town Quay site. A video of this storm shows the attenuation of short-period waves, and therefore the breakwaters provided acceptable protection for small boats, although long-period waves were transmitted. These long-period waves caused the floating breakwaters and moored boats to move simultaneously with limited relative motion. Moreover, the structures and mooring cables were not damaged by the storm.

It is usually preferable for a breakwater to cause the dissipation or reflection of as much wave energy as possible to provide good protection on the leeward side. Some bad experiences with insufficient mooring cable and anchor capacity have motivated an effort to evaluate cable and anchor forces. However, to achieve this, greater understanding of the dynamic behaviour of the complete system is required.

1.2 Process of Analysis

Breakwaters or offshore structures floating in ocean waves are generally exposed to an environment of wind, currents and waves. Loads generated by wind and currents are normally assumed to be constant for short periods of time. In general, they influence the amount of cable pre-tension for a moored structure. Wave loads of the first-order usually dominate the environmental loads. To study the interaction between the bodies and the waves, and the interaction between the bodies, would be the first stage in a general analysis. This work was done a few years ago, and is described in

Paper A. Further work on multiple semi-submerged and submerged bodies was also carried out, and is reported in Paper B.

In the work reported in Papers A and B, the wave forces acting on the bodies, as well as added mass, wave damping and interaction forces through the fluid, were determined by solving the diffraction problem and the radiation problem for bodies at zero forward speed. In the diffraction problem, all of the bodies are held fixed in the incoming waves and the scattered velocity potential of the fluid is calculated. In the radiation problem, the bodies, one at a time, are forced to oscillate in calm water and the radiation potentials are calculated. Although these two problems are physically different, from the mathematical point of view, they involve similar boundary value problems. In general, there exist three major models for solving this type of boundary value problems. They are given in the following.

- *Eigenfunction expansion models* are those by which the domain occupied by water is divided into different regions, one beneath each of the structures and one around them. In each of these regions, the velocity potential is expressed as a series of eigenfunctions satisfying the Laplace equation and the boundary conditions except at the boundaries between the regions. The continuity of velocity and pressure at the common boundaries of the regions can be satisfied by adjusting the coefficients of the series. A number of work were made based on this model. These include the eigenseries solutions of MacCamy and Fuchs (1954), Garret (1971), Black, *et al.* (1971), and Yeung (1981) for a vertical cylinder; solutions of Calisal (1984), Miao & Liu (1985) for composite cylinder, as well as solutions of Chakrabarti (1978), McIver (1986), Lindgren & Björkenstam (1989), Berggren & Bergdahl (1991) and Berggren & Johansson (1992) for the problems of more than one body.

- *Boundary-integral models (or Panel method)* are those in which the model is based on the application of Green's theorem in the entire fluid domain to obtain an integral equation for the velocity potential on the body surfaces (or on the entire boundary surface). The potential at any point, in the fluid or on the boundaries, is considered as the result of a distribution of sources (and sinks), with a contributing function (Green function), on the submerged body surfaces. The source strengths are then determined by discretizing this equation on the body surfaces. The method has been developed by John (1949, 1950), Wehausen & Laitone (1960), Hess and Smith (1962), Faltinsen and Michelsen (1974), Garrison (1974,1975), Newman (1985a, 1985b, 1985c, 1986),

Sclavounos and Lee (1985) and others, and has been applied to various types of structures, for examples, single hemisphere (Garrison, *et al.*, 1970); submerged oil storage tank (Garrison & Chow, 1972); vertical column with variation of section shape (Hogben & Standing, 1975); and Tension-Leg Platform (Korsmeyer *et al.*, 1988, and Newman & Sclavounos, 1988). The boundary-integral methods are also called boundary element methods, panel method, or sink-source method.

- *Finite element models* are those by which the fluid domain is generally divided into two regions, one interior which is near the structures and one exterior. In order to satisfy the radiation condition at infinity, the following techniques are often used in conjunction with a conventional finite element method which is only applied in the interior region to solve numerically diffraction and refraction problems. These methods are: (i) boundary 'dampers' (Lysmer and Kuhlemeyer, 1969, Newton, 1975, Zienkiewicz, *et al.*, 1978 and Huang, 1983), (ii) exterior series solutions (Chen and Mei, 1974, 1975, Mei, 1978, Yue, *et al.*, 1978 and Olsson, 1990), (iii) exterior boundary integral formulation (Zienkiewicz, *et al.*, 1977, 1978), and (iv) 'infinite' elements (Zienkiewicz and Bettess, 1975,1977).

Procedures for applying the FEM to wave radiation and diffraction problems has been reviewed by Chen and Mei (1974) and Bai and Yeung (1974). Zienkiewicz *et al.* (1978) generalized the procedures which can be used to link finite element solutions to any kind of exterior solution.

When the three analytical and numerical models are compared, one can see that the eigenfunction expansion is the most accurate and fastest method. However, this method is applicable only in cases where analytical expressions exist, which requires a simple structural shape. The numerical methods (both BIM and FEM), on the other hand, can be efficient particularly for complex geometry. Eatock Taylor and Zietsman (1981a, 1981b) introduced a technique that permits the fictitious surface to be lifted off the sea bottom, thereby the inner element region could be reduced. This technique remedies the disadvantage of the conventional FEM, especially in deep water, that the element mesh in the inner region must be taken down to the seabed. Application of this technique together with the coupled element approach (combining FEM with BIM) to highly complex 3-D problems has been made by Eatock Taylor and Zietsman (1982).

The dynamic response of floating structures in regular waves is the primary subject studied here. The emphasis is placed on the effects of constraints between the bodies, and the non-linear effects of the mooring lines. Two types of couplings, elastic springs and revolute joints, are discussed in detail. Mooring forces imposed on the structures have been evaluated by a computer code, MODEX, which was developed by Jan Lindahl (Lindahl & Bergdahl, 1987). The theoretical background to this source code is given in the reports 'Dynamic analysis of mooring cables' (Lindahl & Sjöberg, 1983) and 'Implicit numerical solution of the equations of motion of a mooring cable' (Lindahl, 1984). In this study an elastic model has been used in assessing dynamic tension of the cable and its transverse displacement. Since MODEX gives a solution in the time domain, a transformation from time domain to frequency domain is made by means of the Fast Fourier Transform technique. Only the component corresponding to the fundamental frequency is coupled to the body response analysis.

Kwan and Bruen (1991) have made a comparison of different procedures based on time domain, frequency domain and quasi-static analysis for cable dynamics. The conclusions based on their research are: 1) Although quasi-static analysis yields acceptable predictions for suspended lines, it can produce large errors in line tension and anchor force predictions, so this method is suitable only for preliminary design; 2) Time domain dynamic analysis which can account for all primary non-linearities is therefore necessary to all practical mooring configurations; 3) Frequency domain dynamic analysis can produce acceptable line tension and anchor load predictions in most cases if the non-linearities are properly linearized. However, this method may produce substantial error for highly non-linear systems, for example when a large portion of the mooring line lies on the sea floor, a clump weight is close to the touchdown point, or a buoy is close to the surface. For these cases a time domain approach is more appropriate.

The non-linear steady wave drift force cannot be neglected in a moored structure system. Even when its magnitude is one order less than the wave forces, the drifting offset due to this force will cause a change in the static tension and the dynamic behaviour of the cables. In practice, the structures are exposed to irregular waves in the ocean which cause excitation both at low frequencies (difference-frequencies) and at high frequencies (sum-frequencies). In particular, the difference-frequency excitation can cause resonance and, consequently, large slowly varying offset in the horizontal motion of the moored breakwater.

Chakrabarti and Cotter (1983) have made comparisons of linear and non-linear models based on experiments with a conventional barge-type structure exposed to beam sea in regular waves. The results demonstrate that the computational models predict realistic roll motion only if they include a non-linear viscous roll damping term in the motion equation. This is particularly important for a motion near the natural period of the structure.

In solving the equations of motion, the Newton-Raphson method is used to deal with the non-linearity originating from the restoring force imposed by the mooring cables. The 'forward difference' representation is applied for the elements, in the Jacobi matrix, associated with this force. Once the responses are derived, the free-surface elevation is determined according to the dynamic free-surface condition. Waves on the free surface are deformed due to the presence and oscillations of large structures.

As a stage in validating the mathematical modelling, model tests were performed in a wave basin. Box-type floating breakwaters exposed to incident regular, beam, and oblique, waves were investigated. The experiments are fully discussed in Section 4. The results are used for comparison with the theoretical solutions.

Breakwaters have to be properly designed, with an understanding of their limitations, for specific site conditions. It is critical that they maintain their function properly throughout their life. The analysis process mentioned above, including the experiments, is based on the assumption that the waves are regular. However, as ocean waves are random in nature, their statistical properties have to be considered in designing breakwaters. Design waves based on environmental statistics, e.g. wind, current and storm waves, are the most important parameters in determining the dimensions and layout of a particular system. Underestimation of design waves leads to the failure of the structures or penetration of too large waves into the harbour, whereas overestimation results in unnecessary cost. Proposed approaches for selecting design waves are summarized in the next section, *Wave Climate and Design Waves*.

2 WAVE CLIMATE AND DESIGN WAVES

Ocean waves are the most dominant and influential environmental factor affecting the design of coastal and ocean structures. Wave height, wave period and wave direction affect the response of the installed system. For random waves, wave statistics are generally divided into two categories according to the time scales concerned: short-term and long-term wave statistics. Design waves based on the wave information from daily sea states are used to simulate operational conditions. For example, in the design of a breakwater system, such waves are used to determine the dimensions, form and layout of the structures, in relation to the efficiency of the system at the site for normal conditions. Design waves also influence the fatigue characteristics of the mooring cables and coupling elements. The time scale in this type of wave statistical analysis is usually minutes or hours. There are two complementary methods for estimating the short-term design condition. The first method involves the application of wind data, whereas the second has to do with the collection of data directly from wave record devices. The procedures of the estimates based on wind data and on wave data are described briefly below.

For estimates based on wind data two approaches have been used to determine wave characteristics from a known wind field. One of them is termed the "significant wave" method or the Sverdrup-Munk-Bretschneider (SMB) method. By this method, the significant wave height, H_s, and the significant wave period, T_s, are determined directly in terms of representative wind speed, U, fetch, F, and duration, t, (on which the wind acts), and expressed generally in non-dimensional form as

$$gH_s/U^2 = f_1(gF/U^2, gt/U)$$

$$gT_s/U = f_2(gF/U^2, gt/U).$$

Under specific conditions, it is either the fetch or the wind duration that imposes a limit on H_s and T_s. For fetch-limited waves, gt/U is large enough so that it does not influence H_s and T_s; only gF/U^2 controls them. Conversely, for duration-limited waves, these two parameters are simply functions of gt/U. When both the fetch and duration are sufficiently large for H_s and T_s to reach limiting values, these parameters become dependent only on the wind speed U; the condition of a fully arisen sea then exists. Wiegel (1964) and Bretschneider (1958, 1970, 1973) provide some hindcasting curves and empirical equations used to estimate H_s and T_s.

The second approach is to express the wave spectrum directly in terms of the wind characteristics, e.g. the wind speed at 19.5 meters above the mean water level. Examples are the spectra of Pierson-Moskowitz (Pierson & Moskowitz 1964) and JONSWAP (Hasselmann *et al.* 1973), which are the most common spectra used in ocean engineering. A method of applying these formulas with corrected wind speed is provided in the Shore Protection Manual (1984, 1992) of the U.S. Army Coastal Engineering Research Center.

For estimates based on wave data the Fast Fourier Transform algorithm is commonly used to decompose a waveform directly from the recorded data into a set of sinusoidal waves, with corresponding amplitudes and frequencies, in order to determine an energy spectrum. The significant wave height and wave period for each recorded period are subsequently obtained from the spectral moments, $m_n = \int_0^\infty f^n S(f) df$, i.e. by taking $H_s = 4(m_0)^{1/2}$ and by definitions of peak period, $T_0 = 1/f_0$, and zero up-crossing period, $T_z = (m_0/m_2)^{1/2}$, (which is related to T_0 by $T_z = 0.71 T_0$ for the P-M spectrum and by $T_z = 0.714 T_0$ for the JONSWAP spectrum).

A design wave based on the wave information from storm waves over a long period (of the order of $20 - 100$ years) is used to simulate the extreme condition. The prediction of the characteristics of long-term extreme values deals with the occurrence of rare events, as opposed to the short-term statistics which determine the normal variations. When a system is exposed to extreme conditions there is risk of damage. The strength of the structures and mooring cables, as well as the load capacity of the anchors, are affected by such waves. The determination of extreme waves usually involves selecting and fitting a suitable probability distribution to wave height data, and then extrapolating this to find a suitable design wave that corresponds to a chosen return period, T_R, or a chosen encounter probability, E. In general, the long-term probability is obtained from many short-term observations, since storm wave statistics still lack reliable data covering sufficiently long periods.

Mårtensson and Bergdahl (1987) have made investigations of the wave climate in the southern Baltic. Although the purpose of their work was to evaluate the amount of wave energy in Swedish coastal water, some useful information on wave statistics at the measuring sites is provided, and this can be used as a reference.

3 DYNAMIC RESPONSE IN THE FREQUENCY DOMAIN

In the analysis of interaction between waves and structures, wave motion is usually considered to be stationary, ergodic and homogenous. Based on these assumptions, it is permissible for a random process, for instance wave elevation, $\eta(t)$, or wave force, $F(t)$, to be described by a time history or by a spectral representation; it is also accepted that the required information can be sampled during an interval of time, e.g. a few hours, that can be started at different times, and at different locations, within the region considered. For such random dynamic problems, both the excitation and response processes are modelled as random processes. Statistical parameters of the response processes can be predicted from a probabilistic specification of the excitation processes and the equation of motion of the system.

To predict the response of a system to random waves, either time domain analysis or frequency domain analysis may be adopted. In time domain analysis, various combinations of non-linear effects can be modelled in a consistent and direct manner; for a system that is highly non-linear, or if there are difficulties in the linearization of the non-linearities, this method is usually needed to obtain reliable results. Frequency domain analysis, on the other hand, holds only for linear systems. If all of the non-linearities in the equation of motion are replaced by linear approximations, then the method can be used for simplified solution. In comparison with time domain analysis, frequency domain analysis is usually considered simple and efficient; it yields results that are simpler to interpret and apply. All of this may be the reason why frequency domain analysis has been applied extensively to problems of floating-structure dynamics.

For structures floating in ocean waves, the non-linearities of importance in dynamic response are non-linear fluid-drag force, non-linear mooring-line force and non-linear viscous damping. Linear approximations of these non-linear forces have been extensively studied in the past decade. Dynamic analysis of the floating structures is mostly, whenever possible, performed in the frequency domain for simplified solutions.

3.1 Review of Problems and Basic Assumptions

In the design of floating breakwaters or other floating offshore structures, the dynamic response of the bodies to surface waves, currents and wind needs to be taken into account. Since it is possible to translate the regular waves into an irregular sea by means of Fourier transformation, it is

generally sufficient to analyse the structures in regular sinusoidal waves. One of the essential stages in response analysis is the mathematical modelling, which represents the structures by suitably defined mass, damping and stiffness matrices; external constraints; and hydrodynamic forces. To formulate correctly all of these physical characteristics is normally difficult due to uncertainties and non-linearities. Since the effects of physical characteristics on a structure could be different for different systems, it is sometimes possible to simplify the model in order to solve a particular problem. In this primary study, the mathematical model presented represents a basic floating system which can be modified to a more complex or realistic system. In Figure 3.1, an example of a floating breakwater system is shown; it is composed of multiple barge-type bodies, couplings between the bodies and mooring cables between the bodies and the seafloor. In the model the couplings are simulated either as massless springs or as revolute joints, and the cables are modelled taking into consideration their dynamic response to the excitations from the contact (attachment) points and the surrounding fluid. These external effects are discussed separately later. In the model it is assumed that the structures have zero forward speed and that there is no current present.
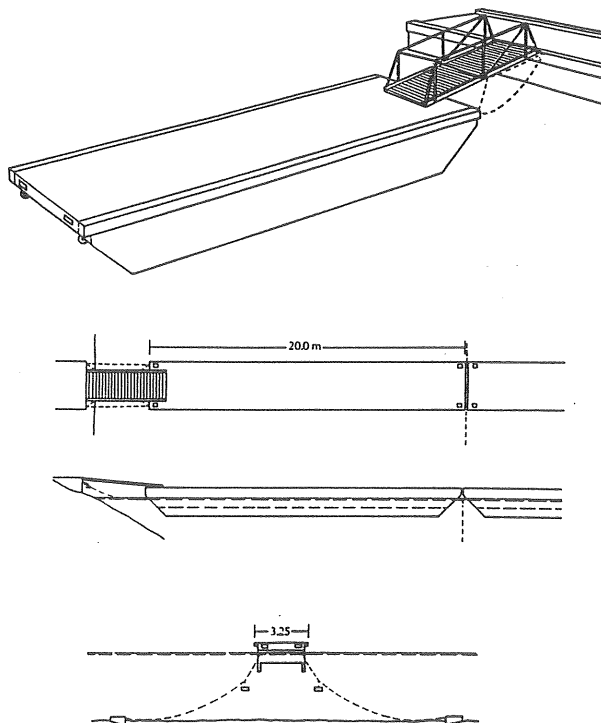

Fig. 3.1   Barge-type floating breakwaters (SF Marina System AB)

12

The hydrodynamic forces exerted by waves on a structure, or on its members, can be expressed as a function of four parameters in a non-dimensional form:

$$\frac{F}{\rho u_0^2 D} = f\left(\frac{t}{T}, \frac{u_0 T}{D}, \frac{u_0 D}{\nu}, \frac{\pi D}{L}\right)$$ (3.1)

in which t is time, T is wave period, L is wave length, D is characteristic dimension of the structure, u_0 is maximum horizontal water particle velocity, ρ is mass density of water, ν is kinematic viscosity, and the parameter $u_0 D/\nu$ is the Reynolds number, $u_0 T/D$ is the Keulegan-Carpenter number (KC), and $\pi D/L$ is the diffraction parameter. Chakrabarti (1980) presents a figure (Fig. 3.2) which indicates the regions where different models for the hydrodynamic forces should be applied. The non-dimensional parameter, ka, presented in Figure 3.2 is equivalent to the diffraction parameter, $\pi D/L$; whereas the KC number is equivalent to the ratio of the particle orbit diameter (2A) to the structure dimension (D = 2a). The KC number plays a role in the flow separation; it measures the importance of drag force effects. The diffraction parameter, ka, determines the importance of the diffraction effect. When the parameter ka << 1, a body is regarded as small and the diffraction is relatively unimportant. The wave force may be dominated by the inertia and/or drag forces, shown in the left part of the diagram. In this part of the diagram, if the parameter 2A/D < 1, as in Regions I and III, the wave amplitude is regarded as small. In such a case the drag force is relatively small compared with the inertia force, i.e. the Froude-Krylov approach is applicable. In the region where the parameter 2A/D is of order O(1) or larger, for instance Region IV, the wave amplitude is regarded as large. Since the flow separation and the drag force are usually significant, the Morison equation is needed to include the effect of the drag force. The inertia force and the drag force are added together linearly. However, when the size of the structure is comparable to the wave length, that is ka ≥ O(1), the presence of the structure alters the wave field near the structure. If no wave break occurs, it is indicated that the drag force is less than 10%, according to the diagram in the regions II and IV, and that the effect of diffraction is predominant. In this case the Froude-Krylov approach and Morison equation are no longer valid. The diffraction theory is then used to take the diffraction of the waves from the structure into account.
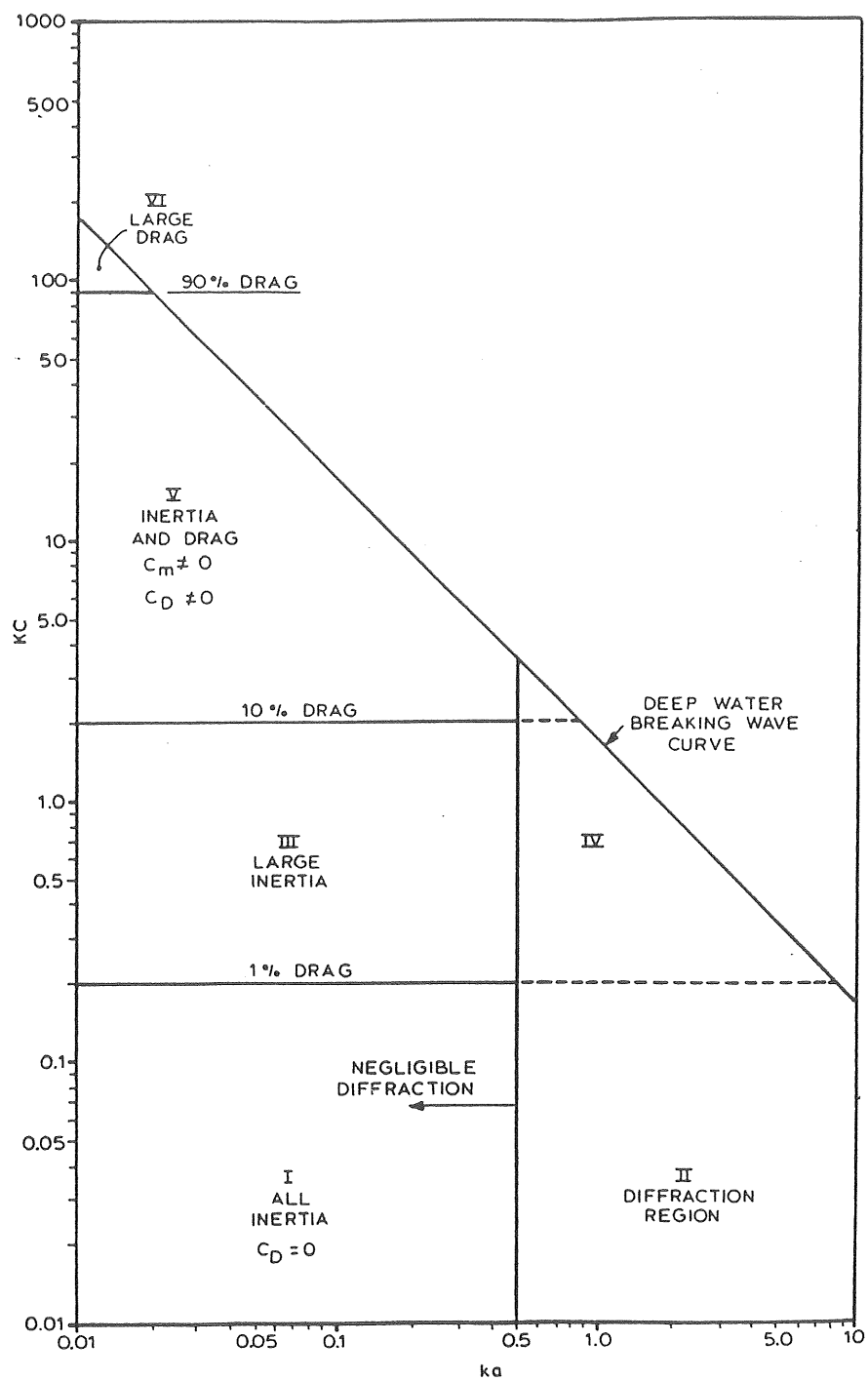
13

Fig. 3.2   Regions of application of wave force formulas,
(Chakrabarti, 1980).

14

The problem discussed here involves large structures (floating bodies) in combination with members (mooring cables) of small diameter in comparison to the wave length. The characteristic dimensions of floating breakwaters are generally in the region of $ka \geq O(1)$ due to the properties of structures and, hence, the diffraction theory has been adopted. In addition to this, the parameter of wave steepness, H/L (wave height / wave length), is assumed to be small, which means that the linear wave theory is applicable as well. The method of computing the linear wave force on large floating and submerged bodies is discussed in Papers A and B. The concepts of added mass, radiation damping, exciting force and interaction force (between the bodies through the fluid) have also been discussed in the above mentioned papers. For the long slender members (cables) the drag force has a significant effect on their dynamic characteristics, especially on the dynamics of transverse displacement. Since an elastic cable combines a soft transverse stiffness with a strong axial stiffness, obtaining its dynamic force and response requires special methods. A detailed computational procedure is described in the paper, "Dynamic Analysis of Mooring Cables", by Jan Lindahl and Anders Sjöberg (1983). The application of this method to computing the dynamic load exerted on the structures is discussed here in Section 3.5.

3.2 The Definition of Motions and Reference Frames

In order to derive a set of equations of motion for a system of several floating bodies and mooring cables in three-dimensional space, three groups of Cartesian reference frames are employed to define the position and orientation of each rigid element, see in Fig. 3.3. The x-y-z frame is a global reference frame with its origin, o, fixed on the mean water surface, and the z-axis is directed upward. This global frame is usually used to define the absolute motion of the bodies, as well as the interrelation of the local frames of the same type or frames of different types.
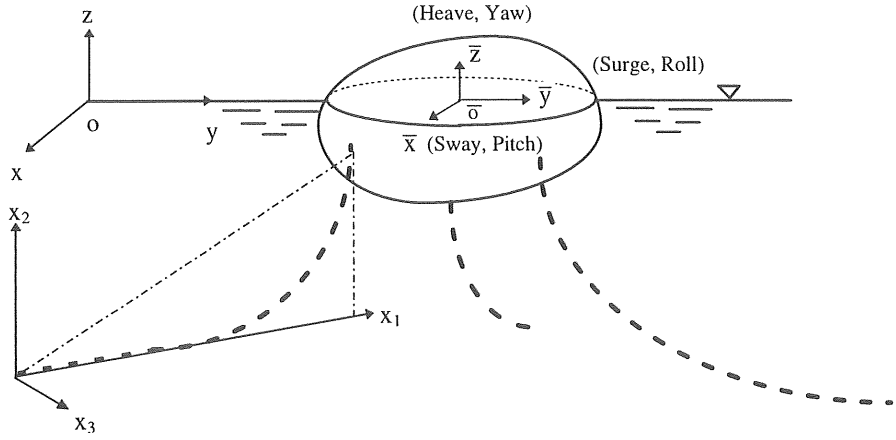
Fig. 3.3 The definition of motions and reference frames for a
floating system

One of the groups of local frames used in dynamic analysis of a system consists of body-fixed reference frames, also called vessel coordinate systems, indicated by $\bar{x}, \bar{y}, \bar{z}$. Each frame is fixed on a body, which means that it moves with the body, in both translation and rotation. All of the axes of a given frame are oriented in the same directions as the axes of the global frame when the body floats at rest in calm water. The geometry of the body is usually specified in the body-fixed frame, and the points of interest on the body can be defined in the x-y-z frame once the $\bar{x} - \bar{y} - \bar{z}$ frame is oriented relative to the x-y-z-frame. Let the reference centre of rotation of the rigid body be Q, and its moving coordinate be expanded as a power series of the perturbation parameter, ε, and truncated up to the second-order. This can be expressed as

$$X(t) = x_0^b + X^{(0)} + \varepsilon X^{(1)}(t) + \varepsilon^2 X^{(2)}(t) + \ldots \tag{3.2}$$

where x_0^b is the vector from the origin of the x-y-z reference frame to the origin of the $\bar{x} - \bar{y} - \bar{z}$ frame, ε is a small quantity denoting the wave steepness, and ($x_0^b + X^{(0)}$) is the resting position of Q independent of time, t. In general, Q need not coincide with the centre of mass of the body. For a body with small motion, the angular displacement is expressed as $\varepsilon\theta^{(1)}(t)$

16

with the components $\varepsilon\alpha$, $\varepsilon\beta$, and $\varepsilon\gamma$ about axes parallel to x, y, and z; the relations between these two frames for any point on the body are

$$x = x_0^b + \overline{x} + \varepsilon\left[\mathbf{X}^{(1)} + \mathbf{\theta}^{(1)} \times \left(\overline{\mathbf{x}} - \mathbf{X}^{(0)}\right)\right] + O\left(\varepsilon^2\right) \tag{3.3}$$

or, in component form,

$$x = x_0^b + \overline{x} + \varepsilon\left[X^{(1)} + \beta(\overline{z} - Z^{(0)}) - \gamma(\overline{y} - Y^{(0)})\right]$$

$$y = y_0^b + \overline{y} + \varepsilon\left[Y^{(1)} + \gamma(\overline{x} - X^{(0)}) - \alpha(\overline{z} - Z^{(0)})\right] \tag{3.4}$$

$$z = z_0^b + \overline{z} + \varepsilon\left[Z^{(1)} + \alpha(\overline{y} - Y^{(0)}) - \beta(\overline{x} - X^{(0)})\right]$$

Another group of local frames consists of cable reference frames; these are used to define the position and movement of the points or elements of the cables. Each of these frames is fixed in space with the origin located at the anchor point. The coordinate plane defined by the axes x_1 and x_3 is parallel to the mean water surface; the plane lies at the seafloor when constant water depth is assumed. The cable hangs in the plane defined by the axes x_1 and x_2. The axis x_1 is positive in the direction towards the upper end point, while x_2 is of the same direction as the axis z. With the angle of rotation of the x_1 axis relative to the x axis, denoted as θ_{1x}, the coordinates of the upper end point P_j in this frame can be expressed as

$$\begin{aligned} x_1 = c_1 + \varepsilon\Big\{&\cos\theta_{1x}X^{(1)} + \sin\theta_{1x}Y^{(1)} - \sin\theta_{1x}\left(\overline{z}_j - Z^{(0)}\right)\cdot\alpha \\ &+ \cos\theta_{1x}\left(\overline{z}_j - Z^{(0)}\right)\cdot\beta - \left[\cos\theta_{1x}\left(\overline{y}_j - Y^{(0)}\right) - \sin\theta_{1x}\left(\overline{x}_j - X^{(0)}\right)\right]\cdot\gamma\Big\} \end{aligned}$$

$$x_2 = c_2 + \varepsilon\Big\{Z^{(1)} + \alpha\cdot\left(\overline{y}_j - Y^{(0)}\right) - \beta\cdot\left(\overline{x}_j - X^{(0)}\right)\Big\} \tag{3.5}$$

$$\begin{aligned} x_3 = c_3 + \varepsilon\Big\{&\sin\theta_{1x}X^{(1)} - \cos\theta_{1x}Y^{(1)} + \cos\theta_{1x}\left(\overline{z}_j - Z^{(0)}\right)\cdot\alpha \\ &+ \sin\theta_{1x}\left(\overline{z}_j - Z^{(0)}\right)\cdot\beta - \left[\sin\theta_{1x}\left(\overline{y}_j - Y^{(0)}\right) + \cos\theta_{1x}\left(\overline{x}_j - X^{(0)}\right)\right]\cdot\gamma\Big\} \end{aligned}$$

where c_1, c_2 and c_3 are the coordinates of the upper end point at the resting position; they are expressed as

$$c_1 = -\cos\theta_{1x}x_0^c - \sin\theta_{1x}y_0^c + \cos\theta_{1x}\left(x_0^b - \overline{x}_j\right) + \sin\theta_{1x}\left(y_0^b - \overline{y}_j\right)$$

$$c_2 = -z_o^c + z_o^b + \overline{z}_j \tag{3.6}$$

$$c_3 = -\sin\theta_{1x}x_0^c + \cos\theta_{1x}y_0^c + \sin\theta_{1x}\left(x_0^b - \overline{x}_j\right) - \cos\theta_{1x}\left(y_0^b - \overline{y}_j\right)$$

where x_0^c is the vector from the origin of the x-y-z reference frame to the origin of the x_1-x_2-x_3 frame. In formula (3.5), the second terms on the right-hand side indicate the first-order displacements of the point P_j in space.

3.3 Equations of Motion

Dynamic responses of a floating structure are determined by the equations of motion, in which all significant dynamic effects (dynamic forces) on the structure needed to be taken into account. Let a system of multiple linked bodies be discretized into rigid bodies, and number them from 1 to NB. For each of the bodies, the interactions between it and connected objects, for example neighbour floats, boats, the seafloor, walls, and so on, are replaced by the corresponding external forces. The interactions between the body and the fluid are replaced by fluid pressure. The computational model is shown in Figure 3.4.
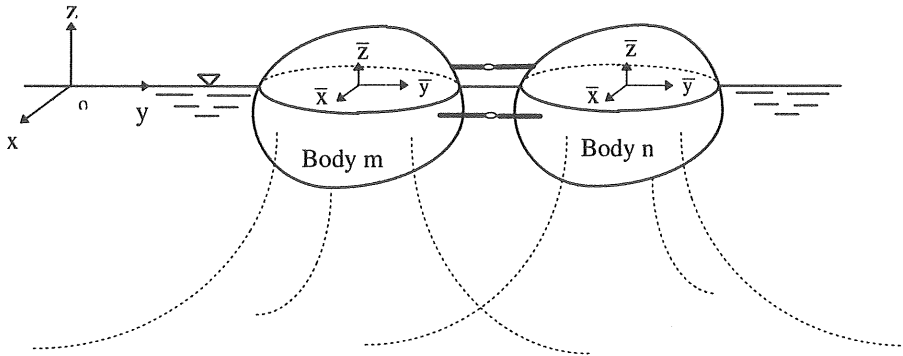

Fig. 3.4   Computational model

For each body, following the conservation law of linear momentum, or Newton's second law, three equations of motion in the x, y and z directions are derived. In addition, by applying the conservation law of angular momentum with respect to the fixed origin, o, together with the equation of linear momentum, another three equations can be obtained in relation to the rotations of the body about the axes passing through the selected centre, Q, and parallel to the x, y and z axes. For a system of small motions, the equations are summarized in matrix form in terms of the generalized displacements and forces

$$\mathbf{M}^m \ddot{\mathbf{x}}^m(t) + \mathbf{C}^m \mathbf{x}^m(t) = \mathbf{F}^m(t) \qquad m = 1,2,..., NB \qquad (3.7)$$

where overhead dots denote the time derivative, and the index, m, is the number of the body; $\mathbf{x}(t)$ is the generalized displacement vector; $\mathbf{M}$ is the mass matrix given in Equation (3.8); and $\mathbf{C}$ is the stiffness matrix due to restoring forces and moments from the displaced position of the body, also given in equation (3.9). Finally, $\mathbf{F}(t)$ represents the load vector.

$$
\mathbf{M} =
\begin{bmatrix}
M & 0 & 0 & 0 & M(\bar{z}_g - Z^{(0)}) & -M(\bar{y}_g - Y^{(0)}) \\
0 & M & 0 & -M(\bar{z}_g - Z^{(0)}) & 0 & M(\bar{x}_g - X^{(0)}) \\
0 & 0 & M & M(\bar{y}_g - Y^{(0)}) & -M(\bar{x}_g - X^{(0)}) & 0 \\
0 & -M(\bar{z}_g - Z^{(0)}) & M(\bar{y}_g - Y^{(0)}) & I_{22}^b + I_{33}^b & -I_{21}^b & -I_{13}^b \\
M(\bar{z}_g - Z^{(0)}) & 0 & -M(\bar{x}_g - X^{(0)}) & -I_{12}^b & I_{11}^b + I_{33}^b & -I_{32}^b \\
-M(\bar{y}_g - Y^{(0)}) & M(\bar{x}_g - X^{(0)}) & 0 & -I_{13}^b & -I_{23}^b & I_{11}^b + I_{22}^b
\end{bmatrix}
$$

$$(3.8)$$

19

$$
C = \begin{bmatrix}
0 & 0 & 0 & 0 & 0 & 0 \\
0 & 0 & 0 & 0 & 0 & 0 \\
0 & 0 & \rho g A & \rho g I_2^A & -\rho g I_1^A & 0 \\
0 & 0 & \rho g I_2^A & \left(\begin{array}{c} \rho g\left(I_{22}^A + I_3^V\right) \\ -Mg\left(\overline{z}_g - Z^{(0)}\right) \end{array}\right) & -\rho g I_{12}^A & \left(\begin{array}{c} -\rho g I_1^V \\ +Mg\left(\overline{x}_g - X^{(0)}\right) \end{array}\right) \\
0 & 0 & -\rho g I_1^A & -\rho g I_{21}^A & \left(\begin{array}{c} \rho g\left(I_{11}^A + I_3^V\right) \\ -Mg\left(\overline{z}_g - Z^{(0)}\right) \end{array}\right) & \left(\begin{array}{c} -\rho g I_2^V \\ +Mg\left(\overline{y}_g - Y^{(0)}\right) \end{array}\right) \\
0 & 0 & 0 & 0 & 0 & 0
\end{bmatrix}
$$

$$(3.9)$$

In these equations $\overline{x}_g$ is the centre of mass of the body; $I_{ij}{}^b$ ($i = 1, 2, 3$; and $j = 1, 2, 3$) are the second moments of inertia. Definitions of $I_{11}{}^b$ and $I_{12}{}^b$ are

$$
I_{11}^b = \iiint_{V^b} \left(\overline{x} - X^{(0)}\right)^2 dm
$$

and

$$
I_{12}^b = \iiint_{V^b} \left(\overline{x} - X^{(0)}\right)\left(\overline{y} - Y^{(0)}\right) dm
$$

where V^b is the volume of the whole body including the part above the free surface. Other moments are similarly defined. The first and second moments of inertia of the cut plane (water-line plane), $S_A^{(0)}$, are denoted respectively by I_i^A and I_{ij}^A ($i = 1, 2, 3$; and $j = 1, 2, 3$); their definitions are given as follow

$$
I_1^A = \iint_{S_A^{(0)}} \left(\overline{x} - X^{(0)}\right) dx\, dy ,
$$

$$I_{12}^A = \iint_{S_A^{(0)}} \left(\overline{x} - X^{(0)} \right) \left(\overline{y} - Y^{(0)} \right) dx \, dy \,, \qquad \text{and so on.}$$

The first moments of the static submerged volume, $V^{(0)}$, are denoted by I_i^V ($i = 1, 2, 3$), and defined as

$$I_1^V = \iiint_{V^{(0)}} \left(\overline{x} - X^{(0)} \right) dx \, dy \, dz \,, \qquad \text{and so on.}$$

Equation (3.7) applies in the time domain. If the mass, damping, or stiffness properties are frequency dependent, the problem is more conveniently formulated in the frequency domain. For a body in harmonic motion, the components of the displacement vector may be described by

$$x_j = \mathrm{Re}\left\{ X_j \cdot e^{-i\omega t} \right\} \qquad\qquad j = 1, 2, ..., 6 \qquad\qquad (3.10)$$

where X_j denotes the complex amplitude of the displacements; index $j = 1$, 2, and 3 indicate, respectively, the translational motions in sway, surge and heave; and $j = 4$, 5, and 6 indicate the rotational motions in pitch, roll and yaw. The linear and angular displacement about the body are noted in the definition sketch, Figure 3.3. For the problem considered here, the time dependent external force $\mathbf{F}(t)$ may consist of the wave force $\mathbf{F}_w(t)$, viscous damping force $\mathbf{F}_v(t)$ and constraining force $\mathbf{F}_c(t)$ from the external supports and connections. The linearized wave force acting on the body m is of the form

$$\mathbf{F}_w^m(t) = \mathbf{F}_I^m(t) - \mathbf{A}^{mm}\ddot{\mathbf{x}}^m - \mathbf{B}^{mm}\dot{\mathbf{x}}^m - \sum_{\substack{n=1 \\ n \neq m}}^{NB} \left(\mathbf{A}^{mn}\ddot{\mathbf{x}}^n - \mathbf{B}^{mn}\dot{\mathbf{x}}^n \right) \qquad (3.11)$$

in which $\mathbf{A}^{mm}$ is the added mass matrix and $\mathbf{B}^{mm}$ is the matrix of radiation damping, both of which are due to the m-th body's own motion. The matrices $\mathbf{A}^{mn}$ and $\mathbf{B}^{mn}$ are the interaction coefficients due to the motion of the neighbor n. The exciting force due to diffraction is $\mathbf{F}_I(t)$. The numerical computations of these coefficients in the frequency domain are fully described in Papers A and B.

Since the viscous damping force and the constraining forces are often non-linear, for example the velocity-squared drag force caused by the viscosity

of the fluid, and the forces due to the mooring lines, they cannot be directly incorporated into the equation of motion when the dynamic analysis is implemented in the frequency domain. All non-linear forces acting on the bodies need to be linearized. The linearization techniques are discussed in the following sections. In general, linearized constraining forces can be given in the following form:

$$
\mathbf{F}_c(t) = \left\{
\begin{array}{l}
\mathbf{F}_c^{(1)} \\[2ex]
\mathbf{T}_c^{(1)} + \mathbf{F}_c^{(1)} \times \left(\mathbf{x}_o^b + \mathbf{X}^{(0)} \right) + \mathbf{F}_c^{(0)} \times \mathbf{X}^{(1)}
\end{array}
\right\}
\tag{3.12}
$$

where $T_c^{(1)}$ denotes the first-order constraining torque due to constrainting influences (including force and moment). With the definitions given in equations (3.10) – (3.12), the equations of motion (3.7) can be rewritten

$$
\left\{ -\omega^2 \left(\mathbf{M}^m + \mathbf{A}^{mm} \right) - i\omega \mathbf{B}^{mm} + \mathbf{C}^m \right\} \mathbf{X}^m e^{-i\omega t} + \sum_{n=1,n\neq m}^{NB} \left\{ -\omega^2 \mathbf{A}^{mn} - i\omega \mathbf{B}^{mn} \right\} \mathbf{X}^n e^{-i\omega t}
$$

$$
= \mathbf{F}_l^m(t) + \mathbf{F}_v^m(t) + \mathbf{F}_c^m(t)
$$

$$
m = 1, 2, ..., NB
\tag{3.13}
$$

In order to eliminate the time factor from the equations and calculate the structural response in the frequency domain, a formal mathematical transformation is used. The basic approach involves the expansion of the time-dependent loads in terms of a series of harmonic functions. One can use an ordinary Fourier series in which the loads, F(t), are expanded in a series of the form

$$
F(t) = \sum_{n=0}^{\infty} A_n \cos \frac{n\pi}{T} t + \sum_{n=0}^{\infty} B_n \sin \frac{n\pi}{T} t
\tag{3.14}
$$

where T is the duration of the loading, or the loads can be expressed as an infinite integral,

$$F(t) = \int_{-\infty}^{\infty} \overline{F}(\omega)\, e^{-i\omega t}\, d\omega. \tag{3.15}$$

The general equations of motion, Eq. 3.7, can be written as

$$\mathbf{M}^m \ddot{\mathbf{x}}^m(t) + \mathbf{C}^m \mathbf{x}^m(t) = \int_{-\infty}^{\infty} \overline{\mathbf{F}}^m(\omega)\, e^{-i\omega t}\, d\omega \qquad m = 1,2,...,\text{NB}. \tag{3.16}$$

Based on the assumption that the structural response to each excitation frequency is confined to that frequency, the following complex set of equations can be solved for various values of ω:

$$(-\omega^2 \mathbf{M}^m + \mathbf{C}^m)\, \mathbf{X}^m(\omega) = \overline{\mathbf{F}}^m(\omega) \qquad m = 1,2,...,\text{NB}. \tag{3.17}$$

Finally, the total response can be calculated from the summation of responses from all of the frequencies.

3.4 Inclusion of Mechanical Couplings

3.4.1 Elastic springs

It is seldom that a floating breakwater consists of a single unit; in general, it is built up by joining units in various ways so that the breakwater will act as one continuous beam. The relative motion between the units is usually restricted by some type of coupling, such as stiff elements or articulated couplings (or joints), among others. The function of an articulated coupling is such that it allows bending in the vertical plane, while it limits horizontal bending and twisting.

Considering that the motion of a breakwater system has been assumed to be small and that the size of the coupling is usually small compared with the characteristic dimensions of the bodies, the stiff elements may be modelled as massless springs with large stiffness. In this study, it is assumed that the springs are placed parallel to the x, y and z axes when the bodies are floating at rest, and that the connections between the body and the springs are hinged connections. Figure 3.5 a) illustrates a simple example of a pair of bodies, m and n, connected by a spring with length l parallel to the y axis and having relative displacements δx and δy in the x

23

and y directions respectively. The horizontal components of the spring force at point p on body m are illustrated in Figure 3.5 b).
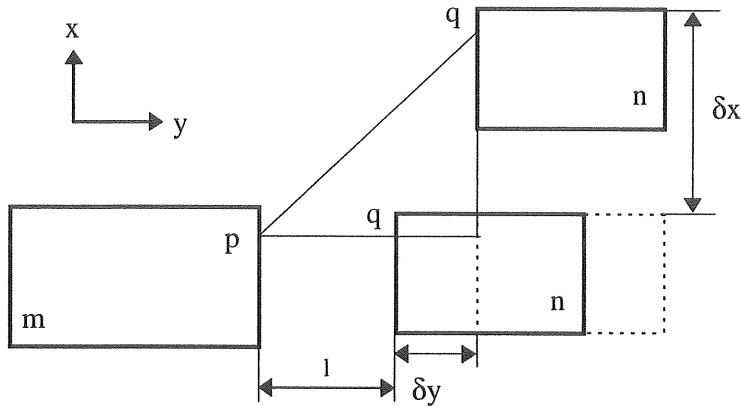

Fig. 3.5 a) Relative displacements for a pair of bodies connected by an elastic spring.

$$\mathbf{F}_x = \frac{\mathbf{F}^{(0)}}{l}\,\delta\mathbf{x} \qquad \mathbf{F} = \mathbf{F}^{(0)} + \mathbf{F}^{(1)} + O(\varepsilon^2)$$

$$\mathbf{F}_y = \mathbf{F}^{(0)} + k \cdot \delta\mathbf{y}$$

b) The horizontal components of the spring force on body m.

The force $\mathbf{F}$ is caused by the axial deflection of the spring. To the first order, the axial deflection is due only to the relative displacement δx; δy induces the second-order deflection. To account for the direction of $\mathbf{F}$, the force on body m can be expressed as

24

$$\begin{bmatrix} k & 0 \\ 0 & F^{(0)}/l \end{bmatrix} \begin{bmatrix} \delta x \\ \delta y \end{bmatrix} = \begin{bmatrix} \mathbf{F}_x^{(1)} \\ \mathbf{F}_y^{(1)} \end{bmatrix}. \tag{3.18}$$

In general, when the bodies move in all six modes of motion, the relative movements between the attached points p on body m and q on body n in the global reference frame are defined as

$$x_p^m - x_q^n = \left(x_0^m - x_0^n \right) + \left(\overline{x}_p^m - \overline{x}_q^n \right) +$$

$$\varepsilon \left[\left(\mathbf{X}^{(1)m} - \mathbf{X}^{(1)n} \right) + \theta^{(1)m} \times \left(\overline{x}_p^m - \mathbf{X}^{(0)m} \right) - \theta^{(1)n} \times \left(\overline{x}_q^n - \mathbf{X}^{(0)n} \right) \right] + O\!\left(\varepsilon^2 \right) \tag{3.19}$$

where the term with the scale ε gives the deflection Δl (δx, δy, δz) of the first order. With similar considerations, the linear forces on body m and their moments about the selected centre of rotation, $\mathbf{X}^{(0)m}$, are summarised in matrix form

$$\mathbf{F}_s^{m(1)} = -\left\{ \sum_{j=1}^{NS} \mathbf{K}_j^{mm} \right\} x^m - \sum_{j=1}^{NS} \left(\mathbf{K}_j^{mn} x^n \right) \tag{3.20}$$

where $\mathbf{F}_s^{m(1)}$ denotes the first-order generalized spring force on body m in which the moments (for components 4, 5 and 6) are evaluated according to Equation (3.12). The stiffness matrix related to the body's own motion is $\mathbf{K}_j^{mm}$, and $\mathbf{K}_j^{mn}$ is related to the motion of the connected body n; both of these are caused by the j-th spring. The number of springs on body m is NS. For the springs parallel to the x axis, the corresponding stiffness matrices are derived as follows:

25

$$\mathbf{\ddot{K}}_j^{mm} = \begin{bmatrix} k_j & 0 & 0 & 0 & k_j h_{zj}^m & -k_j h_{yj}^m \\[8pt] 0 & E_{xj} & 0 & -E_{xj} h_{zj}^m & 0 & E_{xj} h_{xj}^m \\[8pt] 0 & 0 & E_{xj} & E_{xj} h_{yj}^m & -E_{xj} h_{xj}^m & 0 \\[8pt] 0 & -E_{xj} h_{zj}^m & E_{xj} h_{yj}^m & K_{44} & -\begin{pmatrix} E_{xj} h_{yj}^m h_{xj}^m \\ + h_{xj}^m F_{yj}^{(0)} \end{pmatrix} & -\begin{pmatrix} E_{xj} h_{zj}^m h_{xj}^m \\ + h_{xj}^m F_{zj}^{(0)} \end{pmatrix} \\[12pt] k_j h_{zj}^m & 0 & -E_{xj} h_{xj}^m & -\begin{pmatrix} E_{xj} h_{xj}^m h_{yj}^m \\ + h_{yj}^m F_{xj}^{(0)} \end{pmatrix} & K_{55} & -\begin{pmatrix} k_j h_{zj}^m h_{yj}^m \\ + h_{yj}^m F_{zj}^{(0)} \end{pmatrix} \\[12pt] -k_j h_{yj}^m & E_{xj} h_{xj}^m & 0 & -\begin{pmatrix} E_{xj} h_{xj}^m h_{zj}^m \\ + h_{zj}^m F_{xj}^{(0)} \end{pmatrix} & -\begin{pmatrix} k_j h_{yj}^m h_{zj}^m \\ + h_{zj}^m F_{yj}^{(0)} \end{pmatrix} & K_{66} \end{bmatrix},$$

$$(3.21)$$

in which

$$K_{44} = h_{zj}^m F_{zj}^{(0)} + h_{yj}^m F_{yj}^{(0)} + E_{xj}\left[\left(h_{yj}^m\right)^2 + \left(h_{zj}^m\right)^2\right],$$

$$K_{55} = h_{xj}^m F_{xj}^{(0)} + h_{zj}^m F_{zj}^{(0)} + k_j\left(h_{zj}^m\right)^2 + E_{xj}\left(h_{xj}^m\right)^2,$$

$$K_{66} = h_{yj}^m F_{yj}^{(0)} + h_{xj}^m F_{xj}^{(0)} + E_{xj}\left(h_{xj}^m\right)^2 + k_j\left(h_{yj}^m\right)^2,$$

$$h_{xj}^m = \overline{x}_p^m - X_m^{(0)},$$

$$h_{yj}^m = \overline{y}_p^m - Y_m^{(0)},$$

$$h_{zj}^m = \overline{z}_p^m - Z_m^{(0)},$$

$$E_{xj} = \frac{F_{xj}^{(0)}}{\left| \left(x_0^m - x_0^n \right) + \left(\overline{x}_p^m - \overline{x}_q^n \right) \right|},$$

$$E_{yj} = \frac{F_{yj}^{(0)}}{\left| \left(y_0^m - y_0^n \right) + \left(\overline{y}_p^m - \overline{y}_q^n \right) \right|},$$

$$E_{zj} = \frac{F_{zj}^{(0)}}{\left| \left(z_0^m - z_0^n \right) + \left(\overline{z}_p^m - \overline{z}_q^n \right) \right|};$$

and

$$\mathbb{K}_j^{mn} = \begin{bmatrix} -k_j & 0 & 0 & 0 & -k_j h_{zi}^n & k_j h_{yi}^n \\[2ex] 0 & -E_{xj} & 0 & E_{xj} h_{zi}^n & 0 & -E_{xj} h_{xi}^n \\[2ex] 0 & 0 & -E_{xj} & -E_{xj} h_{yi}^n & E_{xj} h_{xi}^n & 0 \\[2ex] 0 & E_{xj} h_{zj}^m & -E_{xj} h_{yj}^m & -\begin{pmatrix} E_{xj} h_{yj}^m h_{yi}^n \\ + E_{xj} h_{zj}^m h_{zi}^{ni} \end{pmatrix} & E_{xj} h_{yj}^m h_{xi}^n & E_{xj} h_{zj}^m h_{xi}^n \\[3ex] -k_j h_{zj}^m & 0 & E_{xj} h_{xj}^m & E_{xj} h_{xj}^m h_{yi}^n & -\begin{pmatrix} E_{xj} h_{xj}^m h_{xi}^n \\ + k_j h_{zj}^m h_{zi}^n \end{pmatrix} & k_j h_{zj}^m h_{yi}^n \\[3ex] k_j h_{yj}^m & -E_{xj} h_{xj}^m & 0 & E_{xj} h_{xj}^m h_{zi}^n & k_j h_{yj}^m h_{zi}^n & -\begin{pmatrix} E_{xj} h_{xj}^m h_{xi}^n \\ + k_j h_{yj}^m h_{yi}^n \end{pmatrix} \end{bmatrix},$$

$$(3.22)$$

in which

$$h_{xi}^n = \overline{x}_q^n - X_n^{(0)},$$

$$h_{yi}^n = \overline{y}_q^n - Y_n^{(0)},$$

$$h_{zi}^n = \overline{z}_q^n - Z_n^{(0)}.$$

For the springs parallel to the y axis, the K_j^{mm} and K_j^{mn} matrices are derived as

$$K_j^{mm} = \begin{bmatrix} E_{yj} & 0 & 0 & 0 & E_{yj}h_{zj}^m & -E_{yj}h_{yj}^m \\[2em] 0 & k_j & 0 & -k_j h_{zj}^m & 0 & k_j h_{xj}^m \\[2em] 0 & 0 & E_{yj} & E_{yj}h_{yj}^m & -E_{yj}h_{xj}^m & 0 \\[2em] 0 & -k_j h_{zj}^m & E_{yj}h_{yj}^m & K_{44} & -\begin{pmatrix} E_{yj}h_{yj}^m h_{xj}^m \\ +h_{xj}^m F_{yj}^{(0)} \end{pmatrix} & -\begin{pmatrix} k_j h_{xj}^m h_{zj}^m \\ +h_{xj}^m F_{zj}^{(0)} \end{pmatrix} \\[2em] E_{yj}h_{zj}^m & 0 & -E_{yj}h_{xj}^m & -\begin{pmatrix} E_{yj}h_{xj}^m h_{yj}^m \\ +h_{yj}^m F_{xj}^{(0)} \end{pmatrix} & K_{55} & -\begin{pmatrix} E_{yj}h_{yj}^m h_{zj}^m \\ +h_{yj}^m F_{zj}^{(0)} \end{pmatrix} \\[2em] -E_{yj}h_{yj}^m & k_j h_{xj}^m & 0 & -\begin{pmatrix} k_j h_{xj}^m h_{zj}^m \\ +h_{zj}^m F_{xj}^{(0)} \end{pmatrix} & -\begin{pmatrix} E_{yj}h_{yj}^m h_{zj}^m \\ +h_{zj}^m F_{yj}^{(0)} \end{pmatrix} & K_{66} \end{bmatrix},$$

$$(3.23)$$

in which

$$K_{44} = h_{zj}^m F_{zj}^{(0)} + h_{yj}^m F_{yj}^{(0)} + E_{yj}\left(h_{yj}^m\right)^2 + k_j\left(h_{zj}^m\right)^2,$$

$$K_{55} = h_{xj}^m F_{xj}^{(0)} + h_{zj}^m F_{zj}^{(0)} + E_{yj}\left[\left(h_{xj}^m\right)^2 + \left(h_{zj}^m\right)^2\right],$$

$$K_{66} = h_{yj}^m F_{yj}^{(0)} + h_{xj}^m F_{xj}^{(0)} + k_j\left(h_{xj}^m\right)^2 + E_{yj}\left(h_{yj}^m\right)^2,$$

and

$$K_j^{mn} = \begin{bmatrix} -E_{yj} & 0 & 0 & 0 & -E_{yj}h_{zi}^n & E_{yj}h_{yi}^n \\[2mm] 0 & -k_j & 0 & k_jh_{zi}^n & 0 & -k_jh_{xi}^n \\[2mm] 0 & 0 & -E_{yj} & -E_{yj}h_{yi}^n & E_{yj}h_{xi}^n & 0 \\[2mm] 0 & k_jh_{zj}^m & -E_{yj}h_{yj}^m & -\left(\begin{array}{c}E_{yj}h_{yj}^m h_{yi}^n \\ +k_jh_{zj}^m h_{zi}^n\end{array}\right) & E_{yj}h_{yj}^m h_{xi}^n & k_jh_{zj}^m h_{xi}^n \\[3mm] -E_{yj}h_{zj}^m & 0 & E_{yj}h_{xj}^m & E_{yj}h_{xj}^m h_{yi}^n & -\left(\begin{array}{c}E_{yj}h_{xj}^m h_{xi}^n \\ +E_{yj}h_{zj}^m h_{zi}^n\end{array}\right) & E_{yj}h_{zj}^m h_{yi}^n \\[3mm] E_{yj}h_{yj}^m & -k_jh_{xj}^m & 0 & k_jh_{xj}^m h_{zi}^n & E_{yj}h_{yj}^m h_{zi}^n & -\left(\begin{array}{c}k_jh_{xj}^m h_{xi}^n \\ +E_{yj}h_{yj}^m h_{yi}^n\end{array}\right) \end{bmatrix}.$$

$$(3.24)$$

For the springs parallel to the z axis, the K_j^{mm} and K_j^{mn} matrices are derived as

$$K_j^{mm} = \begin{bmatrix} E_{zj} & 0 & 0 & 0 & E_{zj}h_{zj}^m & -E_{zj}h_{yj}^m \\[2mm] 0 & E_{zj} & 0 & -E_{zj}h_{zj}^m & 0 & E_{zj}h_{xj}^m \\[2mm] 0 & 0 & k_j & k_jh_{yj}^m & -k_jh_{xj}^m & 0 \\[2mm] 0 & -E_{zj}h_{zj}^m & k_jh_{yj}^m & K_{44} & -\left(\begin{array}{c}k_jh_{xj}^m h_{yj}^m \\ +h_{xj}^m F_{yj}^{(0)}\end{array}\right) & -\left(\begin{array}{c}E_{zj}h_{xj}^m h_{zj}^m \\ +h_{xj}^m F_{zj}^{(0)}\end{array}\right) \\[3mm] E_{zj}h_{zj}^m & 0 & -k_jh_{xj}^m & -\left(\begin{array}{c}k_jh_{xj}^m h_{yj}^m \\ +h_{yj}^m F_{xj}^{(0)}\end{array}\right) & K_{55} & -\left(\begin{array}{c}E_{zj}h_{yj}^m h_{zj}^m \\ +h_{yj}^m F_{zj}^{(0)}\end{array}\right) \\[3mm] -E_{zj}h_{yj}^m & E_{zj}h_{xj}^m & 0 & -\left(\begin{array}{c}E_{zj}h_{xj}^m h_{zj}^m \\ +h_{zj}^m F_{xj}^{(0)}\end{array}\right) & -\left(\begin{array}{c}E_{zj}h_{yj}^m h_{zj}^m \\ +h_{zj}^m F_{yj}^{(0)}\end{array}\right) & K_{66} \end{bmatrix},$$

$$(3.25)$$

in which

$$K_{44} = h_{zj}^{m} F_{zj}^{(0)} + h_{yj}^{m} F_{yj}^{(0)} + k_j \left(h_{yj}^{m} \right)^2 + E_{zj} \left(h_{zj}^{m} \right)^2 ,$$

$$K_{55} = h_{xj}^{m} F_{xj}^{(0)} + h_{zj}^{m} F_{zj}^{(0)} + E_{zj} \left(h_{zj}^{m} \right)^2 + k_j \left(h_{xj}^{m} \right)^2 ,$$

$$K_{66} = h_{yj}^{m} F_{yj}^{(0)} + h_{xj}^{m} F_{xj}^{(0)} + E_{zj} \left[\left(h_{xj}^{m} \right)^2 + \left(h_{yj}^{m} \right)^2 \right] ,$$

and

$$\mathbf{K}_j^{mn} = \begin{bmatrix} -E_{zj} & 0 & 0 & 0 & -E_{zj}h_{zi}^{n} & E_{zj}h_{yi}^{n} \\ 0 & -E_{zj} & 0 & E_{zj}h_{zi}^{n} & 0 & -E_{zj}h_{xi}^{n} \\ 0 & 0 & -k_j & -k_j h_{yi}^{n} & k_j h_{xi}^{n} & 0 \\ 0 & E_{zj}h_{zj}^{m} & -k_j h_{yj}^{m} & -\left(\begin{array}{c} k_j h_{yj}^{m} h_{yi}^{n} \\ +E_{zj}h_{zj}^{m}h_{zi}^{n} \end{array} \right) & -k_j h_{yj}^{m}h_{xi}^{n} & E_{zj}h_{zj}^{m}h_{xi}^{n} \\ -E_{zj}h_{zj}^{m} & 0 & k_j h_{xj}^{m} & k_j h_{xj}^{m}h_{yi}^{n} & -\left(\begin{array}{c} k_j h_{xj}^{m} h_{xi}^{n} \\ +E_{zj}h_{zj}^{m}h_{zi}^{n} \end{array} \right) & E_{zj}h_{zj}^{m}h_{yi}^{n} \\ E_{zj}h_{yj}^{m} & -E_{zj}h_{xj}^{m} & 0 & E_{zj}h_{xj}^{m}h_{zi}^{n} & E_{zj}h_{yj}^{m}h_{zi}^{n} & -\left(\begin{array}{c} E_{zj}h_{xj}^{m} h_{xi}^{n} \\ +E_{zj}h_{yj}^{m}h_{yi}^{n} \end{array} \right) \end{bmatrix} .$$

$$(3.26)$$

3.4.2 Revolute joints (Hinge joints)

Another type of connection that is often encountered in the simulation of articulated couplings is the revolute joint. A revolute joint allows relative rotation about a common axis, but precludes relative translation along this axis, as shown in Fig. 3.6. In order to define the revolute joint, a pair of joint definition frames, x''_m-y''_m-z''_m and x''_n-y''_n-z''_n, are introduced; the frames are attached to bodies m and n, respectively, with their origins at

the centre of the joint, denoted P, that is common to the bodies. Points Q_m and Q_n at one unit of distance from P on the axis of relative rotation, are specified in order to determine the z'' axes of the frames. To orient the frames, unit vectors f_m, g_m and h_m are defined along the coordinate axes of the x''_m-y''_m-z''_m frame, and f_n, g_n and h_n of the x''_n-y''_n-z''_n frame.
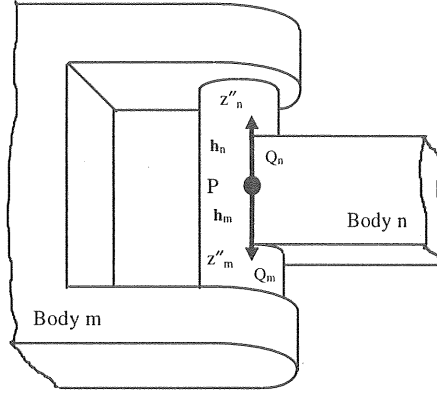
Fig. 3.6   Revolute joint (Hinge)

The analytical formulation of the revolute joint is that points P_m and P_n coincide and that body-fixed vectors h_m and h_n are parallel, leading to the constraint equations

$$\Phi^s\left(P_m, P_n\right) = r_m^P - r_n^P = 0$$

(3.27)

$$\Phi^{p1}\left(h_m, h_n\right) = \begin{bmatrix} \Phi^{d1}\left(f_m, h_n\right) \\ \Phi^{d1}\left(g_m, h_n\right) \end{bmatrix} = \begin{bmatrix} f_m \cdot h_n \\ g_m \cdot h_n \end{bmatrix} = 0$$

for which the second condition states that the vector h_n is parallel to h_m if, and only if, it is orthogonal to f_m and g_m. There are three scalar equations for the first condition, and two for the second one. These equations yield only one relative degree of freedom, i.e. rotation about the common axis of the bearing. In general, if a system has NJ number of joints, all constraint equations encountered can be written in the form

31

$$\Phi_j\left(r_m, A_m, r_n, A_n\right) = 0 \qquad\qquad j = 1, 2, ..., NJ \qquad\qquad (3.28)$$

where index j is the number of the joint between the bodies m and n; r is a space vector of coordinates x, y and z; and A is the direction cosine matrix (or transformation matrix) of the body-fixed frame relative to the stationary x-y-z frame.

The effect of this type of joint on the connected bodies can be replaced by the reaction forces and torques at the connecting point. Since the reaction forces and torques affected by the relative motion of the connected bodies, are usually difficult to determine, a solution based on the principle of virtual work and the Lagrange multiplier theorem is used to obtain the equations of motion which satisfies the constraint conditions for the system.

According to Newton's laws and the virtual work principle, variational equations of motion for a constrained system are reduced to the following compact form

$$\delta r^T\left[M\ddot{r} + \left(A\dot{\tilde{\omega}}' + A\tilde{\omega}'\tilde{\omega}'\right)M\left(\bar{x}_c - X^{(0)}\right) - F_A\right] + \delta\pi'^T\left[M\left(\tilde{\bar{x}}_c - \tilde{X}^{(0)}\right)A^T\ddot{r} + J'\dot{\omega}' + \tilde{\omega}'J'\omega' - T'_A\right] = 0$$

$$(3.29)$$

in which J' is the inertia matrix with respect to the body-fixed frame; F_A and T'_A denote the applied forces and moments (or torques) with respect to the selected centre of rotation; $\omega' = A^T \omega$; ω is the angular velocity of the body-fixed frame relative to the x-y-z-frame; and $\tilde{\omega}$ is a skew-symmetric matrix associated with the vector ω. The effect of the constraint forces is eliminated in this composite equation because the virtual work of all constraint forces is zero. Equation (3.29) must hold for all virtual displacements, δr, and virtual rotations, $\delta\pi'$, that are kinematically admissible for the constraints of equation (3.28) if

$$\Phi_r \delta r + \Phi_{\pi'} \delta\pi' = 0 \qquad\qquad\qquad (3.30)$$

where Φ_r and $\Phi_{\pi'}$ are Jacobian matrices for which computational formulae are given in Table 3.1; for a complete explanation, see Haug (1989).

When Equation (3.29) holds for all δr and $\delta\pi'$ that satisfy equation (3.30), according to the Lagrange multiplier theorem, there exists a Lagrange multiplier vector λ such that

$$\delta r^T\left[M\ddot{r}+\left(A\dot{\tilde{\omega}}'+A\tilde{\omega}'\tilde{\omega}'\right)M\left(\overline{x}_c-X^{(0)}\right)-F_A+\Phi_r^T\lambda\right]+$$
$$\delta\pi'^T\left[M\left(\dot{\tilde{\overline{x}}}_c-\tilde{X}^{(0)}\right)A^T\ddot{r}+J'\dot{\omega}'+\tilde{\omega}'J'\omega'-T_A'+\Phi_{\pi'}^T\lambda\right]=0 \tag{3.31}$$

for arbitrary δr and $\delta\pi'$. The coefficients of these arbitrary variations must be zero, yielding the constrained Newton-Euler equations of motion

$$M\ddot{r}+\left(A\dot{\tilde{\omega}}'+A\tilde{\omega}'\tilde{\omega}'\right)M\left(\overline{x}_c-X^{(0)}\right)+\Phi_r^T\lambda=F_A$$
$$J'\dot{\omega}'+M\left(\dot{\tilde{\overline{x}}}_c-\tilde{X}^{(0)}\right)A^T\ddot{r}+\Phi_{\pi'}^T\lambda=T_A'-\tilde{\omega}'J'\omega'. \tag{3.32}$$

To complete the equations of motion, acceleration equations associated with the kinematic constraints of equation (3.28) must be obtained. By taking the time derivative of equation (3.28), the velocity equation is

$$\Phi_r\dot{r}+\Phi_{\pi'}\omega'=-\Phi_t. \tag{3.33}$$

Next, the time derivative of this equation yields the acceleration equation

$$\Phi_r\ddot{r}+\Phi_{\pi'}\dot{\omega}'=-\Phi_{tt}-\left(\Phi_r r+\Phi_{\pi'}\omega'\right)=\Gamma. \tag{3.34}$$

So far, the equations are set up for a system of large displacements and large rotations. For a spatial system, Euler's theorem and Euler parameters are usually needed to determine the transformation matrix A. For a more detailed derivation of these equations, see Haug (1989). However, for a system of small-amplitude motion, the system acceleration equations can be simplified by eliminating the second order terms, $O(\varepsilon^2)$. Since the

33

approximations of $\sin\alpha \cong \alpha$ and $\cos\alpha \cong 1$ are permissible for a small angular displacement α ($<15°$ or 0.26 rad), the transformation matrix A can be written in the form of elements of θ (α, β, γ):

$$A = \begin{bmatrix} 1 & -\gamma & \beta \\ \gamma & 1 & -\alpha \\ -\beta & \alpha & 1 \end{bmatrix}. \tag{3.35}$$

To the first order, O(ε), the relationships of $\omega = \dot{\theta} = \left(\dot{\alpha}, \dot{\beta}, \dot{\gamma}\right)$ and $\omega' = A^T\omega = \omega$ are derived. According to the formulas given in Table 3.2, the solutions of Γ for all constraint conditions involved are eliminated due to the second order. The Coriolis acceleration effects on the right side of equation (3.32) and the cross-term effects with $\tilde{\omega}'\tilde{\omega}'$ are also negligible for the same reason. Combining equations (3.32) and (3.34), the linearized approximation obtained is

$$\begin{bmatrix} M & M\left(\tilde{\bar{x}}_c - \tilde{X}^{(0)}\right) & \Phi_r^T \\ M\left(\tilde{\bar{x}}_c - \tilde{X}^{(0)}\right) & J' & \Phi_{\pi'}^T \\ \Phi_r^{(0)} & \Phi_{\pi'}^{(0)} & 0 \end{bmatrix} \begin{bmatrix} \ddot{r} \\ \dot{\omega}' \\ \lambda \end{bmatrix} = \begin{bmatrix} F_A^{(1)} \\ T_A'^{(1)} \\ 0 \end{bmatrix} \tag{3.36}$$

with the expressions of

$$\Phi_r^T \lambda = \varepsilon\left(\Phi_r^{T(1)}\lambda^{(0)} + \Phi_r^{T(0)}\lambda^{(1)}\right) + O\left(\varepsilon^2\right)$$

and

$$\Phi_{\pi'}^T \lambda = \varepsilon\left(\Phi_{\pi'}^{T(1)}\lambda^{(0)} + \Phi_{\pi'}^{T(0)}\lambda^{(1)}\right) + O\left(\varepsilon^2\right)$$

where the superscripts (0) and (1) indicate the terms of zero and the first order, respectively. These equations of motion, taken with the kinematic constraint equation (3.28) and the linearized velocity equation (3.33), yield a mixed system of differential-algebraic equations of motion for the system. In addition to this dynamic analysis, an equilibrium analysis of the system is needed to determine the zero-order Lagrange multipliers, and the static forces which depend on the equilibrium position of the bodies.

Furthermore, initial conditions on position and orientation and on velocity may be required for a time domain solution.

Table 3.1

Type of constraint	Constraint function	Φ_{rm}	Φ_{rn}	$\Phi_{\pi'm}$	$\Phi_{\pi'n}$
Spherical constraint	$\Phi^s\,(P_m,P_n)$	$-[\,\mathbf{I}\,]$	$[\,\mathbf{I}\,]$	$A_m\!\left(\widetilde{\overline{x}}_m^P - \widetilde{X}_m^{(0)}\right)$	$-A_n\!\left(\widetilde{\overline{x}}_n^P - \widetilde{X}_n^{(0)}\right)$
Dot-1 constraint	$\Phi^{d1}\,(f_m,h_n)$	0	0	$-h_n'^T A_n^T A_m \widetilde{f}_m'$	$-f_m'^T A_m^T A_n \widetilde{h}_n'$
Dot-1 constraint	$\Phi^{d1}\,(g_m,h_n)$	0	0	$-h_n'^T A_n^T A_m \widetilde{g}_m'$	$-g_m'^T A_m^T A_n \widetilde{h}_n'$

Table 3.2

Type of constraint	Γ functions	
Spherical constraint	$\Gamma^s\,(P_m,P_n)$	$A_m \widetilde{\omega}_m' \widetilde{\omega}_m' \left(\overline{x}_m^P - X_m^{(0)}\right) - A_n \widetilde{\omega}_n' \widetilde{\omega}_n' \left(\overline{x}_n^P - X_n^{(0)}\right)$
Dot-1 constraint	$\Gamma^{d1}\,(f_m,h_n)$	$-h_n'^T\!\left(A_n^T A_m \widetilde{\omega}_m' \widetilde{\omega}_m' + \widetilde{\omega}_n' \widetilde{\omega}_n' A_n^T A_m\right)f_m + 2\omega_n'^T \widetilde{h}_n' A_n^T A_m \widetilde{f}_m' \omega_m'$
Dot-1 constraint	$\Gamma^{d1}\,(g_m,h_n)$	$-h_n'^T\!\left(A_n^T A_m \widetilde{\omega}_m' \widetilde{\omega}_m' + \widetilde{\omega}_n' \widetilde{\omega}_n' A_n^T A_m\right)g_m + 2\omega_n'^T \widetilde{h}_n' A_n^T A_m \widetilde{g}_m' \omega_m'$

3.5 Inclusion of Mooring Lines

A mooring system is generally required to keep floating breakwaters on station. For the purpose of assessing the influence of mooring lines on the dynamics of a breakwater system, a study of different methods was undertaken, based on the published articles of other researchers. This study yielded considerable information. Kwan and Bruen (1991) made calculations by three different methods, conventional quasi-static analysis, time domain and frequency domain analysis, for 13 cases of different types of mooring and different wave conditions. Results from these three methods were compared. The comparison shows that quasi-static analysis gives a very poor representation of wave frequency tensions, which may result in large errors in fatigue damage calculation. However, when the total tensions are considered, the difference in the results based on quasi-static and time domain analysis is less dramatic. Quasi-static analysis underestimates total tensions by 4 to 40% for all of the thirteen cases studied. From these extensive comparisons, it is evident that quasi-static analysis is a very approximate approach, especially for systems floating in deep water. Generally, it is not sufficient that the cable force be determined only by the fairlead position. For an accurate prediction of cable tension, dynamic analysis is needed, to include not only the loads induced by the motions of the fairlead but also the dynamics of the mooring line itself.

In studying the methods used in the dynamic analysis, extensive comparisons of the dynamic computations (parameters), based on frequency domain and time domain simulations, for mooring cables, have also been made and reported in the Kwan and Bruen paper. Results obtained by these methods have been compared in terms of maximum line tensions, tension spectra and their transfer functions (tension to tangential motion), and maximum anchor loads. A major conclusion based on these comparative studies is that the frequency domain analysis can produce acceptable line tension and anchor load predictions in most cases if the non-linearities are properly linearized. Furthermore, similar conclusions have been obtained by Larsen and Sandvik (1990) from a similar study.

In this dissertation an approach based on dynamic analysis in the time domain is employed using a computer programme, MODEX, developed by Lindahl (1983) at the Department of Hydraulics, Chalmers University of Technology. The method has been verified by model test data (Lindahl, 1985, Bergdahl & Rask, 1987). The program MODEX is based on the theory reported in the paper "Dynamic Analysis of Mooring Cables" by Lindahl and Sjöberg (1983). In this paper, a model is used that incorporates the elasticity of the cable, inertia forces, the hydrodynamic

force, drag forces and the frictional forces between the sea bottom and the cable. Among these forces, the drag forces acting on the cable give rise to important non-linear terms in the governing equations. A sea bottom effect, such as the contact between the cable and the bottom, also causes non-linearities. The bottom effect is particularly significant in shallow water where a large portion of the cable may lie on the bottom. The non-linearity caused by a change of the geometry of the cable is also taken into account. In the numerical computation, the position of the mooring line is updated at each time step, except for the global mass matrix (including the added mass) which may be updated for each n:th time increment where n is larger than one. The damping term, stiffness term and load in the equation of motion for the cable are recalculated at each time step. Hence the computation is complex and time consuming.

According to equations (3.15)-(3.17) and the principle described in Section 3.3, the cable force reacting on the structure can be decomposed into a series of periodic components at different frequencies by means of the Fast Fourier Transform (FFT) technique. Response of the system to wave excitation is then calculated by solving the equations of motion incorporating only the cable force of wave frequency.

3.6 Inclusion of Wave Drift Forces

In addition to linear wave forces, floating structures are also affected by a non-linear steady wave drift force when exposed to regular waves. This non-linear force may be partially attributable to the velocity-squared terms in Bernoulli's equation, and partially attributable to the surface elevation or run-up on the structures at the waterline when the structure is surface piercing. The drift force is of the second order with respect to the wave height and, thus, generally a small percent of the first-order force. However, under certain circumstances, the drift force can be of considerable significance. The dynamic behaviour of moored floating structures is, for instance, influenced by this force since, in the equations of motion, it changes the restoring forces and moments caused by the mooring lines. The equilibrium position of the floating system and the initial tensions of the cables are determined by this steady force, as well as the steady forces caused by wind and current.

Moreover, the non-linear steady wave force may become oscillating forces, due to the difference in frequencies of wave components in irregular waves. For a given wave energy spectral density, a random wave profile can be generated in terms of components of frequency ω_j (j = 1,2,...,N). An

important contribution to the non-linear oscillating forces is due to the velocity-squared terms in Bernoulli's equation. The solution of the second-order problem results in: mean forces, slowly-varying excitation forces with difference frequency $(\omega_j-\omega_k)$, and excitation forces with double frequencies $(2\omega_j, 2\omega_k)$ and sum frequencies $(\omega_j+\omega_k)$. Due to the long natural periods in a moored system in the surge, sway, and yaw motions and low damping near these periods, the slow oscillations and, hence, the mooring loads increase. This may be critical for a large moored structure. The large horizontal displacement of the structure near resonance can result in failure of the anchor system. The high frequency forces can also play an important part in exciting the resonance oscillations in heave, pitch and roll, since the natural periods in these motions are generally small for a barge-type (or ship-like) structure. Normally, their resonance periods fall within the range of a few seconds.

Many authors have made investigations of the non-linear wave force effects on the dynamic behaviour of a large moored-structure system. Nielsen and Herfjord, et al. (1994) have made investigations of large floating platforms, such as deep draft floaters (DDFs), Troll Olje platforms and tension leg platforms (TLPs), which are used for oil and gas production. These studies provide the basis for observation that the low frequency wave induced motions, in the horizontal and vertical planes, are more important than the first-order motions. Figure 3.7 illustrates clearly the various contributions to the total mooring load, as well as the load in the most heavily loaded line, under extreme conditions. For this type of offshore structure, both mean wind force and mean wave drift force are the main contributions to the total steady force. The dynamic part of the load is dominated by the slow drift motion.
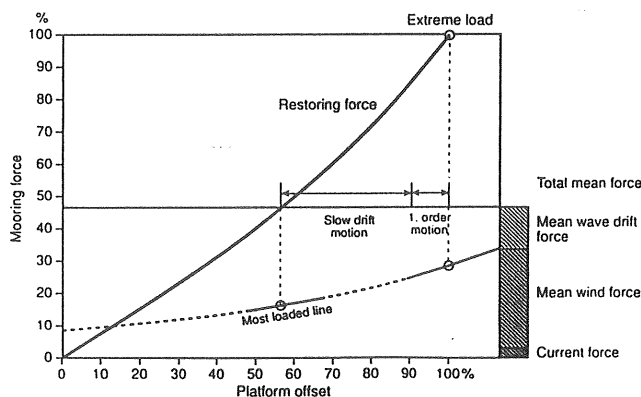
Fig. 3.7 Mooring force versus platform offset. (Nielsen *et al.* 1994)

38

Takaki and Tango (1994) have made studies on a very large floating structure system consisting of multiple barge-type modules, each one of the same length L, floating in regular waves in a head sea condition. It is verified experimentally that the coefficients of wave drift force on the multiple connected floating structures have values of more than 2 to 3 in the case of rationally-hinged connector(s). They found that the wave drift force on the multiple structures with hinge connectors becomes zero, in the range of a long wave length, when the number of the modules with the hinge connectors becomes larger. The effect of different kinds of connections on the wave drift forces has also been investigated. Results from their studies show that the wave drift forces on the multiple structures connected with hinge connectors are smaller than those on the structures with rigid connectors in the long wave length λ range, larger than $\lambda/L = 3.0$, but that there is no difference in the short wave length range of $\lambda/L \leq 1.0$. In the range of $1.0 \leq \lambda/L \leq 3.0$, the wave drift forces associated with the hinge connectors are much larger than those associated with the rigid connectors.

While studying the response problem, the trend was observed that the mean wave drift force is more important for large structures than for small ones. Wave diffraction seems to be an important factor behind this phenomenon. Slow drift excitation loads are large when the mean wave loads are large. Kinoshita, *et al.* (1986) have made similar investigations on multi-body-type floating breakwaters. The breakwater consists of several slender flat plates with floats, and is placed parallel to head seas. The wave energy of the incident waves, which is locked in the interval between the adjacent plates by resonance, is dissipated into the water through the power of the eddies. For this particular type of breakwater, the wave drift force is small, because there are almost no reflected waves. Therefore the quadratic response of the waves is smaller than for a conventional breakwater. However, these experimental studies show that the damping due to wave drift force has a strong effect on the system response in both regular and irregular waves. Herfjord and Nielsen (1988) also found that the wave drift damping is an important contribution to the low frequency damping for a large volume structure, even if this damping is dominated by viscous effects. Low-frequency motion is the result of a low-damped system at resonance. Accordingly, for accurate prediction of the system response, it is critical to account for all damping mechanisms.

Viscous effects make a contribution to the mean drift forces when the drift forces become small. Although these effects cause a third-order drift-force,

proportional to the cube of the wave amplitude, the effects can become increasingly important with rising wave amplitude.

In order to determine the extreme loads in the mooring lines, reliable estimates on the motions are needed. A moored structure could possibly oscillate with combined low frequencies and wave frequencies. The low frequency motions can be determined by solving the following ordinary differential equation which is decoupled from the high-frequency components.

$$\left(M_{ij} + A_{ij}\right)\frac{d^2X_j(t)}{dt^2} + W_{ij}\frac{dX_j(t)}{dt} + C_{ij}X_j(t) = D_i \tag{3.38}$$

In regular waves, the wave drift force, D_i, and wave drift damping coefficient, W_{ij}, are constant functions of the square of the wave amplitude. Moreover, their values are independent of the slow drift displacement, X_j. However, in random waves, these quadratic forces are time dependent. They become slowly-varying quantities and depend parametrically upon the slow drift displacements of the structure. When evaluating the mean forces on a structure, it is not necessary to solve the second-order problem. The second-order potential does not result in mean wave forces. All of the information that we need can be obtained from the first-order solution. However, this is not true for the slow-drift excitation forces. A contribution from the second-order potential is needed. At present, the viscous damping and wave drift damping estimates are very uncertain. Their values are usually obtained by analysing the experimental data from free decay tests of the structure in calm water and in regular waves. The final estimated motions are a combination of the first-order motion with different components of the slow drift motions.

In the work presented here, no computation of wave-drift offset is made. The mean offset, needed for the calculation of the mooring line load, is taken from experimental data.

3.7 Inclusion of Nonlinear Drag Damping

Non-linear drag force can have significant effect on structural motions. As mentioned in Section 3.1, the problem we look at is the diffraction problem. The parameter kD is assumed to be of the order $O(1)$. According to Fig. 3.2, the drag force on a structure is usually less important in the

region this order. However, for certain motions the drag force has a small but significant effect on the amplification of the dynamic response, e.g. the roll motion of a long floating body (barge or ship) in beam (90° wave) sea. The effect is particularly important for a motion near the natural period of the structure. When comparing theoretical calculations with experimental data from model tests, it was also found that the response amplitudes were considerably overestimated near the system resonance in cases where viscous damping was ignored. In many practical applications, the natural frequency of a barge-type structure in roll often falls within the range of wave frequency where the wave energy is dominant; therefore an accurate prediction of roll damping is of importance. In order to reduce the roll motion, bilge keels are often recommended as a method of increasing roll damping.

Standing and Jackson (1992) made an experimental investigation of roll damping for a barge-type structure. A series of typical cross sections, such as a basic rectangular section with either sharp or rounded corners, and with and without bilge keels, was tested. From their studies, notable features were found: first, that the contribution from the wave-radiation damping to the roll damping is very small, while the frictional contribution is negligible; and second, that the roll damping coefficient increased linearly with roll velocity amplitude for sections with sharp corners and no bilge keels, and almost linearly for all sections with bilge keels. The measured wave radiation damping was also found to be fairly constant and independent of roll velocity amplitude.

To include the effect of drag force on the roll motion, the non-linear damping term, $C_D |\dot{x}|\dot{x}$, is incorporated into the equations of motion as follows,

$$\sum_{j=1}^{6}\left[M_{ij}{}^{m} \ddot{x}_{j}{}^{m}(t) + C_{Dii}|\dot{x}_{i}|\dot{x}_{i} + C_{ij}{}^{m} x_{j}{}^{m}(t)\right] = F_{i}^{m}(t) \qquad (3.39)$$

$$i = 1, 2,..., 6; \; m = 1, 2,..., NB$$

in which the drag coefficient, C_{dii}, is evaluated from the drag damping part of the Morison equation based on structure motion. The drag force due to the water particle velocity, which is often insignificant compared to the inertia term, is left out. When the system of equations given in Equation. (3.39) is solved, it is usual to linearize the non-linear term by introducing a linear term so that the work done over one period is the same for this linear

term as for the non-linear term. The linearization is carried out with respect to time, t, in the following way:

$$|\dot{x}_i|\dot{x}_i \approx \frac{8}{3\pi}(\omega X_i)\cdot\dot{x}_i. \tag{3.40}$$

In this equation the right hand side is the first term of the Fourier series expansion of the left hand side. On substitution of $|\dot{x}_i|\dot{x}_i$ into Equation (3.39) and the elimination of time, a set of complex equations with unknown X is obtained.

The drag damping coefficient is usually difficult to determine. In the present study, the C_D parameter is based on the experimental data provided by Standing and Jackson (1992), and others.

3.8 Solution Techniques

Since the primary non-linearities in the system considered have already been linearized with respect to time, the dynamic analysis is reduced to a solution of the complex equations in the frequency domain. To account for the effects mentioned in Section 3, the equations of motion at an incident wave frequency are derived as follows with the additional acceleration equations already obtained from the kinematic constraint equations.

$$\begin{cases} \left\{-\omega^2\left(M^m + A^{mm}\right) - i\omega\left(B^{mm} + \frac{8}{3\pi}C_D\omega\left|X^m\right|I\right) + C^m + \sum_{j=1}^{NS}K_j^{mm} - H^m\right\}X^m + \\ \\ \sum_{n=1,n\neq m}^{NB}\left\{-\omega^2 A^{mn} - i\omega B^{mn}\right\}X^n + \sum_{j=1}^{NS}\left(K_j^{mn}X^n\right) + \Phi_{X^m}^{(1)T}\lambda^{(0)} + \Phi_{X^m}^{(0)T}\lambda^{(1)} - F_{m2}^m = F_I^m(\omega) \\ \\ -i\omega^2\sum_{m=1}^{NB}\Phi_{X^m}^{(0)}X^m = 0 \end{cases}$$

$$m = 1, 2, ..., NB \tag{3.41}$$

Here $\Phi_{x^m}\left(\Phi_r, \Phi_{\pi'}\right)$ is an $NC \times 6$ Jacobian matrix associated with body m; NC is the number of constraint equations and depends on the type and number of couplings. Since the viscous damping term and the mooring line force, F_{m2}^m, in Equation (3.41) are non-linear with respect to X (amplitude

42

of motions), a Newton-Raphson method is used for finding the solution. In many cases, if the iteration begins at a point near the root of interest, this iterative scheme gives a very efficient convergence to the roots of the equations. For the problem studied here, the solution, excluding the non-linear effects with respect to X, is often expected to be near the solution of the complete equations; its values can therefore be used as the initial values in the iterative process. In practically all of the cases I have tested, the convergence of this iterative scheme has been achieved in only a small number of iterations.

In each of the iterations, the computation involves a solution of the linear equations. For a system of many connected bodies moving in all six directions, the number of complex equations, equal to NB $\times$ 6 + NC, may become very large. During the process of design, the equations may have to be solved for many different frequencies of a random sea state and for different couplings, mooring lines and mooring arrangements. Consequently, an efficient solution method for this phase would be very worthwhile. The most important aspect in the computation of the solution is effective computer implementation in both operation speed and data storage. To this end, the LU (Lower triangular and Upper triangular) decomposition method is employed to find the linear solution. This method has an operations count (=1/3 N^3) which is as small as that for Gaussian elimination, but it does not share the disadvantage that all right-hand sides must be known in advance. In the sample computations, however, it was found that the coefficient matrix of the linear equations is ill-conditioned. The direct solution methods of LU decomposition or Gaussian elimination failed to give satisfactory results. Another method is therefore needed. Singular value decomposition, SVD, is one of the powerful techniques for dealing with sets of equations or matrices that are either singular or else numerically very close to singular (ill-conditioned). SVD can diagnose precisely what the problem is by the use of a condition number, and in some cases this will also solve it. A matrix is singular if its condition number is infinity, and it is ill-conditioned if its condition number is too large. When the method was tried on the cases that were studied here, rational estimates of the solution were obtained.

3.9 Surface Elevation

Predicting wave attenuation is a major task in breakwater design. The problem that arises, when a wave train of small amplitude encounters a semi-submerged and fixed breakwater, corresponds to the diffraction problem. A part of the incident wave energy is reflected, while the other

part is transmitted and dissipated. For breakwaters of rectangular configuration, the energy dissipation is usually small. The superposition of the reflected and incident waves forms a combined wave in front of the breakwaters, as sketched in Fig. 3.7 a). The combined velocity potential, Φ, is the sum of components describing the incident and scattered wave motions:

$$\Phi = \Phi_I + \Phi_s \tag{3.41}$$

where Φ_I denotes the incident wave potential, and Φ_s the scattered potential. The free surface elevation is obtained from the dynamic free-surface condition

$$\eta(t) = -\frac{1}{g}\left(\frac{\partial\Phi}{\partial t}\right)_{z=0}. \tag{3.42}$$

The effect of a breakwater on water waves can be determined by examining the average wave-energy fluxes (proportional to the square of the wave height) across the various regions around the breakwater. For a long fixed breakwater (2-D problem), it is convenient to define a reflection coefficient K_r as the ratio of reflected wave height H_r to incident wave height H_I, and a transmission coefficient K_t as the ratio of transmitted (H_t) to incident wave height. If there were zero wave dissipation, H_r and H_t would then be related by the following equation

$$H_I^2 = H_r^2 + H_t^2 \tag{3.43}$$

or

$$K_r^2 + K_t^2 = 1. \tag{3.44}$$

The coefficients of K_r and K_t vary with the wave period, wave steepness, and the structural configurations.

For the more general three-dimensional case of a wave train that approaches a moored floating breakwater, the affected wave field includes the components of wave diffraction (reflection and transmission) and wave

44

radiation caused by the motion of the body as shown in Fig. 3.7 b). The velocity potential for the combined wave motion is

$$\Phi = \Phi_I + \Phi_S + i\omega \sum_{m=1}^{M} \sum_{j=1}^{6} X_{mj} \Phi_{mj} \qquad (3.45)$$

in which Φ_{mj} denotes the radiation potential due to the motion of body m in mode j with the amplitude X_{mj}. According to the free surface condition given in Equation (3.42), the surface elevation of the combined wave pattern is then written as

$$\eta(t) = -\frac{1}{g}\left(\frac{\partial \Phi}{\partial t}\right)_{z=0}$$

$$= \frac{i\omega}{g}\left(\Phi_I + \Phi_s\right) + \frac{\omega^2}{g} \sum_{m=1}^{M} \sum_{j=1}^{6} X_{mj} \Phi_{mj} \qquad (3.46)$$

For this general case, the combined wave field, as well as the wave energy in the area of interest, can be described by the coefficient of the total wave height to the incident wave height or by the sum of the components with coefficients defined in a way similar to the reflection and transmission coefficients.

Incident   Reflected   Transmitted   Radiation   Radiation
wave   wave   wave   wave   wave
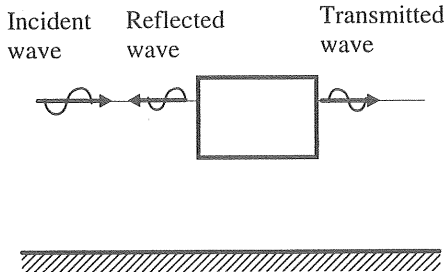
Fig. 3.7 a) Wave trains for a fixed   b) Wave trains caused by the
        breakwater.   breakwater motion (e.g. heave).
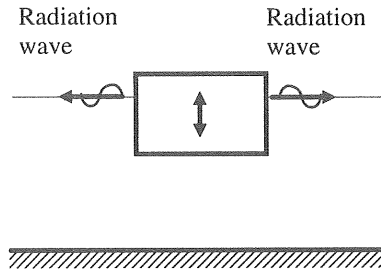
4 EXPERIMENTAL INVESTIGATION

Preliminary model tests have been carried out in the wave basin in the Department of Hydraulics. The purpose of the tests was to evaluate the prediction accuracy of the theories used in the numerical computations. For this purpose many tests, according to four different models described in Table 4.1, were planned to be carried out in steps in order to facilitate the understanding of different effects on the dynamic characteristics of the system.

Table 4.1 Cases studied in model test.

Model No.	Structure arrangements	Wave directions
I	Two units connected by two revolute joints (No mooring chains used)	180° (beam wave)
II	Two units connected by two revolute joints There are 4 mooring chains on each of the units	180° (beam wave)
III	The same as II above	165°
IV	The same as II above	150°

All of the tests were performed in regular waves. In addition to these tests, free-decay tests for one unit with 4 mooring chains in all six modes of motion were carried out in calm water in order to evaluate natural periods of the systems.

In addition to the mathematical modelling to be verified by the model tests, the experiments were intended to be as realistic as possible. Therefore, a scaling procedure was needed to obtain a testing model dynamically similar to its prototype.

4.1 Dimensional Analysis

Dimensional analysis is often a useful approach to obtain relationships (or scaling laws) between variables pertaining to a model and its prototype. By carrying out this approach to the system being analysed, several dimensionless parameters (or numbers) may be derived. The main advantage of using these dimensionless parameters is that the similarity of two systems generally results when the systems are geometrically similar and when the governing dimensionless parameters for the systems are correspondingly the same for both. Hence, the results of studies on one system can be applied to a similar system; the characteristics of one system can be represented by the characteristics of a similar system.

There are three general methods of dimensional analysis. These are: a) the Buckingham π theorem, which states that there will be at least one set of n-m (n = quantities involved, m = fundamental dimensions) independent dimensionless groups in a dimensional analysis; b) Group theory in which dimensionless parameters are obtained by normalizing the differential equations of motion; and c) obtaining dimensionless parameters by taking the ratio of the significant forces that exist in the system being analysed. In any fluid in motion, the forces that could be relevant generally include inertia, viscosity, gravity, pressure, elasticity, surface tension and compressibility forces. Since the fluid inertia force is usually important in fluid dynamic problems, any other relevant force is conveniently introduced as a ratio to this inertial force: for example inertia/viscous force (= Reynolds number); inertia/gravitational force (= Froude number); inertia/pressure force (= Euler number); inertia/compressibility force (= Mach number); etc. Of the three methods, the first two have been adopted for the experimental work discussed here, and their application is described next.

For problems involving wave motion, the following conditions were imposed for practical reasons:

a) $\rho_m/\rho_p = 1$, water is used in model tests;

b) $g_m/g_p = 1$; and

c) $\left(U/\sqrt{gL}\right)_m \big/ \left(U/\sqrt{gL}\right)_p = 1$, Froude similarity is maintained.

The subscripts m and p denote values pertaining to the model and prototype, respectively. From these three conditions and from relevant

47

defining relations, the following relationships may be derived for systems of geometric similarity:

1) $u_m/u_p = t_m/t_p = C_L^{1/2}$;

2) $f_m/f_p = C_L^{-1/2}$;

3) $F_m/F_p = C_L^3$; and

4) $M_m/M_p = C_L^4$;

in which C_L is the length-scale factor between the model and prototype; u represents the velocity; t, time; f, frequency; F, force, and M, moment.

The Buckingham π theorem has been used to obtain the dimensionless parameters for the problem of wave-structure interaction. In general, any time-invariant force, F, i.e. a maximum in-line force, on a fixed rigid structure of characteristic size, D, subjected to a plane wave propagating in finite water depth, could depend on the density of water ρ, gravity g, viscosity ν, body length D, wave amplitude A, wave length L, wave direction θ, water depth d, and time t. Their relationship may be expressed in functional form as

$$F = f(\rho, g, \nu, D, A, L, \theta, d). \tag{4.1}$$

In this equation there are totally nine dimensional quantities. According to the Buckingham π theorem, six non-dimensional parameters will be used to define the non-dimensional form of equation (4.1). The dimensional analysis of equation (4.1) yields

$$F/(\rho g A D^2) = f(A/L, d/L, D/L, \theta, Re) \tag{4.2}$$

where A/L is half the wave steepness and d/L is the wave-depth parameter. These two independent dimensionless parameters are sufficient to define the incident waves. Re is a characteristic Reynolds number

48

$$\left(= \frac{u_0 D}{\nu} = \frac{2\pi AD}{T\nu} \right)$$ which accounts for the consequences of fluid viscosity.

D/L is the diffraction parameter and is used to indicate the importance of wave diffraction or scattering in the problem. When D/L is sufficiently large (say D/L > 0.2), wave diffraction or scattering is significant, see Fig. 3.2; when this is so and also A/D is small, the effect of drag force and the influence of the Reynolds number may be omitted from equation (4.2). When D/L is small, on the other hand, the flow separation may dominate the loading behaviour, while the incident wave field may remain relatively unaffected. This situation implies that the effect of wave diffraction no longer need to be taken into account. Instead of the diffraction parameter, D/L, the Keulegan-Carpenter number (= $u_0 T/D$, or = $2\pi A/D$) may be used to indicate the relative importance of the drag and inertia forces, where u_0 is the velocity amplitude of water particle.

For body motion in waves without any external constraints, the body mass must be added to the nine physical parameters upon which the wave force depends. Thus the non-dimensional form of the body motion in one direction, for example in heave motion, is expressed as

$$z/A = f\left(A/L, d/L, D/L, \theta, Re, m/\rho D^3 \right). \tag{4.3}$$

Since $m = \rho \forall$ holds for freely floating bodies, the added parameter, $m/\rho D^3$, is equal to $\forall/D^3$. For a given body shape, this parameter is independent of the length scale. Thus, it can be omitted from equation (4.3). The discussion of equation (4.2) applies to this problem as well, although there are some important exceptions for viscous forces that may significantly affect the motion of structures, even in cases where the diffraction parameter D/L is large. Examples are: 1) roll motion of bodies with a sharp corner cross-section, as discussed in Section 3.7; 2) surge motion of flat plates or streamlined bodies, for which types of bodies the inertial forces are often small compared to the frictional forces due to viscous shear; and 3) body motion near the resonant region, in which case even small viscous damping may have a marked effect on the amplitude of response. It should be pointed out, however, that it is usually impossible to have complete dynamic similarity, that is to ensure constancy of both a Froude and a Reynolds number. If the effect of viscosity has to be taken into account, further assumptions or hypotheses may be necessary. Moreover, the model test results may not predict exact prototype values in amplitude of motion

49

if the viscous damping in roll motion is neglected; fortunately the viscous damping often has little effect on the natural frequency.

For this study, the values of D/L are in the region where the diffraction is important. The wave steepness, A/L, and the parameter, A/D, are considered to be small. With these assumptions, the linearizing approximation has been made such that the wave force varies linearly with wave amplitude; then the parameter A/L can be omitted from equations (4.2) and (4.3). For the linear diffraction problem, equation (4.3) reduces to

$$z/A = f(d/L, D/L, \theta). \qquad (4.4)$$

In practice, it is not difficult to obtain the same identities of the parameters d/L, D/L, and θ in the model test as those in the prototype. The constancy of d/L and D/L entails the equality of the ratios

$$L_m/L_p = d_m/d_p = D_m/D_p = C_L .$$

In contrast to large floating objects, mooring cables are usually considered to be long slender members of small D/L values. As already mentioned, when D/L is small the viscous effect on the cable dynamics cannot be omitted and, consequently, the requirement of having the same Reynolds number in two dynamically similar systems must be met. If, in addition, the elasticity of a cable is taken into consideration, the dynamics of the cable will be influenced by its elastic stiffness. Hence, the dynamic similarity is ensured when the elasticity of the cable is properly modelled together with other independent parameters. Ideally, all of the independent parameters should be held constant between the model and the prototype, but in practice this may not be possible. Therefore, special techniques are often needed to overcome the difficulties.

In finding the non-dimensional parameters for the dynamic similarity of the mooring cables, a method involving the governing equations was used. This approach has been developed by M.L. Collier (1972); J. Lindahl (1985) has applied this method in his experimental studies. Both of them have demonstrated that model scaling is possible for an elastic cable. For a detailed description of the dimensional analysis, refer to their papers. In this thesis, only their results are given. From the dimensional analysis, it is indicated that the following relationships must be satisfied:

50

$$s_m / s_p = C_L, \qquad \text{a)}$$

$$T_m / T_p = C_L^{1/2}, \qquad \text{b)}$$

$$K_m / K_p = \varphi C_L \vartheta^2, \qquad \text{c)}$$

$$(C_M)_m / (C_M)_p = \varphi, \qquad \text{d)} \qquad (4.5)$$

$$(C_{DN})_m / (C_{DN})_p = \vartheta \varphi / C_L \qquad \text{e)}$$

$$(C_{DT})_m / (C_{DT})_p = \vartheta \varphi / C_L, \qquad \text{f)}$$

$$(T_F)_m / (T_F)_p = \varphi C_L \vartheta^2, \text{ and} \qquad \text{g)}$$

$$(Re)_m / (Re)_p = \vartheta C_L^{1/2} ; \qquad \text{h)}$$

with the assumptions that $\nu_m = \nu_p$ and $(\rho_c)_m = (\rho_c)_p$, same cable material is used, and the definitions $\varphi = (C_V)_m / (C_V)_p$ and $\vartheta = (D_c)_m / (D_c)_p$; where s denotes the total unstretched length of cable; T, the period; K, the cable stiffness; C_M, the added mass coefficient; C_{DN} and C_{DT}, the normal and tangential drag coefficients; T_F, cable tension; C_V, volume coefficient $(= \dfrac{cross-section\ area}{\pi D_c^2 / 4})$; and D_c, characteristic diameter of the cable.

In this approach a distorted scaling (a length scale different from the diameter scale, $C_L \neq \vartheta$) has been introduced to achieve dynamic similarity in a way that is possible to carry out. Since the distorted diameter scale has been used, the Reynolds number is no longer the same in the two similar systems (model and prototype). Additional similarity relations given in equations 4.5 e) and h) must be satisfied. The scale factor, C_L, is chosen on the basis of the length of the cable, and ϑ is determined from equations 4.5 e) and h) such that $(C_{DN})_m$ and $(Re)_m$ are points on the drag vs Reynolds number curve for the model cable chosen. The determination of ϑ is based on the normal drag similarity. It should be noted that the similarity in tangential drag may not be satisfied even if equation 4.5 f) is satisfied. This is due to cable roughness which may have different effects on the tangential drag in the model and the prototype. In model tests, the Reynolds number may be low enough that the tangential drag coefficient is independent of roughness, but this may be not true for the prototype. For mooring cables having large transverse oscillation, the lack of similarity in the tangential force does not have any significant effect on the cable tension or amplitude of motion.

In practice, it is difficult to satisfy the requirement that $K_m/K_p = \varphi C_L \vartheta^2$ (equivalent to $E_m/E_p = C_L$), because it is impossible to find a material which can match the required (very small) value of Young's modulus, E, in model scale. To overcome this difficulty, a spring of appropriate stiffness is inserted in series with the cable at its lower end. This technique has been used by various researchers in the modelling of elastic members.

When a cable is attached to a floating body oscillating in waves with zero forward speed, the upper end of the cable follows the body with a velocity that is proportional to the amplitude times the frequency of the body's motion, $U \propto a\omega$. Hence, the similarity of the Strouhal number based on the amplitude of the cable motion at the upper end is satisfied when $a_m/a_p = C_L$, since $\omega_m/\omega_p = C_L^{-\frac{1}{2}}$ and $U_m/U_p = C_L^{\frac{1}{2}}$.

The models tested were based on concrete barge-type floating breakwaters. Such breakwaters are produced by a company, SF Marina System AB, in Sweden. For their TYPE300 breakwaters, the principal dimensions in full scale are: length, 20 m; breadth, 3 m; draft ≈1.2 m; and weight ≈38 tonnes. Each floating breakwater unit is moored by 3 to 4 chains with the following characteristics:

Total unstretch length, l	= 30 m, about 3 × water depth,
Chain diameter, D_c	= 23 mm,
Mass per unit unstretched length	= 12 kg/m,
Density	= 7800 kg/m^3 , and
Water depth	= 10 m.

The models were constructed to a scale of 1/10 (= C_L). The principal parameters in the model scale were obtained according to the theories described above. In spite of the fact that only standard sizes of chain are available, the chains used are actually quite similar to those computed. The difference in full-scale is also small. The parameters in both full-scale and scaled-down are given in Table 4.2. For Table 4.2 c) and d), $\vartheta = 0.1296$, and $\varphi = \dfrac{M_m}{M_p}\dfrac{1}{\vartheta^2} = 0.7714$.

Table 4.2 a) Wave characteristics for regular waves in prototype and model

Period (sec)		Wave Length (m)		Wave Steepness	Wave Height (cm)	
T_m	T_p	L_m	L_p	H/L	H_m	H_p
0.6	1.90	0.562	5.62	0.02	1.12	11.2
				0.03	1.69	16.9
				0.04	2.25	22.5
0.7	2.21	0.764	7.64	0.02	1.53	15.3
				0.03	2.29	22.9
				0.04	3.06	30.6
0.8	2.53	0.998	9.98	0.02	2.00	20.0
				0.03	3.00	30.0
				0.04	4.00	40.0
0.9	2.85	1.264	12.64	0.02	2.53	25.3
				0.03	3.79	37.9
				0.04	5.06	50.6
1.0	3.16	1.559	15.59	0.02	3.12	31.2
				0.03	4.68	46.8
				0.04	6.23	62.3

b) Water depths and principal parameters of the floating bodies in prototype and model

Water depth $h_m = C_L h_p$		Length of body $l_m = C_L l_p$		Breadth of body $b_m = C_L b_p$		Draft of body $T_{dm} = C_L T_{dp}$	
h_m (m)	h_p (m)	l_m (m)	l_p (m)	b_m (m)	b_p (m)	T_{dm} (m)	T_{dp} (m)
1.0	10.0	2.0	20.0	0.3	3.0	0.119	1.19

c) Parameters of mooring cables in prototype and model

Length of cable $s_m = C_L\, s_p$		Diameter of cable $(D_c)_m = \vartheta\,(D_c)_p$		Mass / length $M_m = \varphi\vartheta^2\, M_p$	
s_m (m)	s_p (m)	$(D_c)_m$ (mm)	$(D_c)_p$ (mm)	M_m (kg/m)	M_p (kg/m)
2.965	29.65	3.5	27	0.215	16.586

d) Stiffness of cables and couplings in prototype and model

Stiffness of cable $(K_c)_m = \varphi\vartheta^2 C_L (K_c)_p$		Stiffness of coupling $K_m = C_L{}^2\, K_p$	
$(K_c)_m$ (kN)	$(K_c)_p$ (kN)	K_m (kN)	K_p (kN)
regarded as rigid	regarded as rigid	rigid (except for restriction in pitch)	rigid (except for restriction in pitch)

4.2 Experimental Arrangement and Measurements

Testing Facility

The experiments were performed in a 3-D wave basin which is 11.5m by 19.4m and has water depths up to 1.2m. Two synchronised wave generators at one end of the basin were used to provide regular waves. Each generator consists of a plane blade and a piston so that the wave amplitude and period can be varied by adjusting an input signal given to the pistons. A sloping beach covered with small crushed stone was located at the opposite end of the basin to reduce the wave reflections. For the removal of undesired cross waves in the basin, i.e. waves perpendicular to

the main wave propagation direction, absorbers were placed at the side walls of the basin.

Before the models were placed in the basin, the waves of interest were carefully calibrated and the surface elevation time series were measured in the area where the model should be during the execution of the tests.

Models and instruments

The breakwater units used in the model tests were constructed from PVC with rectangular section and symmetrically loaded with steel plates. Each of the units is of the same size, as illustrated in Figure 4.1. This figure also shows the main dimensions of the units which are determined according to the dimensional analysis given in the previous section, refer to Table 4.2. The mechanical quantities of the scaled cables are also given in the same table.
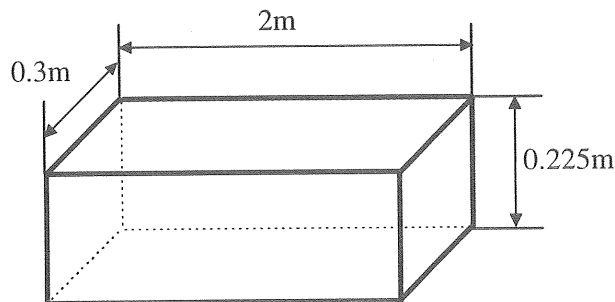
Fig. 4.1   Dimensions of the floating units used in the model tests.

Model motions in 6 degrees of freedom were measured by the MacReflex system, which was provided by the company Qualisys AB. The system is a newly developed position and motion analysis system. It consists mainly of three parts: a specially developed precision CCD camera, a video processor and MacReflex software used in a Macintosh environment. Video monitors are optional, however they can make it possible to obtain better experimental conditions during the system set up. For 3-D measurements, at least one extra camera and video processor are required.

The camera has an internal LED flash for infrared illumination of a measured object and its attached markers which are made with retro-reflective tape. The camera has an exposure time of only 800 microseconds; it samples all the markers at the same time with a frequency of 50 Hz. When the short-flash light-pulses illuminate the markers, they become the brightest shining objects in the field of view. The camera automatically reduces its sensitivity so that only the markers are visible in the video image. The video processor is used to detect the markers in a picture and to calculate the centre point of each marker in video (real time) speed. The MacReflex software is used for two purposes: 1) to collect data from the video processor; and 2) to sort and track the sampled data, since the video processor cannot distinguish one marker from another. Data exported from MacReflex in a readable form can be further processed by other analysis programs, such as a WingZ based application program.

The line tensions and the surface wave elevations were measured by ring-shaped force transducers and conductive wave probes, respectively. All of the data from the sensors were collected by the data acquisition system MP100 which was provided by BIOPAC Systems, Inc. This system consists of a collection unit and system manager software which works with the AcqKnowledge waveform analysis program. The data collected can be saved in the format of the application program or in the text format. The MP100 system can take samples at different rates. However, in these experimental studies 50 samples per second was selected since it was being used with the MacReflex system.

An MRMP-1 synchronization unit was also used in order to synchronize the MacReflex system with the MP 100 system. The data from MacReflex and from all of the channels in the MP100 were therefore sampled at the same time.

Measurement setup

The photograph shown in Fig. 4.2 illustrates the arrangement of the experiments for oblique waves. Arrangement of breakwater modules, mooring chains and measurement points are illustrated in Figure 4.3. Two units (modules) were connected with two revolute joints, see Figure 4.4. Three reflective markers (at least three markers for 3-D measurements) were attached to each of the units at selected positions. Of the eight mooring chains, chains from m3 to m6 were hung at an angle of about 45 degrees from the vertical symmetry plane in the longitudinal direction, while the others were in the planes parallel to their transverse symmetry

planes. The force transducers were placed at the connection between the model and the chain, for example on mooring lines m1, m2 and m4. Since the model and the mooring arrangement were transversely symmetric, only the lines at one side of the system were measured when the system was exposed to beam sea (180° waves). Six wave probes, A2 to A7, were placed 0.5 m in front of and 0.5 m behind the model, three at each side, and the distance between them was about 1 m.
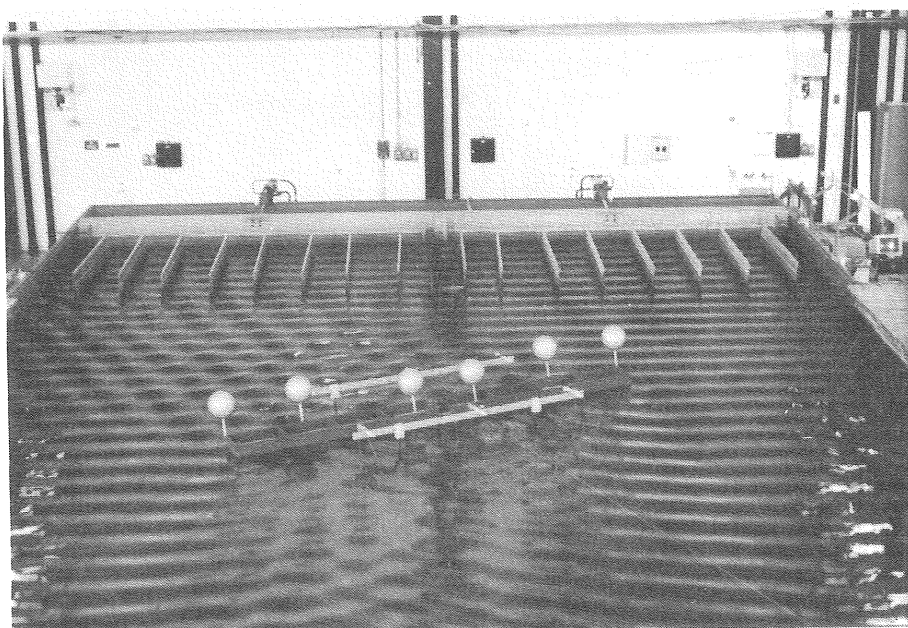
Fig. 4.2   Photograph of the experimental arrangement.

For free floating models, only the motions were measured. Wave probe A1 located about 5 m from the model, was intended to be used to control the incoming waves during each test. All models were placed about 7 m from the wave generator.

57
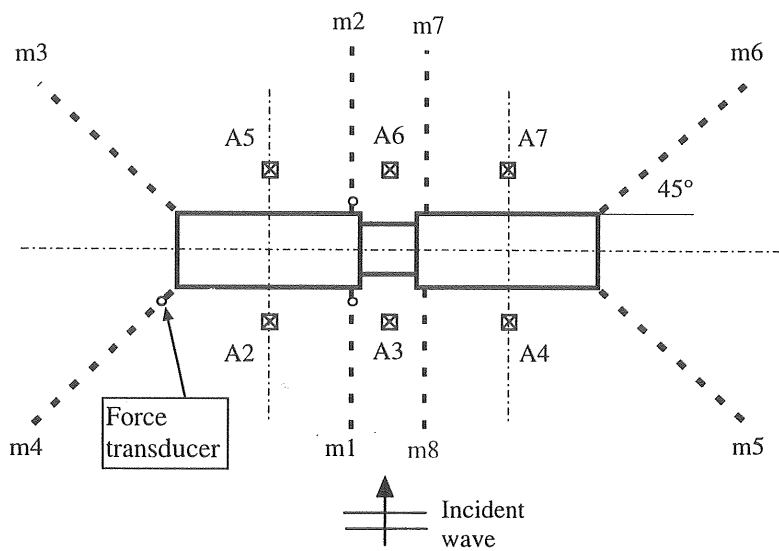
Fig. 4.3   Arrangement of breakwater modules, mooring chains and
measurement points.
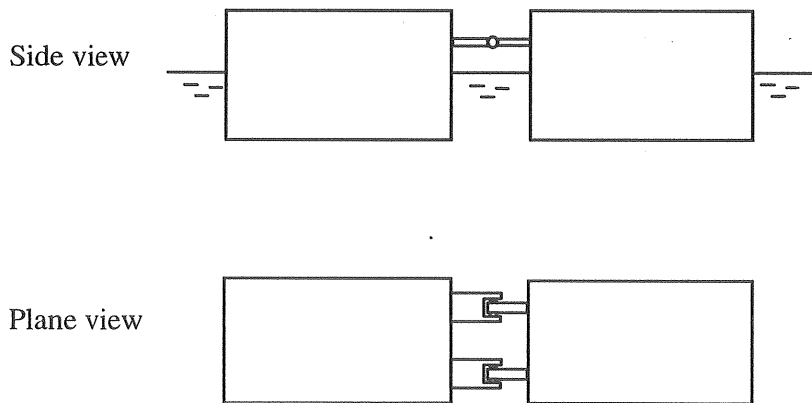
Fig. 4.4   Connecting arrangement of revolute joints

58

Figure 4.5 illustrates the connection of the hardware of the recording systems MacReflex and MP100, and Figure 4.6 shows a typical measurement setup for MacReflex. A maximum of 10 analog channels in MP100 were used for data acquisition. The sampling time for each test was determined to be 20 sec., which should be less than the time required for the reflected wave to travel from the model to the wave generator and back again.
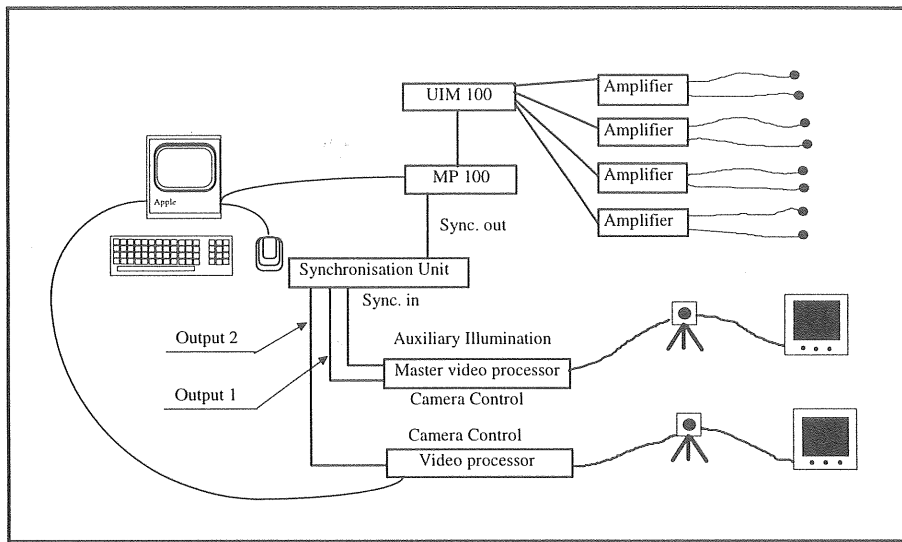
Fig. 4.5   Arrangement of measuring equipment

Measurements

Before a series of tests was conducted, the measurement accuracy of the MacReflex system was checked by testing a marker position while the model was floating at rest. Figure 4.7 shows the registration of the marker position. The marker movement as registered was less than 2 mm in the x direction and less than 1.5 mm in the y and z directions.

a) Free decay tests

The free decay tests were performed in all six modes of motion for a single moored body. The natural periods for these modes, evaluated from the tests. It can be seen that the natural periods of the motion in the horizontal

plane, i.e. sway, surge and yaw, are clearly larger than those in the vertical plane, i.e. heave, pitch and roll; they are in the range of 5 - 10.5 sec. The natural periods of 0.98 and 1.03 sec. in heave and roll motions are near the tested wave periods given in Table 4.2 a).
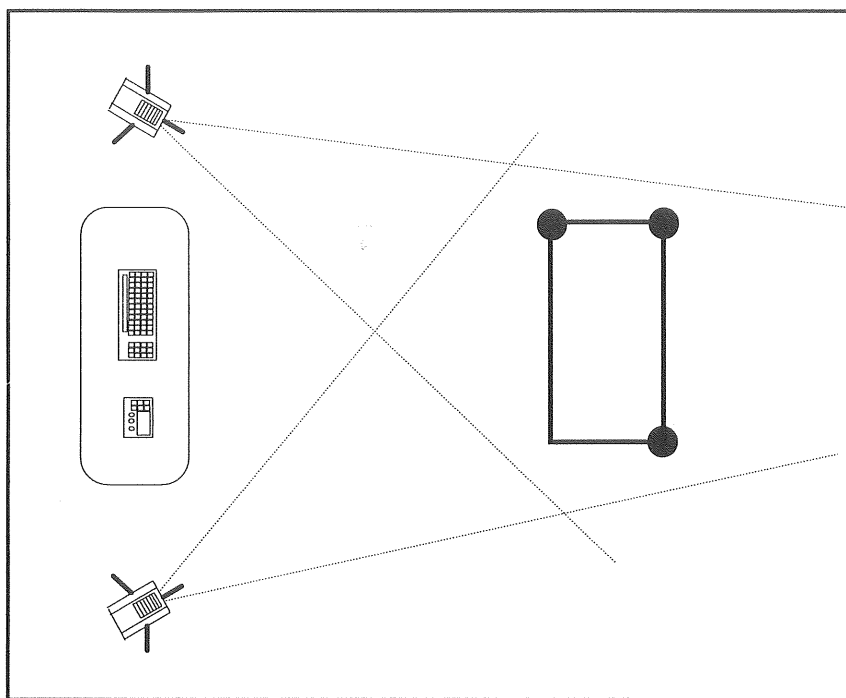
Fig. 4.6   A typical measurement setup for MacReflex

b) Wave tests

Four models were used in wave tests. For model I, the motions of the model were measured; for model II, III and IV, the motions of the model, mooring line tensions, and waves near the model were measured. For each model, experiments were carried out at five different wave periods; there were three variations of wave steepnesses for each wave period. These experimental wave conditions are given in Table 4.2 a).

60
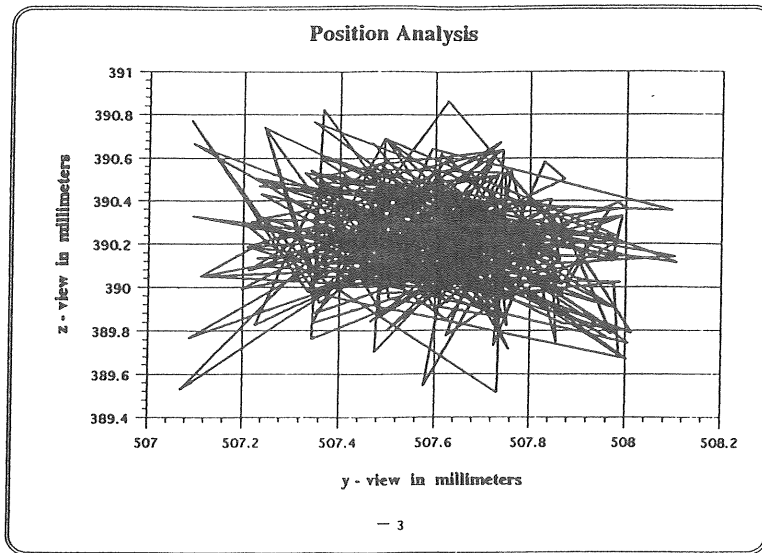
Fig. 4.7   Diagram showing a typical registration of a marker (No. 3) while Model I was floating at rest.

5 COMPARISONS AND DISCUSSION

5.1 Analysis of Sampled Data

The Data acquired from the MacReflex and MP100 systems is in the form of time series. Since the MacReflex and its supporting analysis program, WingZ for MacReflex, provided motion data only for markers, further computation of the bodies' motion in the six degrees of freedom was needed. Six markers (three for each unit) were measured and the results were used to determine the body motion. Figures 5.1.a) and b) present an example of the resulting motions. Effects due to the non-linear drift force are clearly seen in the sway, surge and yaw motions. The curves in these figures present the total motion comprising first-order wave-induced motion and slow-drift motion. Since only regular waves were modelled, the amplitude of the slow-drift motion decreased with time, due to damping. The body then continued its wave-frequency motion around the mean drift position. Examples of the recorded wave elevation in front of and behind the measured bodies are presented in Figures 5.1. c) and d). The low frequency motion was not observed to have any significant effect on the water waves. The variation in cable tension is illustrated in Figure 5.1.e). The slow-drift oscillation and wave-frequency motion appear again in the dynamic tension, due to the fact that the upper end of the cable follows the body to which it is attached.

For recorded time series, the frequency response characteristics can be analysed by means of Fast Fourier Transformation (FFT). As an illustration, Figure 5.2 shows a transformation of the sway motion given in Figure 5.1.a). Magnitudes in this figure indicate that the slow-drift motion can be very much greater than the high frequency motion. Even when the impulse load is small, large oscillation may occur in a resonant system. For a moored slender body system, natural frequencies associated with the motions in the horizontal plane (sway, surge and yaw) are normally lower than those in the vertical plane (heave, pitch and roll), see Table 4.3. This may also be the reason why the modes with high natural frequencies show hardly any low frequency effect. In addition, the effect of damping is very important.
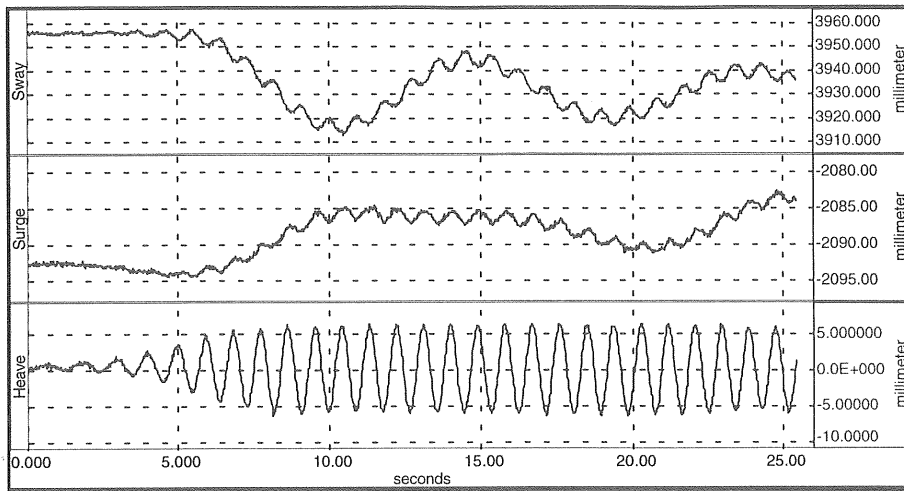
Fig 5.1 a) Measured sway, surge and heave motion of Body I in
Model IV, T = 0.9 sec. and H/L = 0.03.
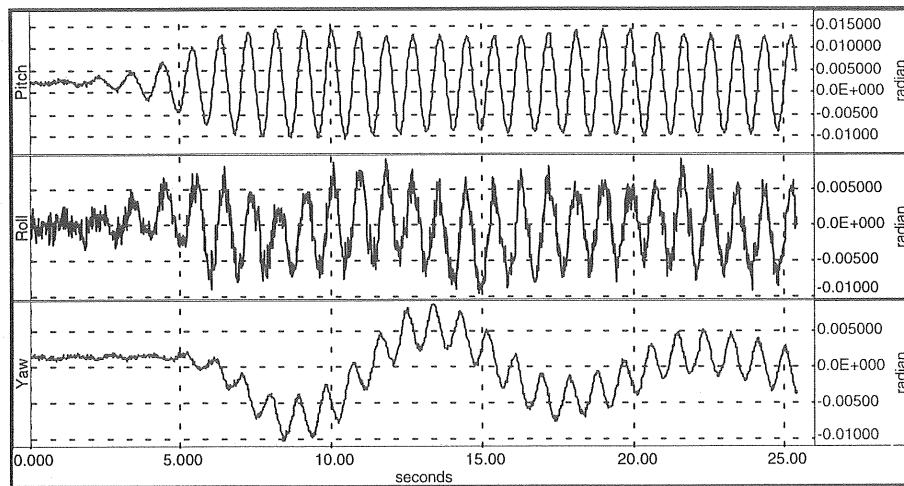
Fig. 5.1 b) Measured pitch, roll and yaw motion of Body I in Model IV.
T = 0.9 sec. and H/L = 0.03.
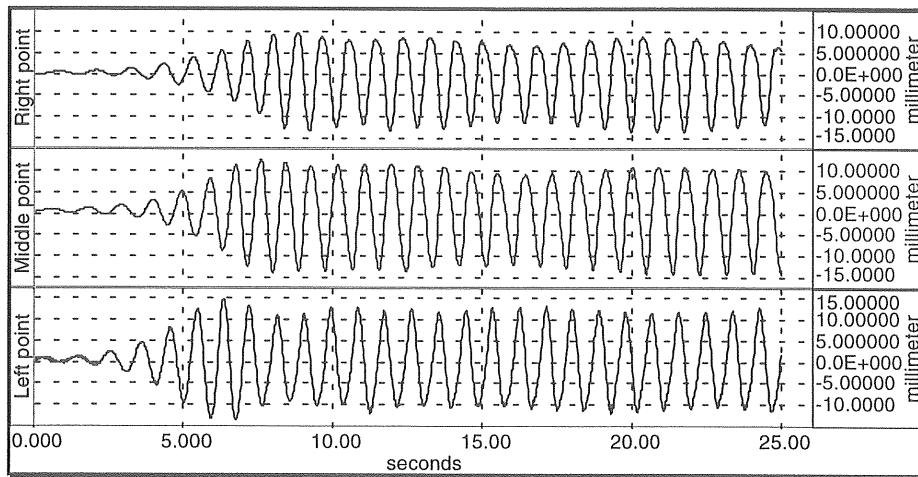
Fig. 5.1 c)   Measured windward wave elevation in Model IV,
              T = 0.9 sec. and H/L = 0.03.
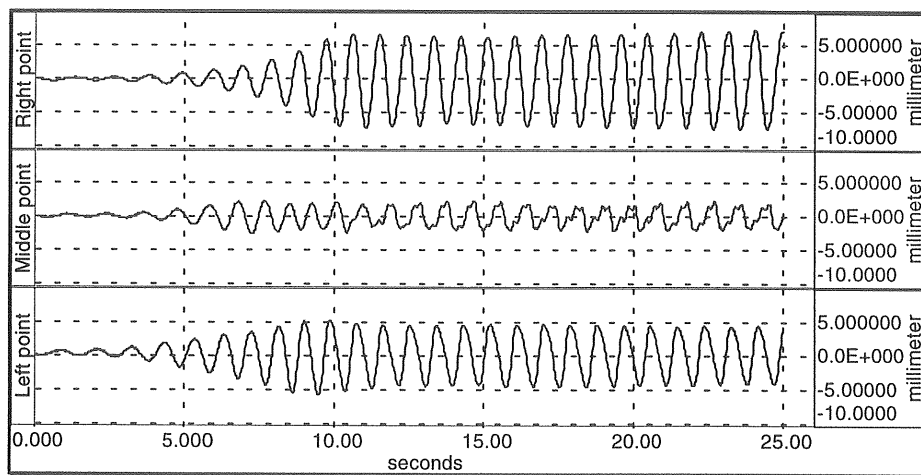
Fig. 5.1 d)   Measured leeward wave elevation in Model IV,
              T = 0.9 sec. and H/L = 0.03.

64
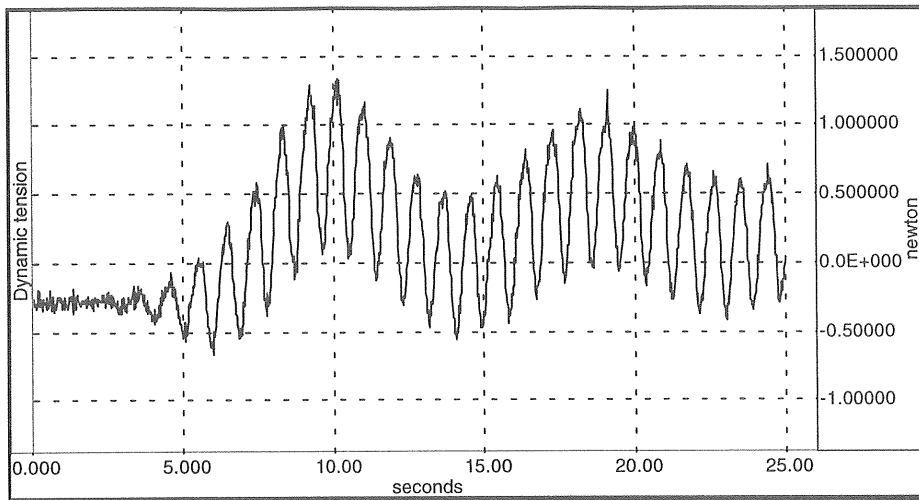
Fig. 5.1 e)   Dynamic tension at the upper end of Cable 4 in Model IV,
T = 0.9 sec. and H/L = 0.03.
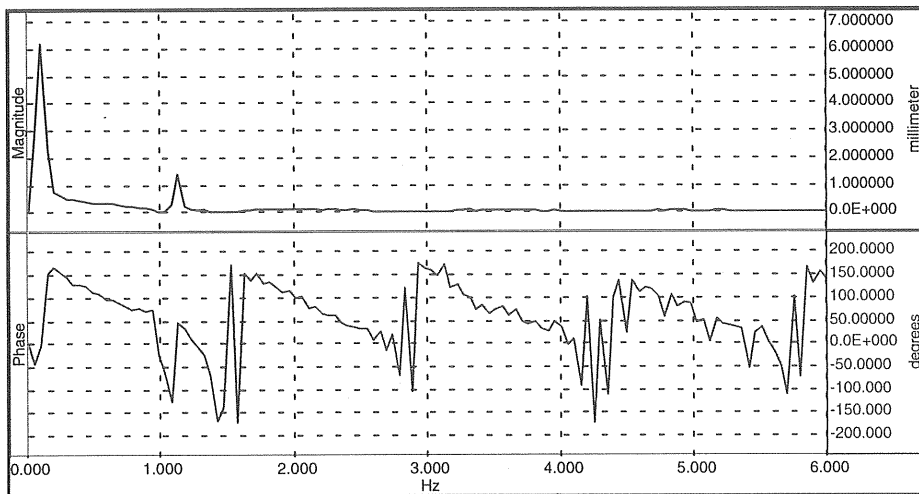
Fig. 5.2   Amplitude spectrum and phase for sway motion in Figure 5.1.a).

The present study is focused on the first order responses of the considered problem. Therefore, amplitudes with frequencies corresponding to the incident wave frequency will be decomposed from the other components and used in comparisons with results obtained from numerical computations.

65

5.2 Numerical Computations

All of the experimental models and the wave conditions given in Table 4.2 a) were studied theoretically. According to the mathematical modelling and the scheme described in Paper A, the wave loads on each of the bodies were initially calculated for each of the wave frequencies. Computational experience shows that the computation of the horizontal wave loads requires a fine discretization of the body surfaces. This may be due to the fact that the bodies have relatively small draft, the wetted body surfaces are close to the free surface where most of the wave energy is found; and may also be due to the large velocity gradients around the sharp corners of the bodies. The number of panels required for discretization depends on the wavelength. Although increasing the number of the panels usually produces better results, this is time consuming, specially when using a PC computer. One way to refine the discretization is to use a cosine distribution of the panel size in the horizontal directions. Figure 5.3 shows a mesh of cosine distribution, with more panels around the sharp corners and fewer close to the middle. This technique can efficiently reduce the number of panels without any practical loss of accuracy. I have made test runs with different numbers of panels, for example 440, 516, 548 and 620 panels, for each of the bodies. The cosine distribution was applied in most of the cases studied. The results show that the number of panels required to achieve acceptable accuracy is 548. It is noted that this number may be reduced by improving the distribution.
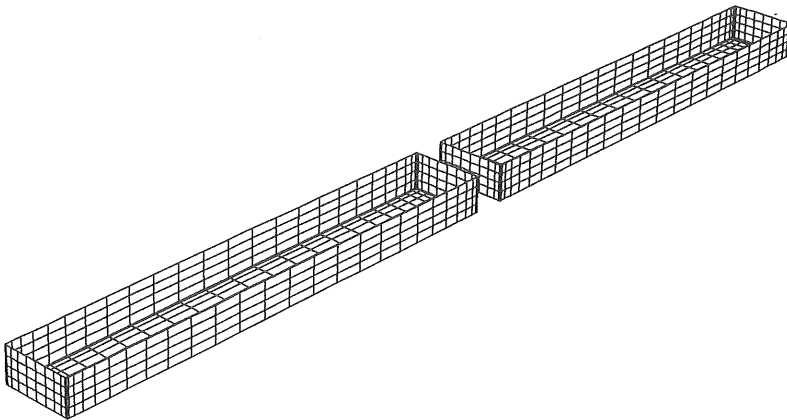
Fig. 5.3   Wetted body surfaces discretized with 2×548 panels

66

The validity of the solution of the hydrodynamic coefficients has been confirmed and reported in Papers A and B where comparisons are made with results provided by different authors. For the other solutions, such as motion response, wave elevation and line tension, the computations were performed following the approaches described in Section 3. In the computation of the line tensions and wave elevations at the positions near the moored breakwater, it is important to be aware of the effects of offset caused by the mean drift force. The breakwaters are assumed to undergo oscillations around their mean positions. In the present study, these mean positions were evaluated directly from the test results. In order to check the validity of the computations, numerous comparisons were made. Values resulting from the various simulations are presented below together with those from the measurements.

5.2.1 Results for high frequency (1st order) motions

The first example discussed here is a simulation of the response of the moored breakwater (Model II) to the beam waves, as given in Table 4.2 a). Since only beam waves are taken into consideration, the motion response of the breakwaters is limited to sway, heave and roll motions; also, Body I shows the same motions as Body II. Results of the motions for Body I are presented in Fig. 5.4. In view of quality control, results from numerical computation are generally compared with results from model tests before the analysis moves into detail. The translational responses shown in the plots are defined as the ratio of the amplitude of the breakwater motion over the amplitude of the incident waves, and the rotational responses are presented directly in the diagrams in radians.

Similar simulations were also made for oblique waves, i.e. waves coming from 165° (Model III), and waves from 150° (Model IV). In these cases, the comparisons were made separately for the two connected bodies, see Fig. 5.5 through Fig. 5.8. Motions in surge, pitch and yaw are also presented, since the limitation mentioned above is no longer valid.
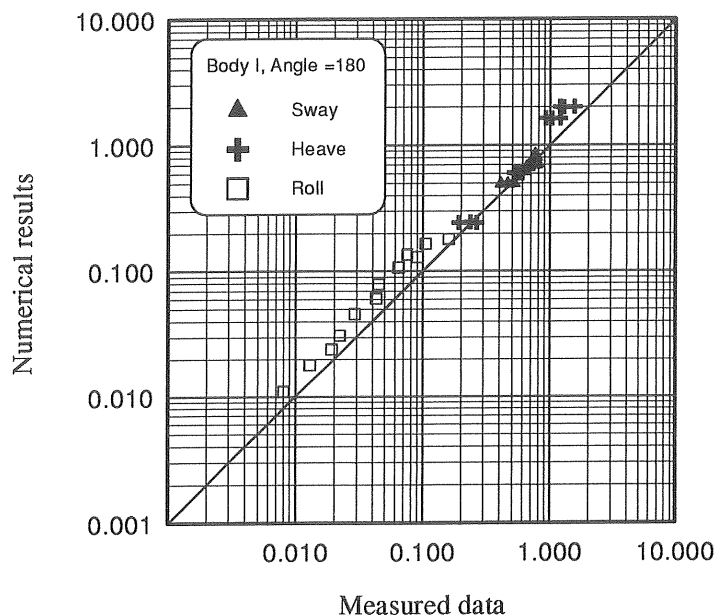
Fig. 5.4   A comparison of the computed and measured results
          for Body I in Model II
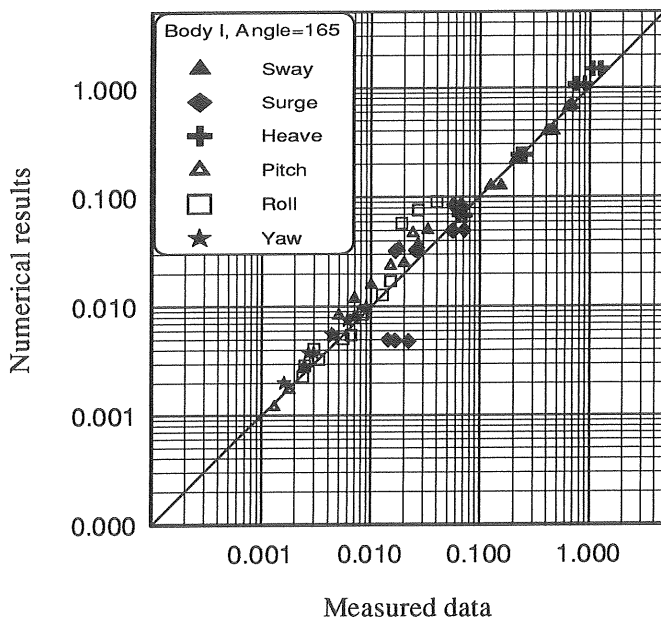
Fig. 5.5   A comparison of computed and measured results
          for Body I of Model III

68
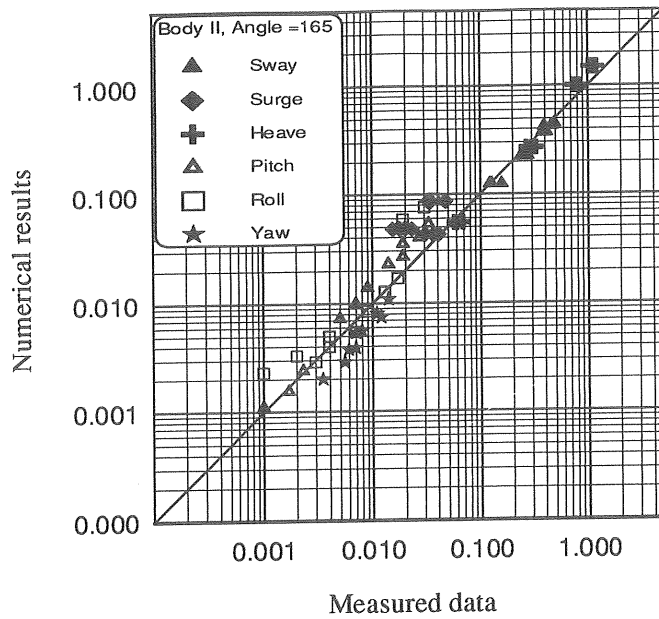
Fig. 5.6   A comparison of computed and measured results
            for Body II of Model III
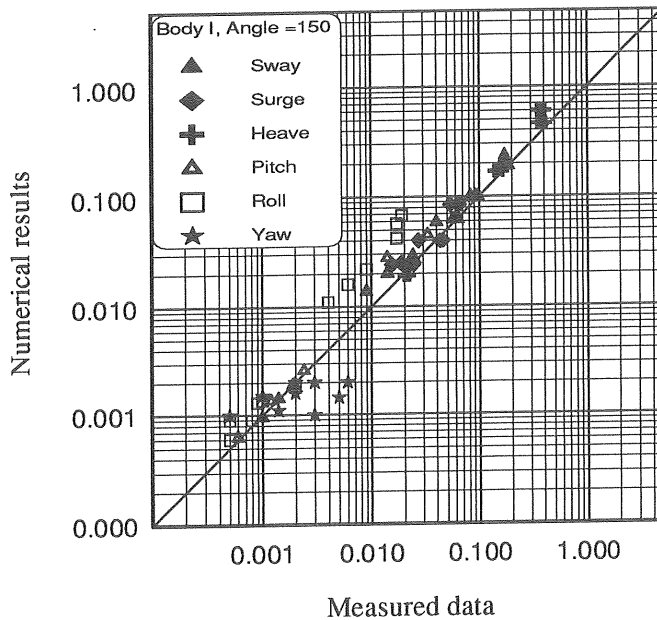
Fig. 5.7   A comparison of computed and measured results
            for Body I of Model IV

69
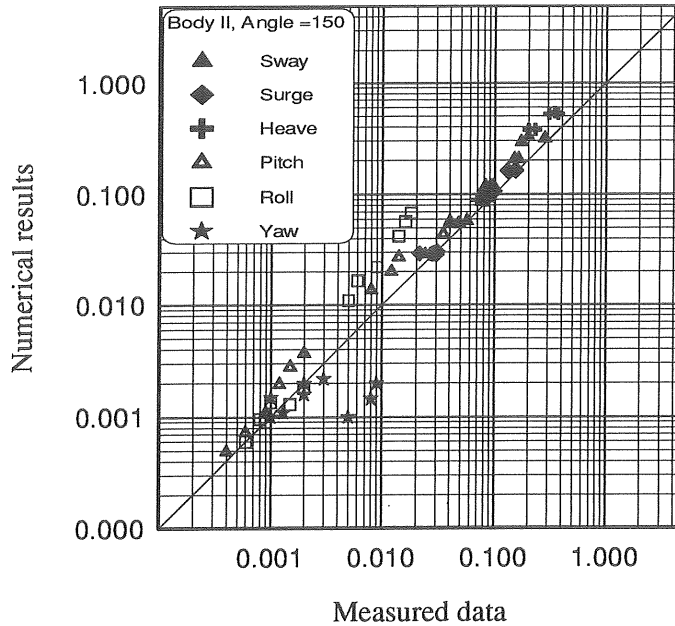
Fig. 5.8   A comparison of computed and measured results
for Body II of Model IV

As seen from the comparisons, the theoretical computations correspond
fairly well in general with the measurements. However, in some cases the
discrepancy is large. This is particularly noticable in the motions of very
small amplitude, such as the responses in surge, pitch, roll and yaw. The
major contributions to the scatter could be experimental error, especially for
the measurements of small motions, and the damping estimation. An
estimate of the accuracy of the measured motion is ±0.5 ~ 2.0 mm. For the
small motions, the amplitudes are approximately of the same order as this
variation. However, for practical reasons, our interest is focused on the large
motions. From the comparisons it can also be seen that, except for yaw
responses in oblique waves, the numerical solution generally overestimates
the motion response.

In determination of the motion response for Model II, we found that the
mooring system used in the model tests was so compliant that the 1st order
responses, except for the roll motion, were hardly affected by the mooring
system. This can be confirmed by comparing the measured responses of
Model I (free floating) and Model II (connected with mooring chains), see
Figures 5.9 and 5.11. Curves from numerical prediction are also shown in
these figures for direct comparison. Results for sway motion seem to show

70

very good agreement between computation and experiment. For heave and roll motions, as indicated in Figures 5.10 and 5.11, experimental points remain very well fitted to the theoretical curves, as long as the periods are outside the resonant region. For periods inside the resonant region, the fit is poorer. For the motions in these two modes, the essential contribution to the disagreement between the numerical results and the experiments could be an underestimation of the damping. In sway motion, the results from both methods show that the motion responses are almost linear to the incident waves, even for the case when H/L = 0.04, which is slightly in excess of the region of linear wave theory. The same behaviour can be observed in heave motion. However, in roll motion the theoretical results display a considerable difference in the region close to the resonant period, unlike the measured values in which the linear behaviour remains. This may indicate that the solution of roll damping, especially in the resonant region, needs to be improved.
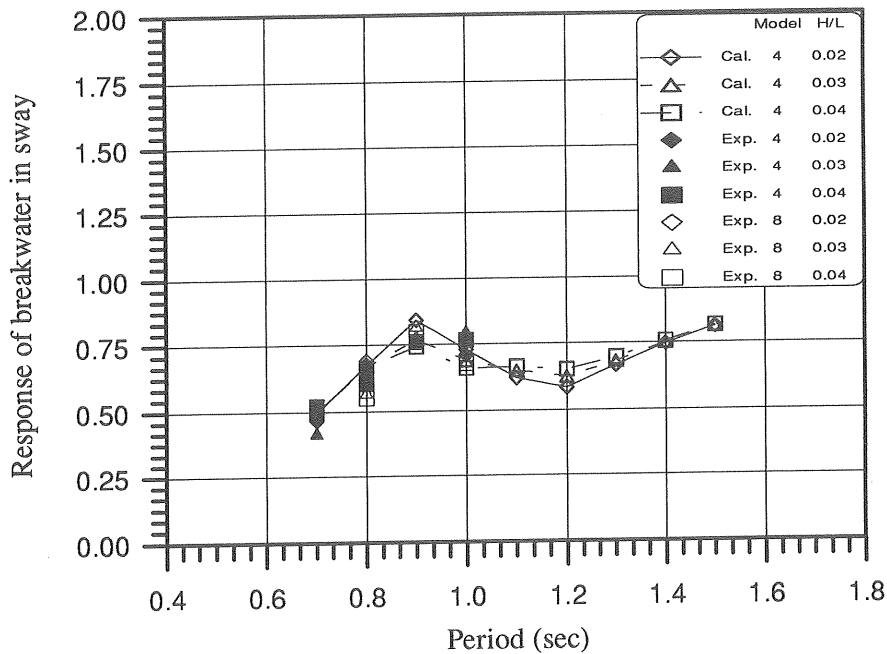
Fig. 5.9   Sway responses of Body I in Model I (free floating) and Model II (with 4 mooring chains).
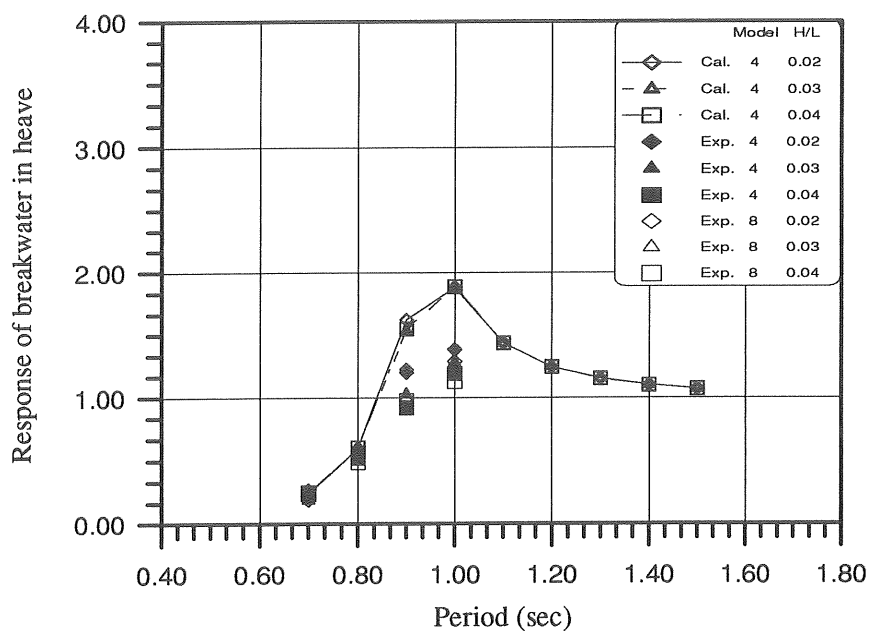
Fig. 5.10 Heave responses of Body I in Model I (free floating) and Model II (with 4 mooring chains).
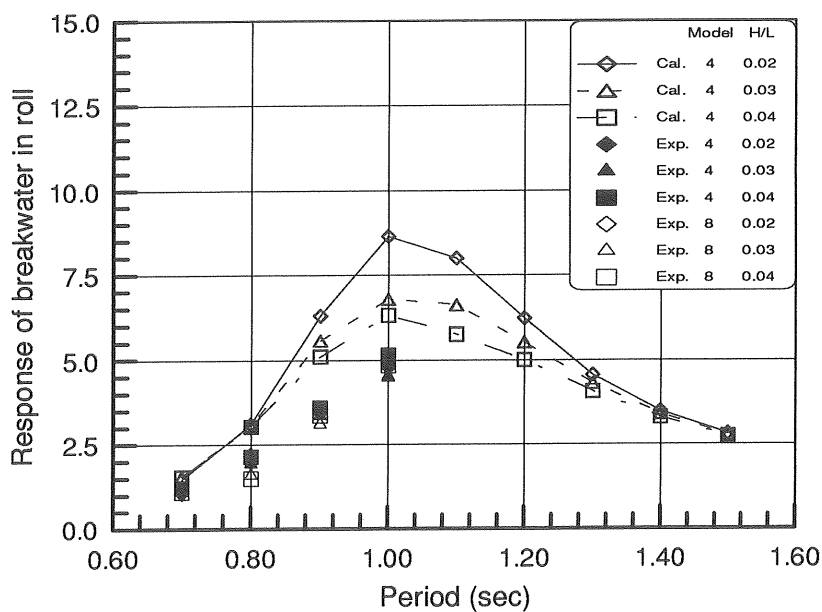
Fig. 5.11 Roll responses of Body I in Model I (free floating) and Model II (with 4 mooring chains).

72

In order to examine the effect of wave direction on motion response, similar plots are made including the results for Models III and IV. As expected, the roll amplitudes shown in Figures 5.14 and 5.17 reached a maximum in a beam sea, and decreased as the breakwaters were turned 165° and 150° from the main propagation direction of the waves, which indicates that a minimum would be reached in a head sea or in a following sea. For short waves this observation seem to be applicable to sway and heave, see Figures 5.12 and 5.13 for Body I, and Figures 5.15 and Fig. 5.16 for Body II. The motions in beam waves have been observed to be greater than the motions in oblique waves.

To examine the differences of motion between the connected bodies the figures 5.18 to 5.23 are presented for Models III and IV. In Figures 5.20 and 5.23, the property of infinite stiffness of the couplings in roll (relative rotation is allowed only in pitch) is demonstrated which indicates that the roll motions of Bodies I and II are the same. Approximately the same responses in heave motion are indicated as well. The difference found in sway motions, shown in Figures 5.18 and 5.21, could be caused by the fact that the global co-ordinate system used in the computation is located at the centre of the water plane of Body I (selected centre of Body I at rest) and the sway motion of Body II is related to a selected centre of its own. There is a difference between these two centres in the sway motions because the bodies are rigidly connected and have the yaw motion about the z axis through the selected centre of Body I. It may be that the yaw motion becomes more pronounced in long waves. Note that the sway motion of Body I in Model III is greater than that of Body II at T = 1.0 sec., while it becomes less in Model IV at the same period.

73
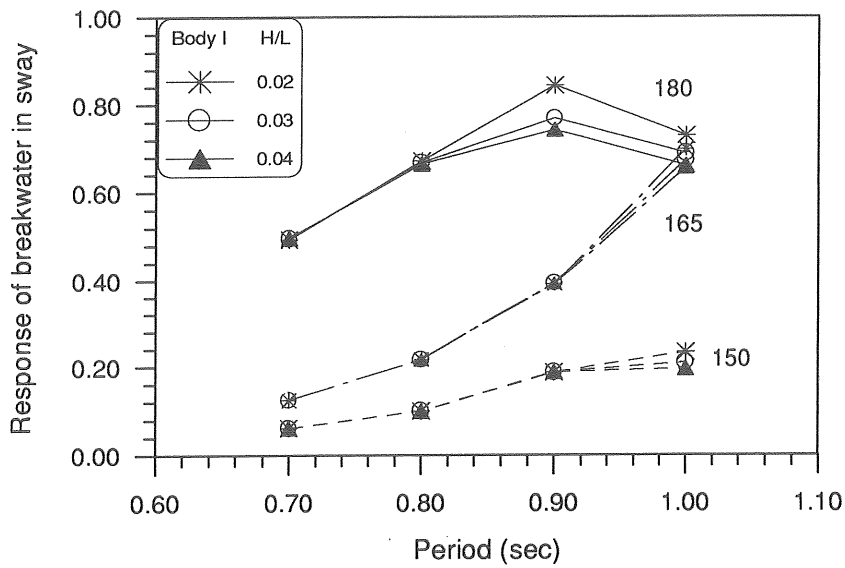
Fig. 5.12 Calculated sway response of Body I in waves from 180°, 165° and 150°.
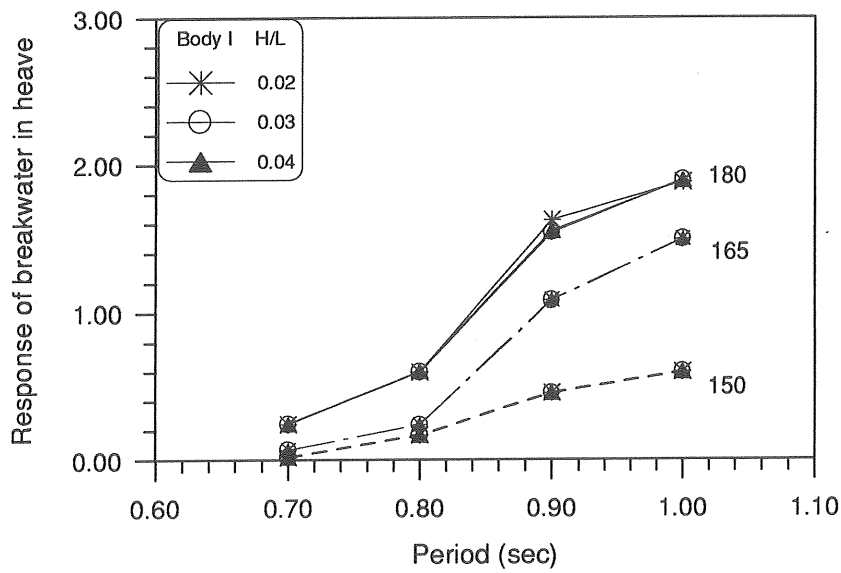
Fig. 5.13 Calculated heave response of Body I in waves from 180°, 165° and 150°.

74
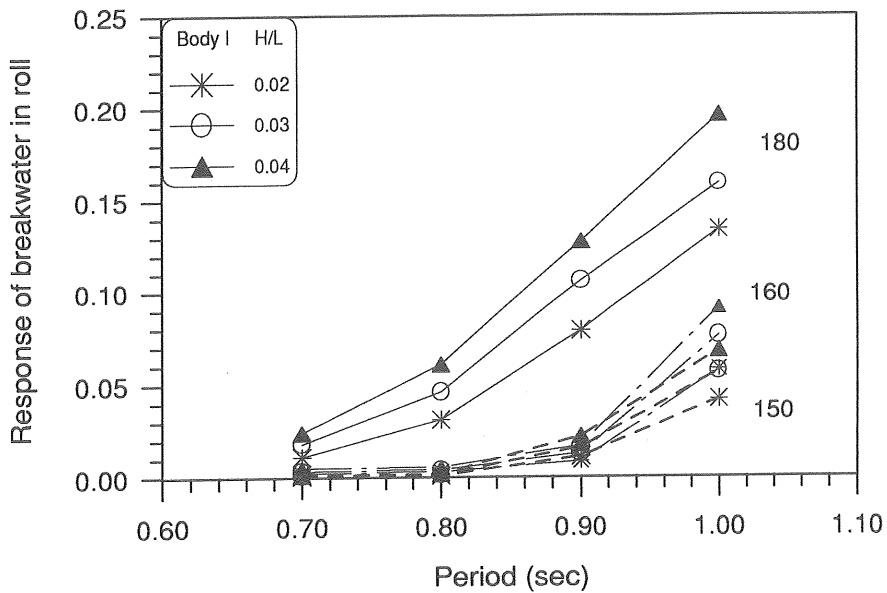
Fig. 5.14 Calculated roll response of Body I in waves from 180°, 165° and 150°.
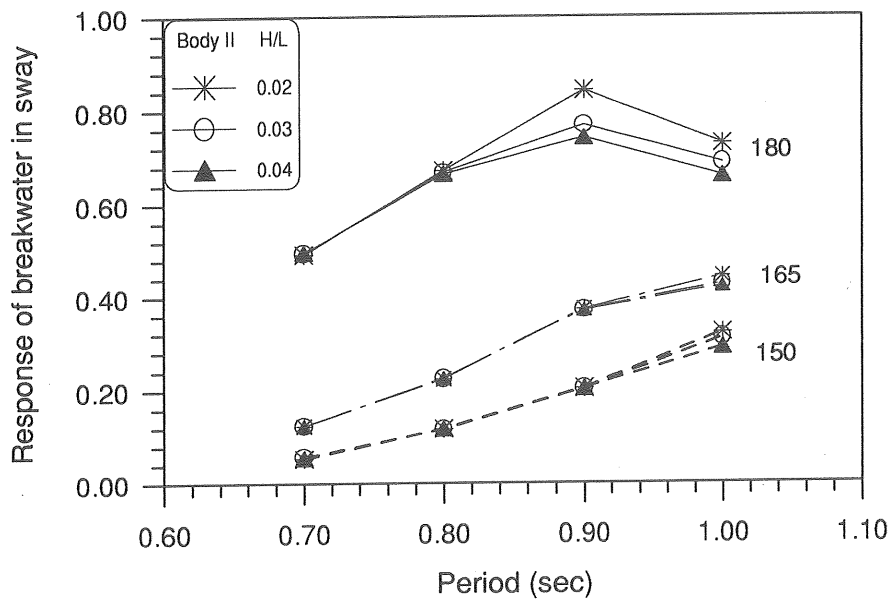
Fig. 5.15 Calculated sway response of Body II in waves from 180°, 165° and 150°.
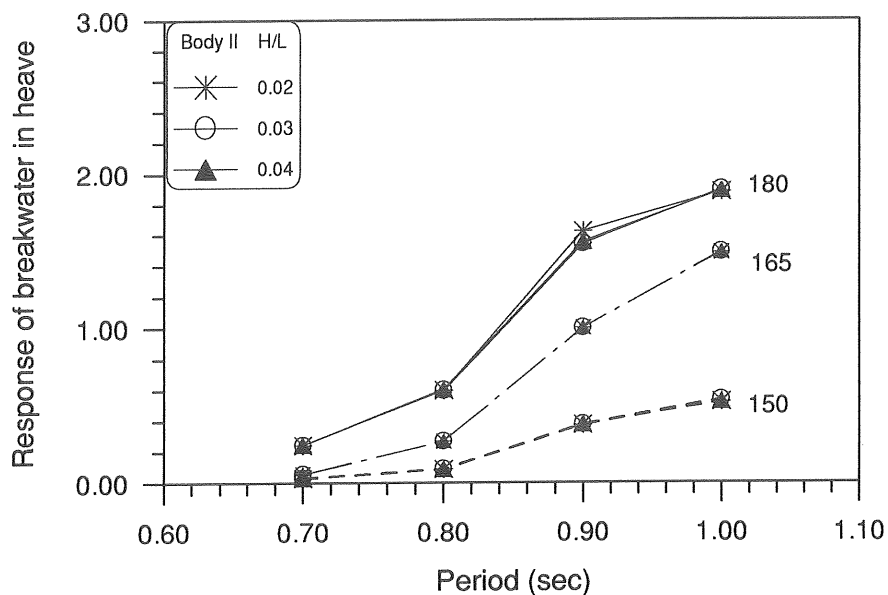
Fig. 5.16 Calculated heave response of Body II in waves from 180°, 165° and 150°.
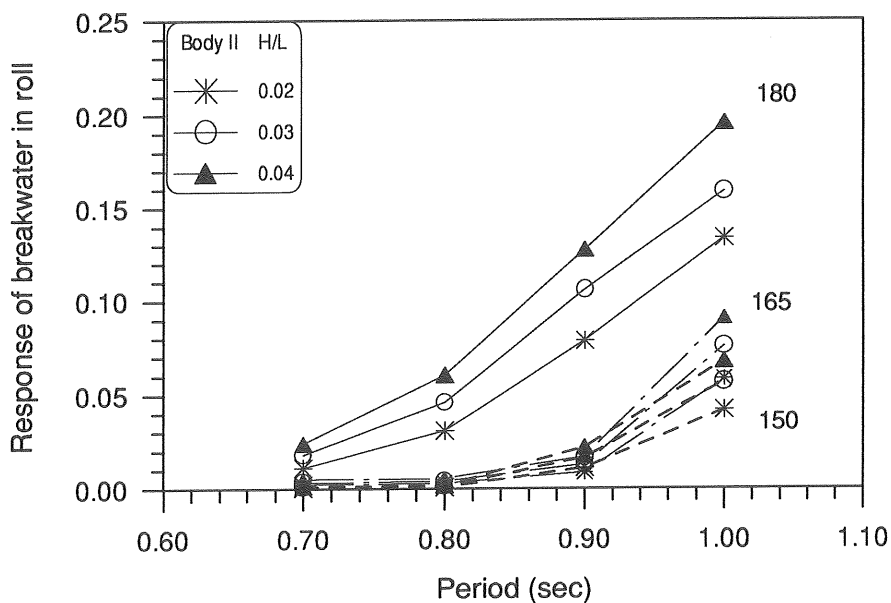
Fig. 5.17 Calculated roll response of Body II in waves from 180°, 165° and 150°.

76
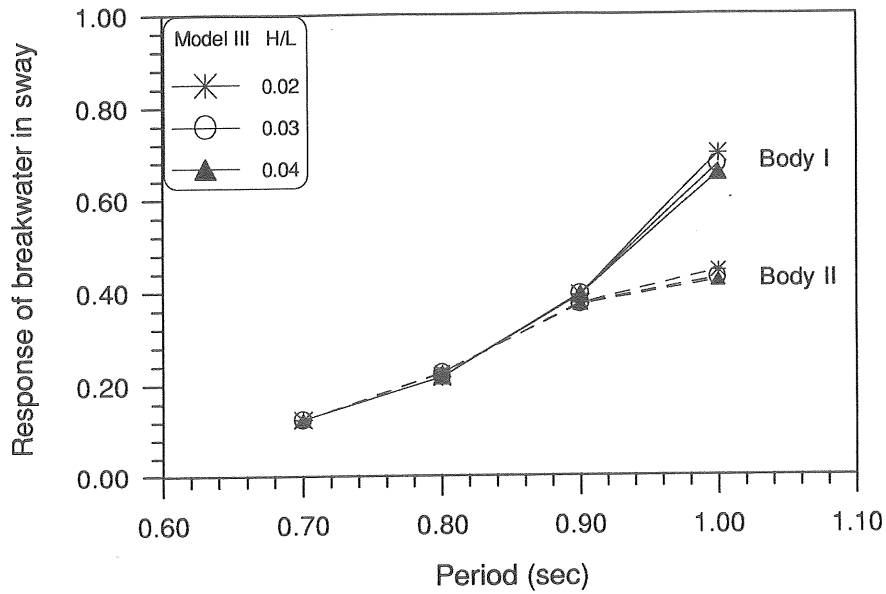
Fig. 5.18 Calculated sway response of Body I and Body II in Model III.
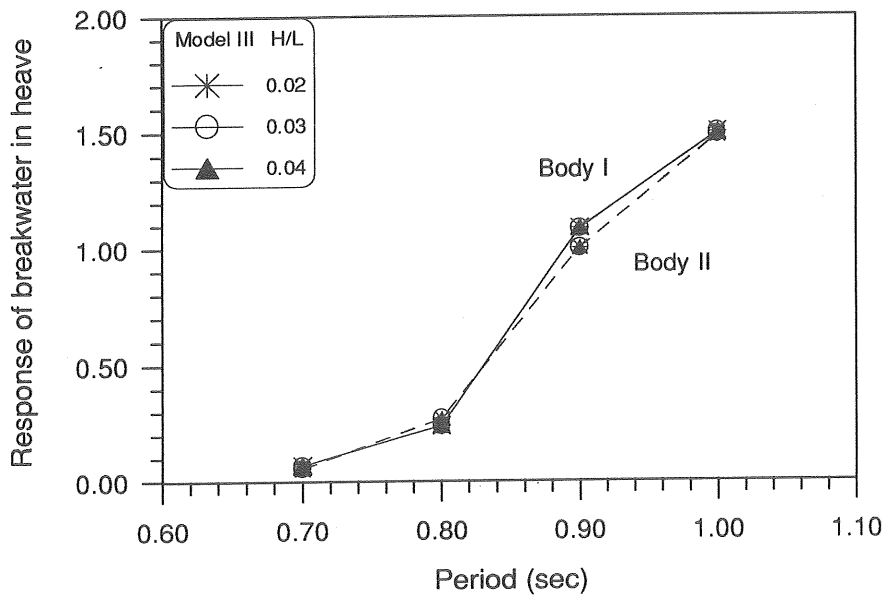
Fig. 5.19 Calculated heave response of Body I and Body II in Model III.
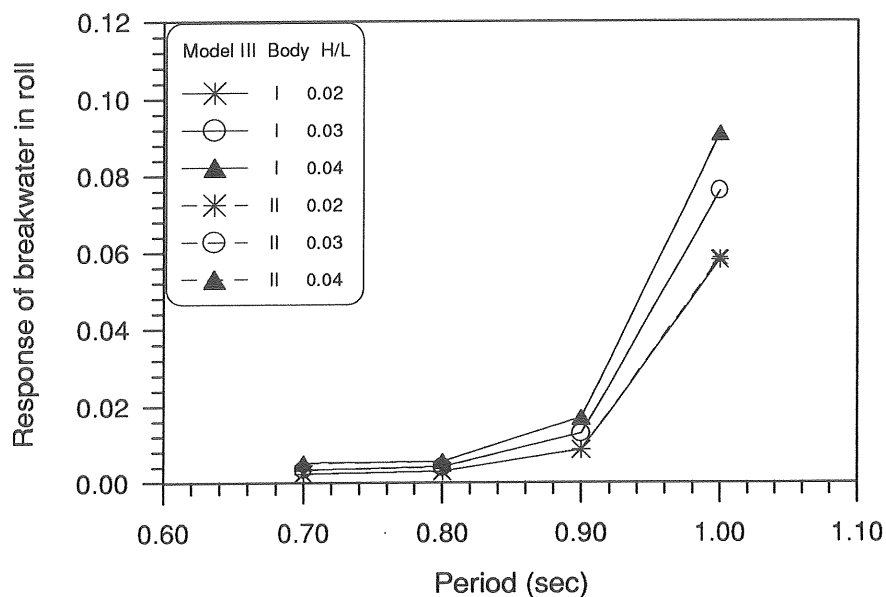
Fig. 5.20 Calculated roll response of Body I and Body II in Model III.
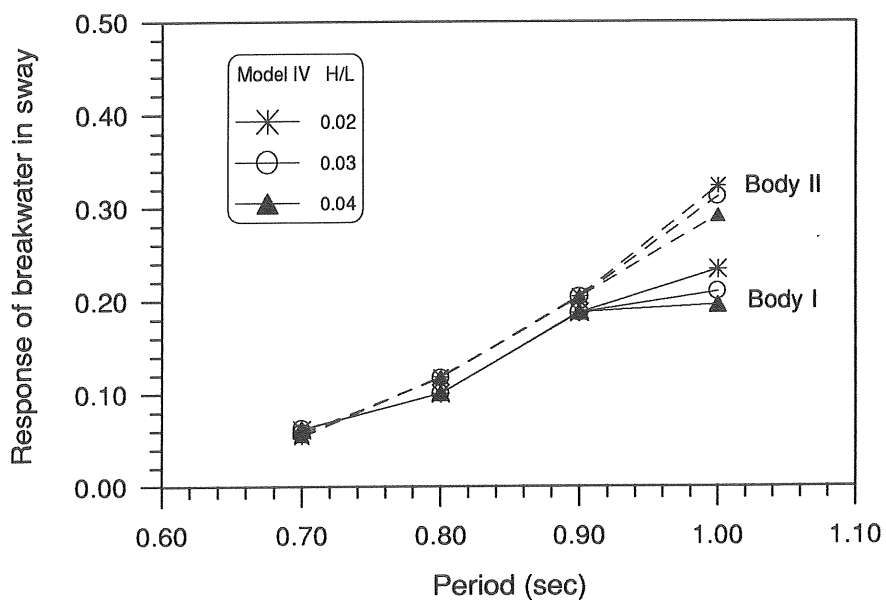
Fig. 5.21 Calculated sway response of Body I and Body II in Model IV.

78
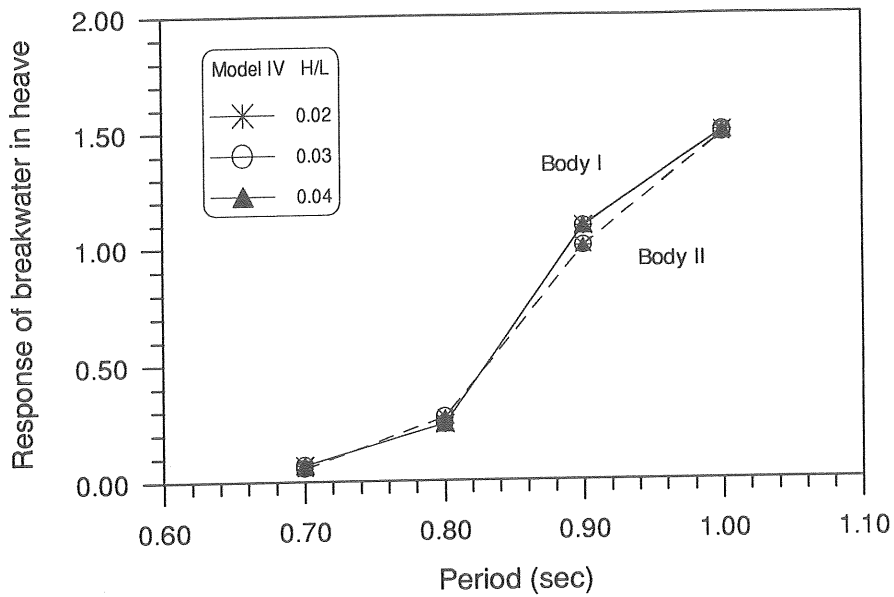
Fig. 5.22 Calculated heave response of Body I and Body II in Model IV.
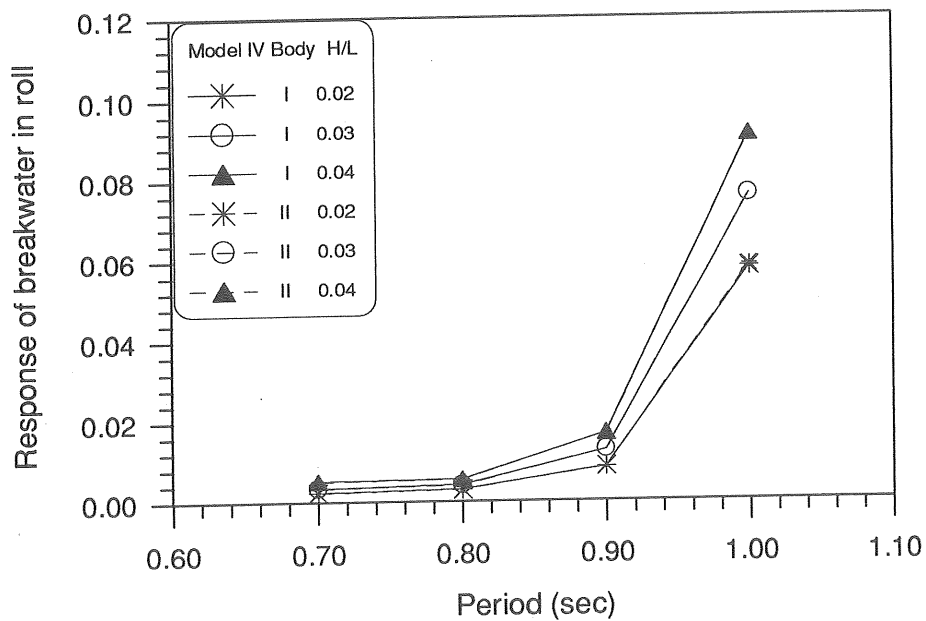
Fig. 5.23 Calculated roll response of Body I and Body II in Model IV.

5.2.2 Surface elevation

The validation of the calculated wave elevation is made by comparing the results of the numerical predictions with measured values from the model tests. Fig. 5.24 presents the results for Model II. The computations were performed for the same positions as were measured in the model tests, see Fig. 4.3 in Section 4.2. Results marked windward refer to the waves on the incident wave side, while leeward refers to the side protected by the breakwater from the incident wave. Furthermore, the results presented are expressed as the ratio of the amplitude of the total wave to the amplitude of the incident wave at a given point. Similar comparisons were made for Models III and IV and are presented in Figures 5.25 and 5.26, respectively. In general, the results obtained from the theoretical approach were found to be in agreement with the measured values, especially when keeping in mind that certain errors contaminated the measured data. These errors may come from: 1) inaccuracy of the record sensor, for instance a ±1 mm variation in measured wave amplitude due to the wave probes used; 2) the effect of reflexions (cross waves) in the wave basin, due to the side walls; and 3) the varying distance from the breakwaters to the measuring points, due to the slowly-varying motion in sway. On the other hand, some errors could also have been introduced in the computation of the total waves, as a consequence of over or underestimation of the motion of the breakwaters. These variations should be accounted for in any interpretation of the calculated results, including the line tensions shown in Section 5.2.3. It should also be noted that in these plots it is the linear axis scale that is applied, not the logarithmic scale.

Variations of the total wave amplitude ratio over the period range from 0.7 sec. to 1.0 sec. are presented in Figures 5.27 to 5.35. In this series of plots, results from both theory and experiment are compared directly, and the values from the weather side are displayed together with the values from the lee side. Figures 5.27 to 5.29 show the results for Model II at each pair of points, e.g. A1 and A4, A2 and A5, and A3 and A6. Similar plots are presented also for Model III in Figures 5.30 to 5.32, and for Model IV in Figures 5.33 to 5.35. Again the results presented show a good correlation in most cases, even in the area (points A2 and A5) where the water field is strongly affected by diffracted waves from both bodies. Linear response of water waves was observed, in spite of that the responses to waves of steepness H/L = 0.04 deviate slightly from the others to waves of H/L = 0.02 and 0.03. Both the experimental and theoretical curves exhibit a consistent trend for the wave performance on the weather side, as well as for the performance on the lee side. In Model II, waves on the weather side reach a maximum at T = 0.8 sec., and have an amplitude slightly larger than

the incident wave height (H = 2A), and reach a minimum amplitude of about 30% of A at T = 0.9 sec.

In order to obtain an impression of the variation of wave attenuation with the direction of the incident waves at the lee side, the coefficients of the wave amplitudes are presented in Fig. 5.36 for incident waves of· H/L = 0.03. It can be seen clearly that for high frequency waves the breakwaters provide better protection in oblique waves than in beam waves, but that for waves of low frequency, there is no significant difference. In this figure the differences between the values at points A4 and A6 are indicated as well. In Fig. 5.37, similar comparisons are made for the waves at the weather side.
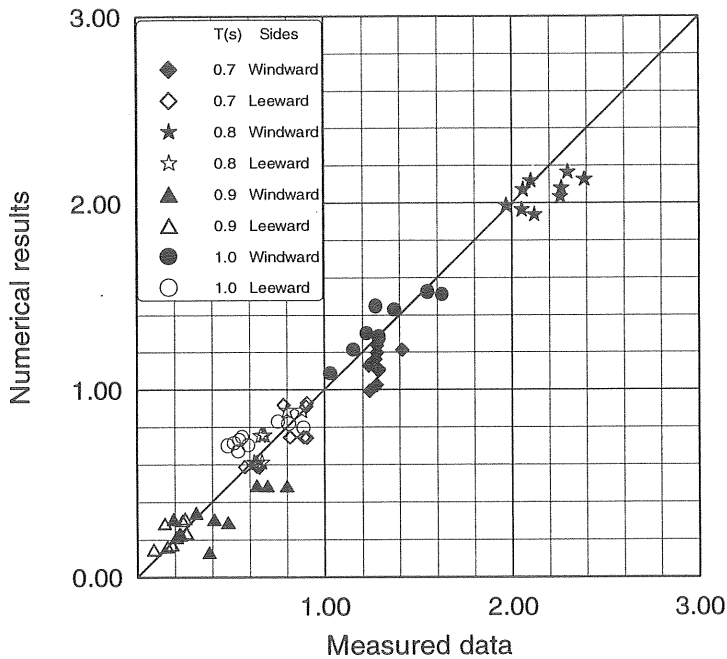
Fig. 5.24 A comparison of the model test and the numerical prediction for wave amplitudes at all six given points of Model II.
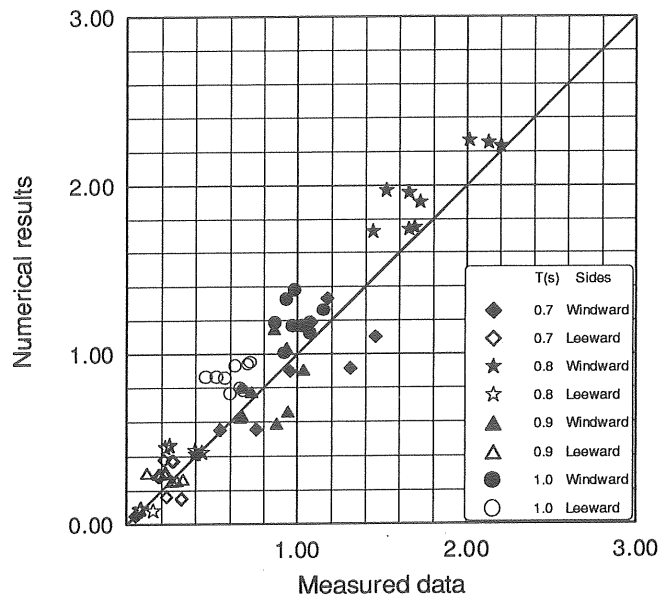
Fig. 5.25 A comparison of the model test and the numerical
prediction for wave amplitudes at all six given points
of Model III.
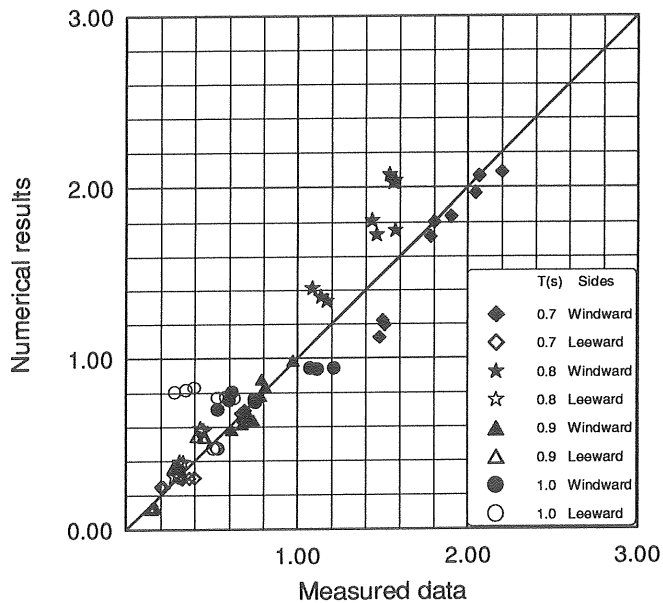
Fig. 5.26 A comparison of the model test and the numerical
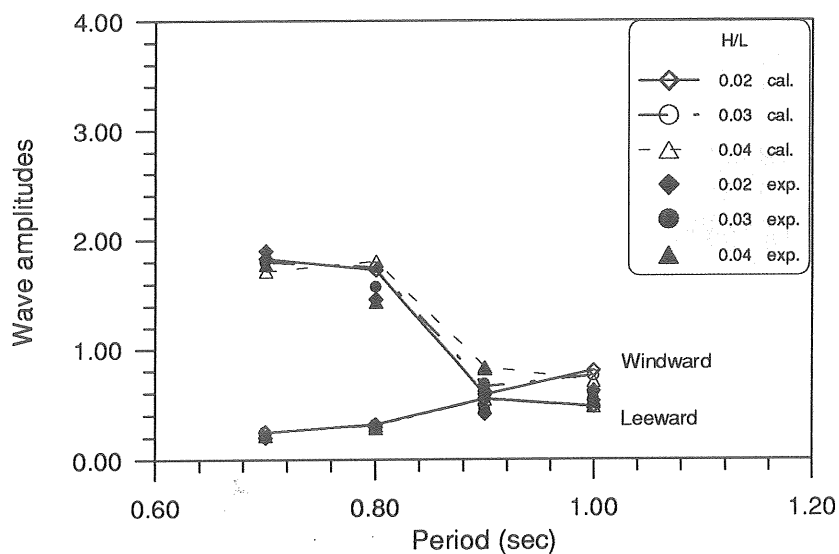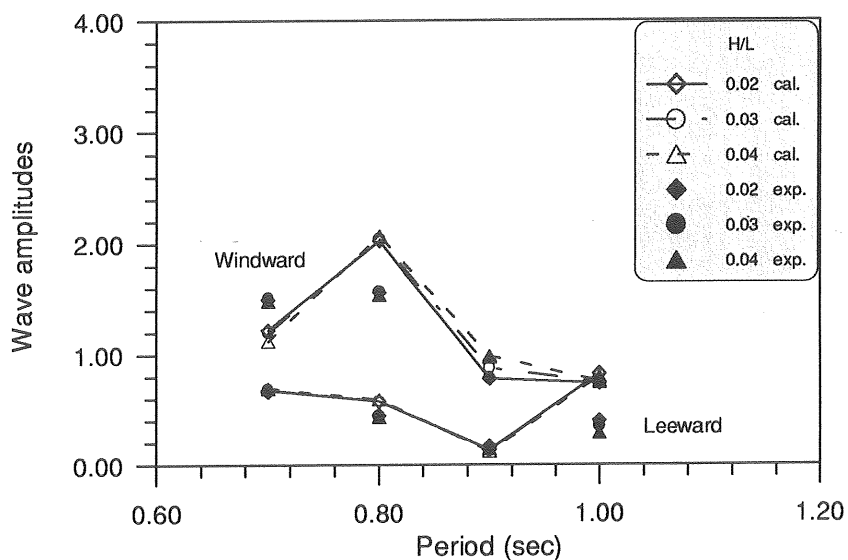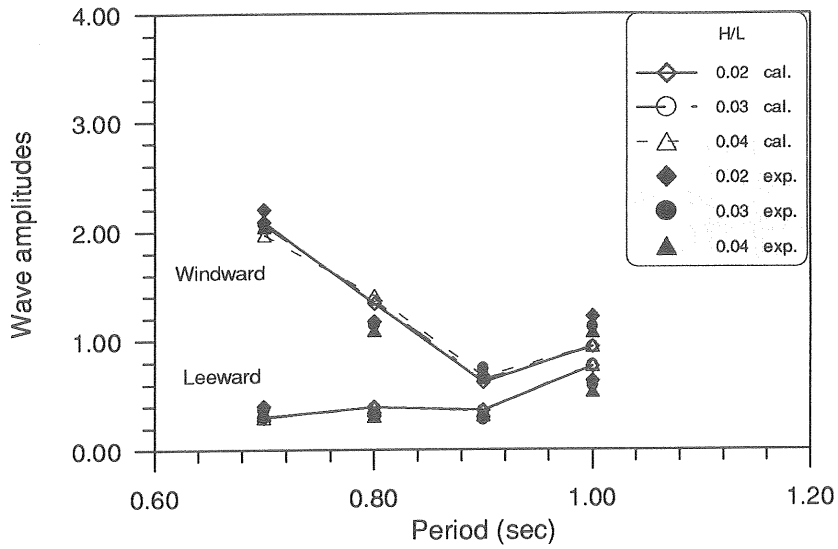prediction for wave amplitudes at all six given points
of Model IV.

82
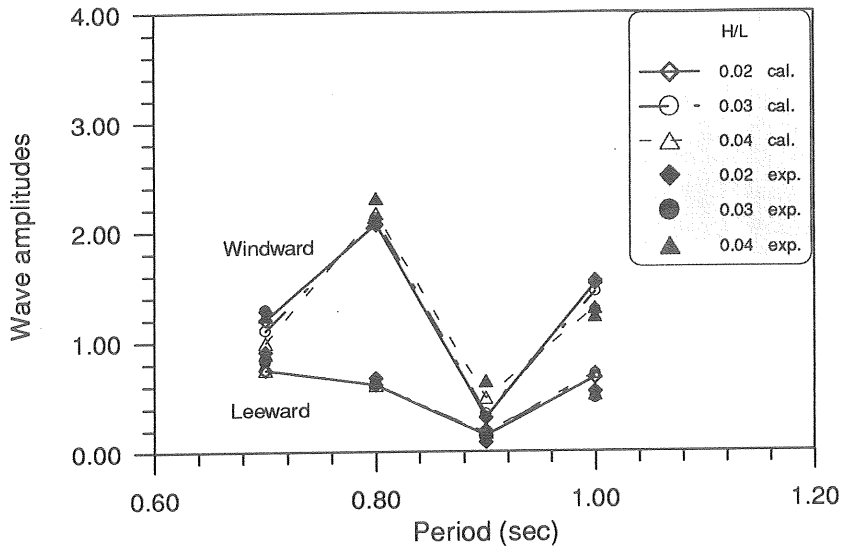
Fig. 5.27 Non-dimensional wave amplitudes as a function of wave period for various wave steepnesses valid for Model II at points A1 and A4.
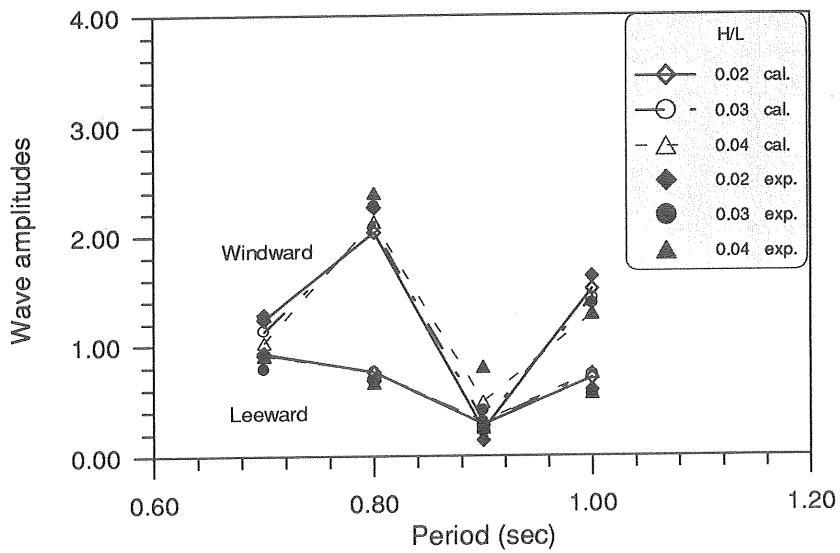
Fig. 5.28 Non-dimensional wave amplitudes as a function of wave period for various wave steepnesses valid for Model II at points A2 and A5.

83
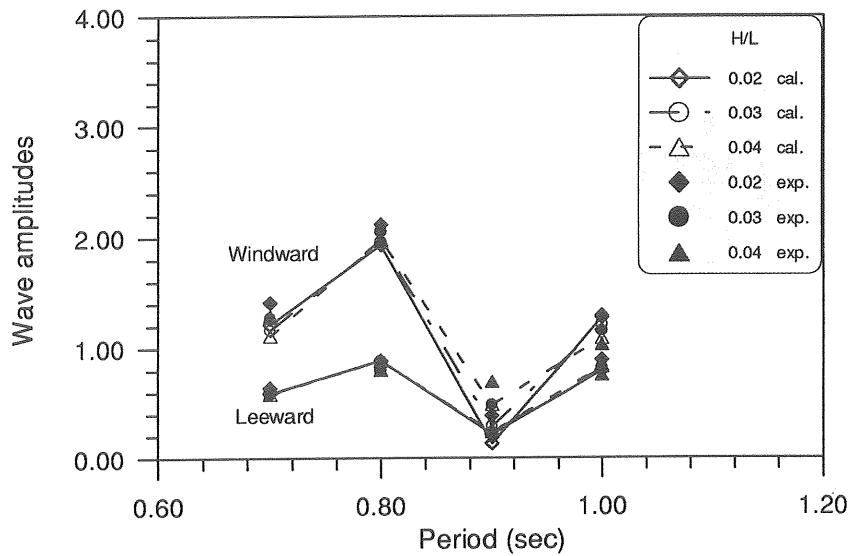
Fig. 5.29 Non-dimensional wave amplitudes as a function of wave
period for various wave steepnesses valid for Model II at
points A3 and A6.
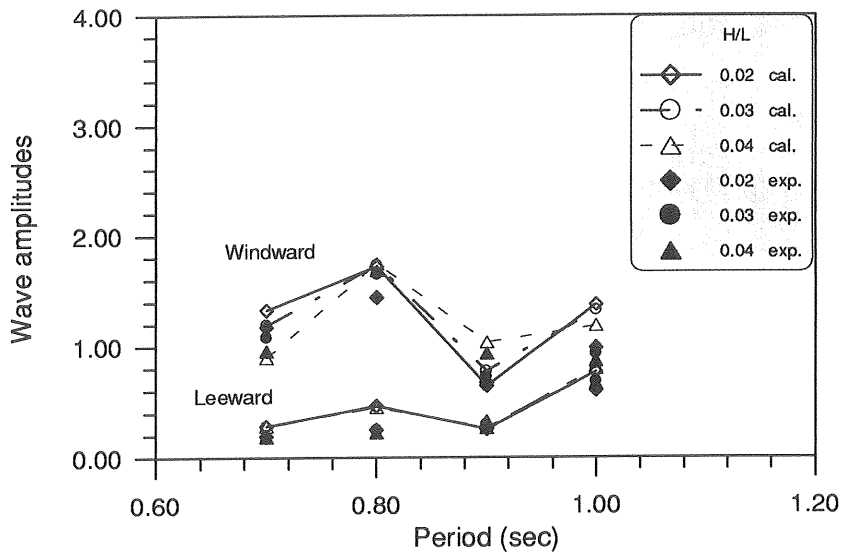
Fig. 5.30 Non-dimensional wave amplitudes as a function of wave
period for various wave steepnesses valid for Model III at
points A1 and A4.
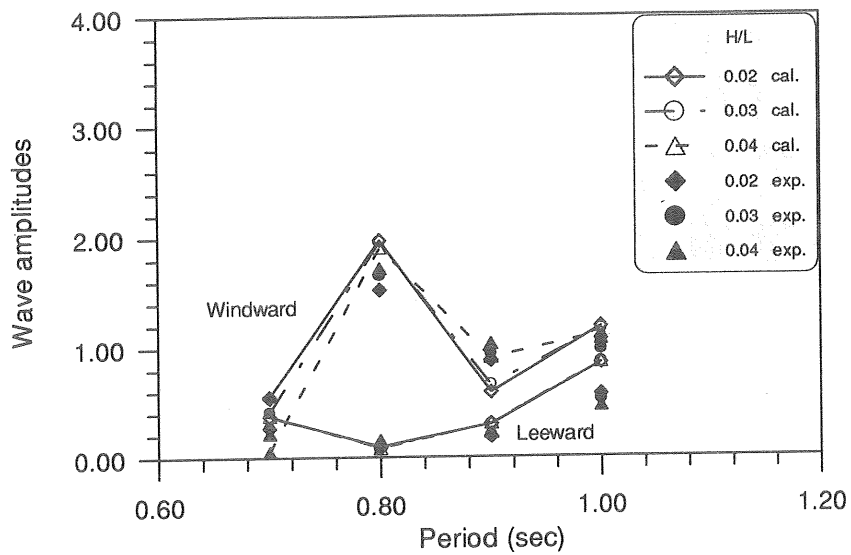
Fig. 5.31 Non-dimensional wave amplitudes as a function of wave period for various wave steepnesses valid for Model III at points A2 and A5.
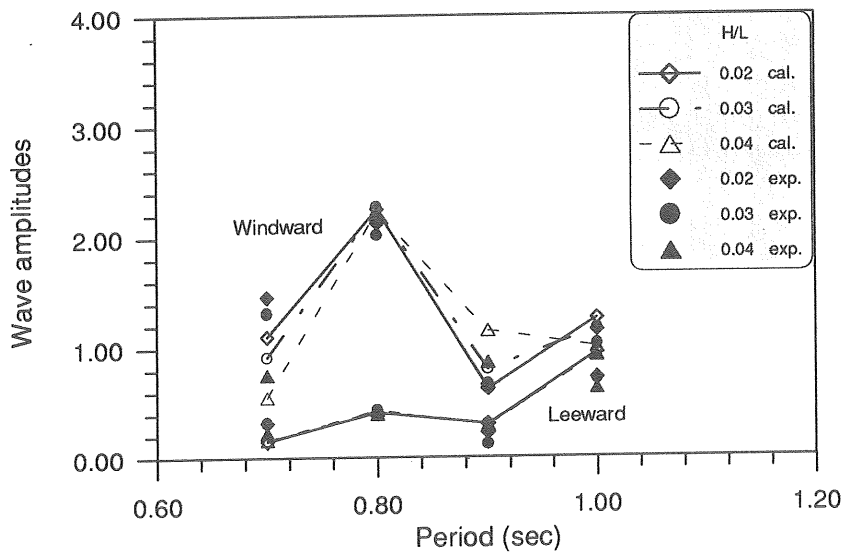
Fig. 5.32 Non-dimensional wave amplitudes as a function of wave period for various wave steepnesses valid for Model III at points A3 and A6.

85

Fig. 5.33 Non-dimensional wave amplitudes as a function of wave period for various wave steepnesses valid for Model IV at points A1 and A4.

Fig. 5.34 Nondimensional wave amplitudes as a function of wave period for various wave steepnesses valid for Model IV at points A2 and A5.

Fig. 5.35 Non-dimensional wave amplitudes as a function of wave period for various wave steepnesses valid for Model IV at points A3 and A6.
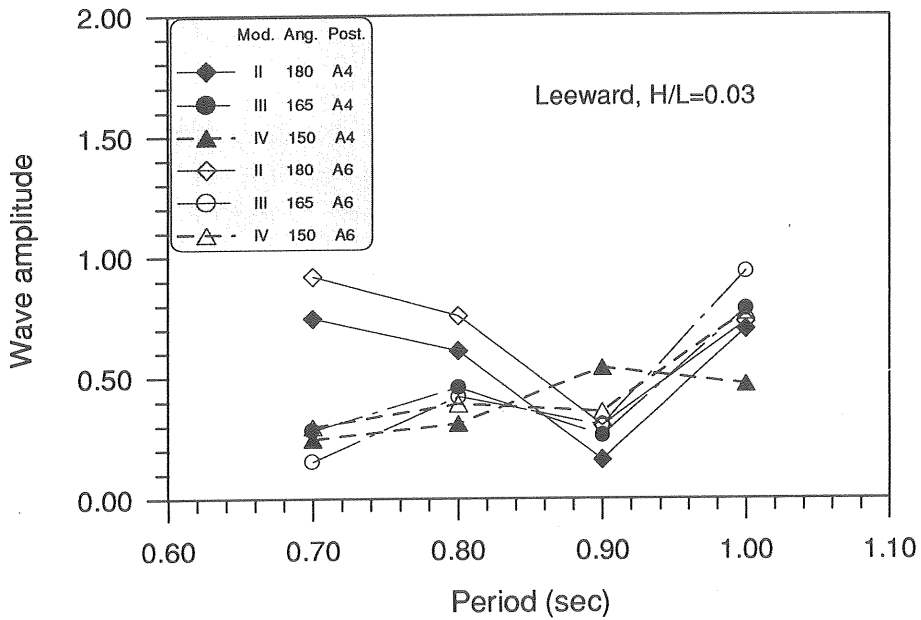
Fig. 5.36 Wave attenuation for incident waves from 180°, 165° and 150°.
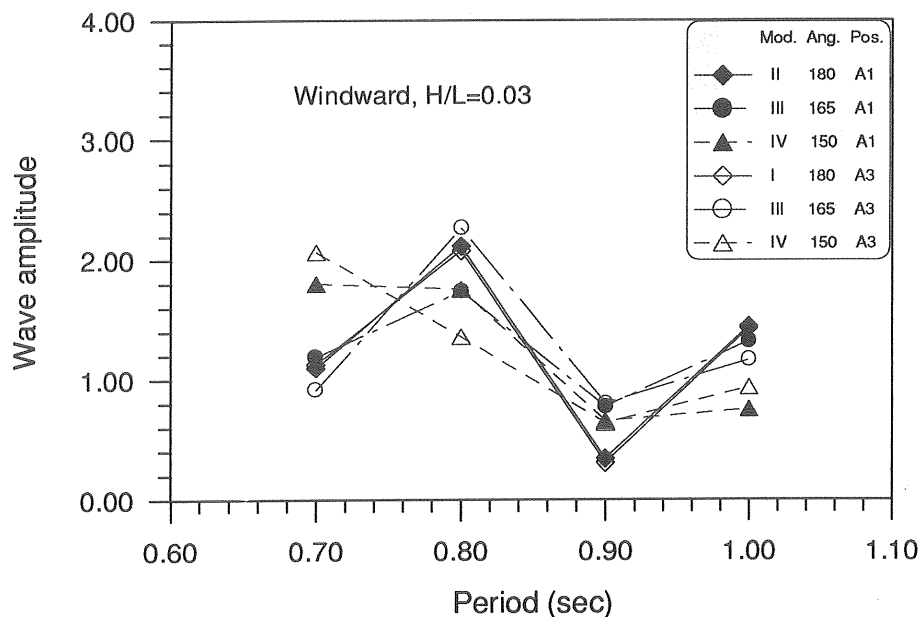
Fig. 5.37 Total waves on the weather side of the breakwaters for incident
waves from 180°, 165° and 150°.

5.2.3 Mooring cables

The performance of a moored breakwater is closely related to the static
properties of its mooring system, such as the mean position of the
breakwater, the system holding capacity for static load, the individual cable
load capacity for maximum load (static + dynamic load), the system
restoring force, etc. Figures 5.46 a) to f) present the relationships between
the system restoring force and the breakwater offset of Body I. In these
figures, all six components of the restoring force are plotted against the
offset in one of the modes. The computations were carried out by applying
the program MODEX to each of the cables. As shown in the results, the
system stiffness ($K = F/X$) is small compared with the stiffness caused by
the buoyancy, especially in heave, pitch and roll; which indicates that their
effects on the wave induced motions could be relatively unimportant. This
corresponds to the observations from the model tests and the numerical
predictions given in Section 5.2.1.

Figures 5.47 a) − f) show the line tensions for each of the individual cables
versus the breakwater offset. In the sway mode, the breakwater can be
expected to exhibit a large mean offset, in particular in a beam sea state. As

88

is shown in Figure 5.47 a), the maximum load may occur in Cable 1 or Cable 4. This depends, of course, on the contributions from the dynamic part of the load caused by the dynamic oscillation at the position of the fairlead. Moreover, the static analysis shows that, at the wave frequencies studied, the motion responses of the moored breakwaters are not significantly affected by the non-linearties of the mooring system.

The dynamic analysis of the mooring cables was also carried out with the program MODEX, a time domain simulation program calculating line position, line tension, line strain etc., for an arbitrary mooring cable. As mentioned in Section 5.1, the static tension caused by the mean drift motion and the dynamic tension caused by the slowly varying motion were abstracted from the sampled data by means of Fast Fourier Transformation. The computed results presented herein refer always to the first order component of the dynamic part of tension. A sample of the numerical simulations is shown in Figures 5.48 to 5.50 where the results are expressed as functions of time. The calculations were performed for Cable 4 in Model IV with wave of H/L = 0.03 and T = 1.0 sec. In Figure 5.38 the load time series are directly comparable.

Results obtained by MODEX and the model tests were compared in terms of dynamic tension at the upper end of the cable. Figure 5.39 shows the results from Cables 1, 2 and 4 in Model II. As indicated in the comparisons, the computed results are very close to those measured. Similarly good agreement was also found for the cables in Models III and IV. For those results, the comparisons are made directly in the plots of tension versus the wave period.

In order to illustrate the dynamic properties of the line tension, the numerical results shown in Fig. 5.40 are plotted against the wave period for various H/L, where the tensions are scaled by wave amplitudes. It is shown that Cable 1 would be the most heavily loaded cable in the system and that the maximum response of the cable load occurs at T = 0.9 sec.
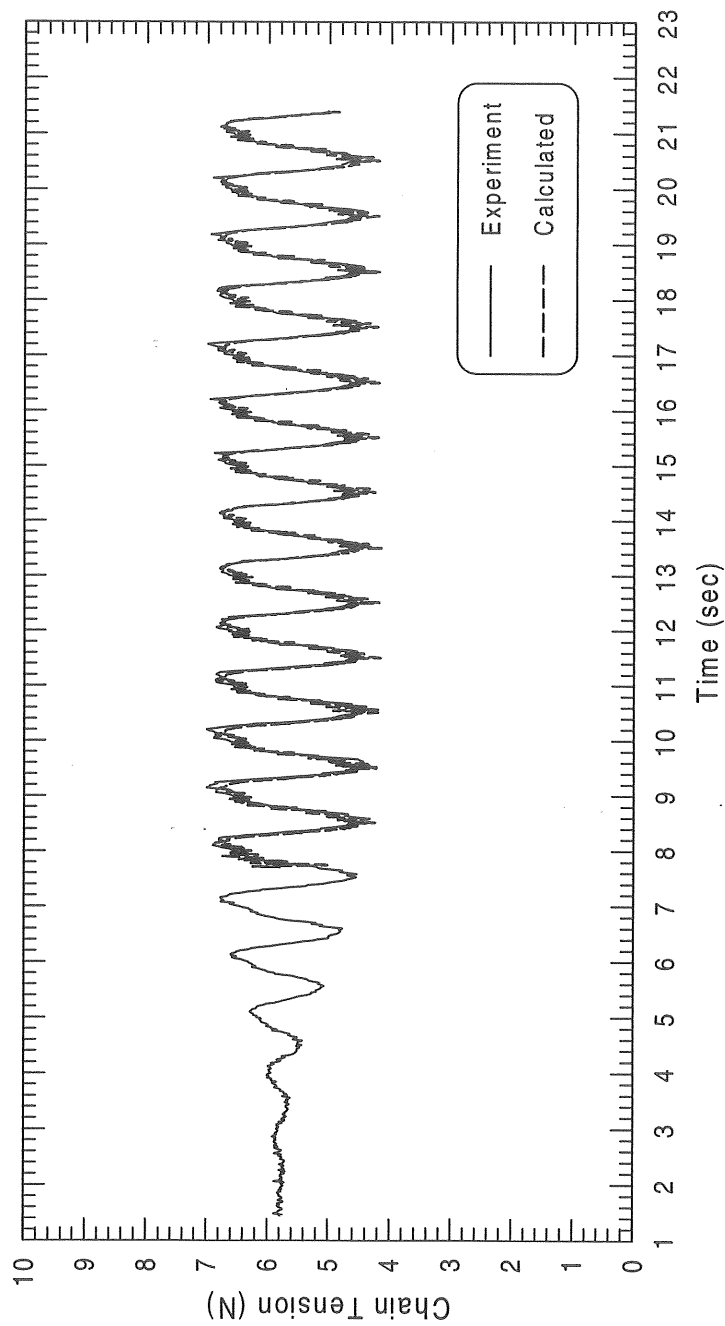
Fig. 5.38 Time history of the line tension at the upper end of Cable 4 in
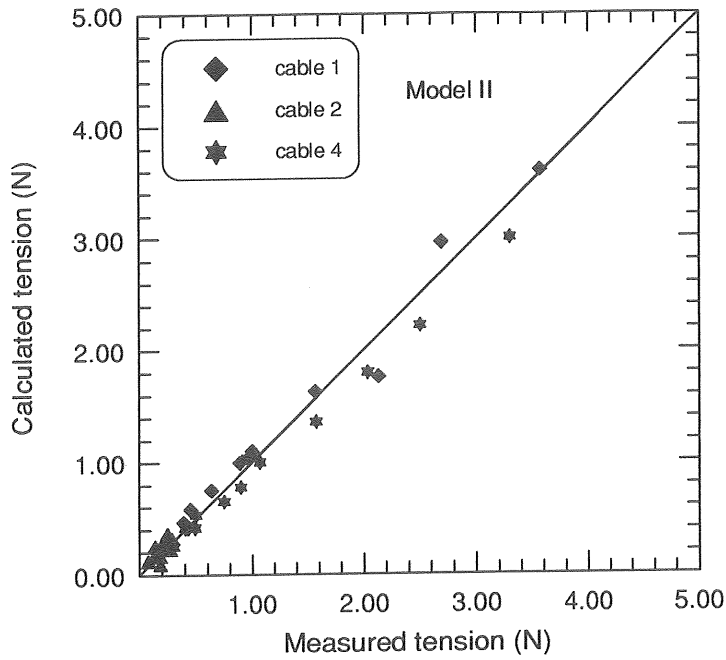Model IV for a wave of H/L = 0.03 and T = 1.0 sec.

Fig. 5.39 Comparison of measured dynamic tension with the tension obtained in conjunction with the program MODEX for Cables 1, 2 and 4 in Model II.
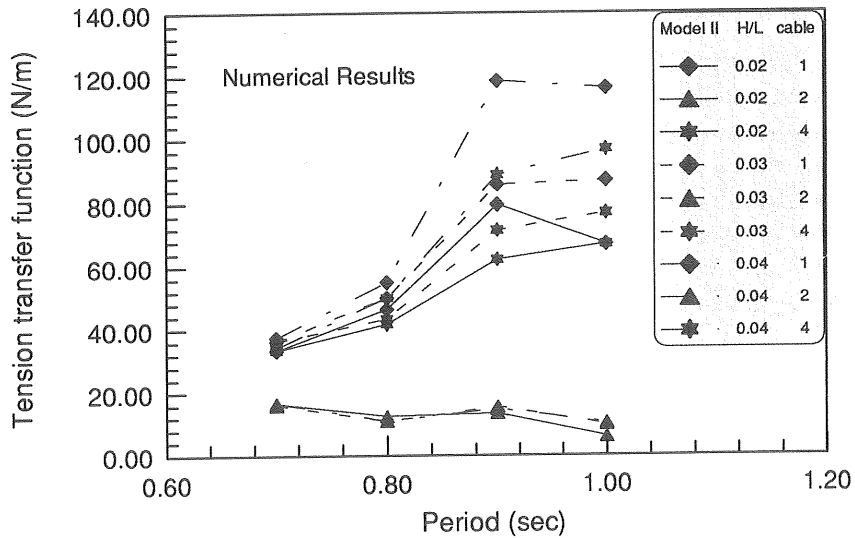

Fig. 5.40 Dynamic tension at the top of the mooring lines as a function of wave period for Cables 1, 2 and 4 in Model II.

91

Figure 5.41 presents the dynamic tension in Cable 1 versus the amplitude of the incident waves. A non-linear relationship between the line tension and the incident wave appears for the waves of low frequency.
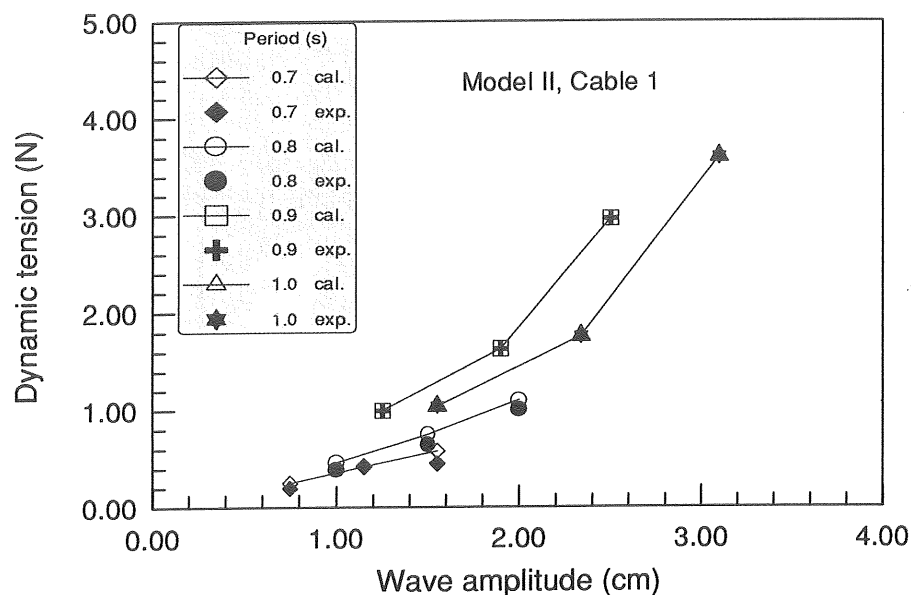
Fig. 5.41 Dynamic tension versus wave amplitudes of the excitation.

The next series of comparisons concern the tension response in oblique waves. Some introductory results are presented as the ratio of dynamic tension to the wave amplitude. Figure 5.42 shows results from the sampled and the calculated data for Cables 4 and 5 in Model III. Except for the maximum response at T = 0.9 sec., the agreement between the two sets of data is quite reasonable. Considerable discrepancy occurs at T = 0.9 sec., the reason for which could be overestimation of the excitation at the fairlead. As shown in Fig. 5.43, the same reason could apply to the results for Model IV, except the maximum dynamic load which no longer occur at T=0.9 sec. It is noted that in this case the heaviest load could be in Cable 4, rather than in Cable 1. This may be due to the motion of the body in sway when the oblique waves are taken into account.

Finally, comparisons are made for the dynamic tensions in different sea states. Figures 5.44 and 5.45 present the results for Cable 1 and Cable 4, respectively. It can be clearly seen that the dynamic tensions for beam waves are greater than those for oblique waves.
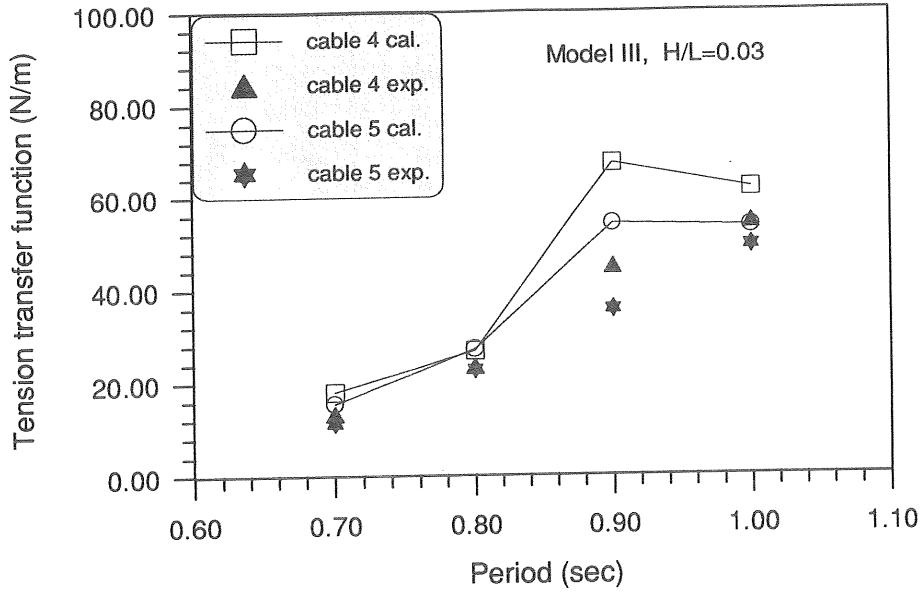
92

Fig. 5.42 A comparison of the measured and the calculated dynamic
tensions for oblique waves, θ =165°.
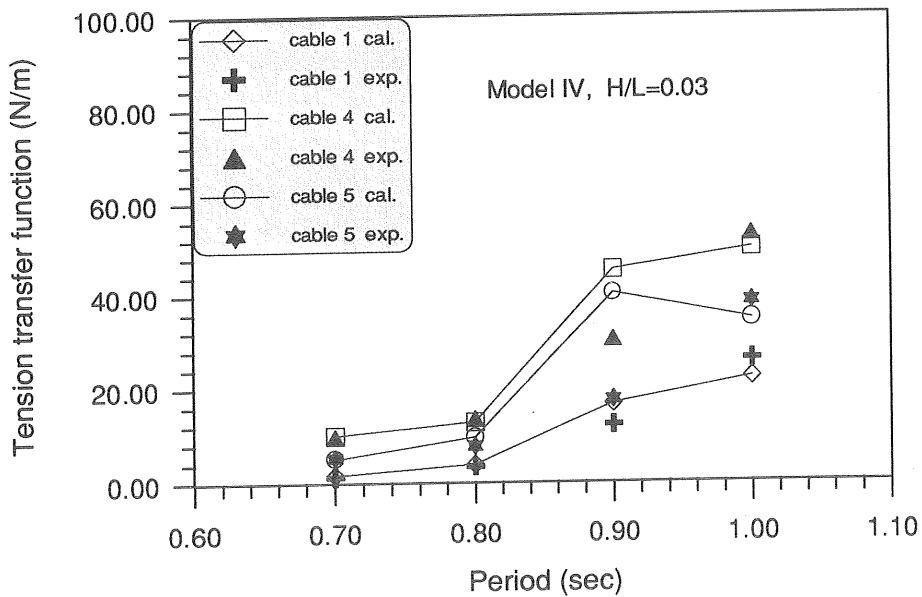

Fig. 5.43 A comparison of the measured and the calculated dynamic
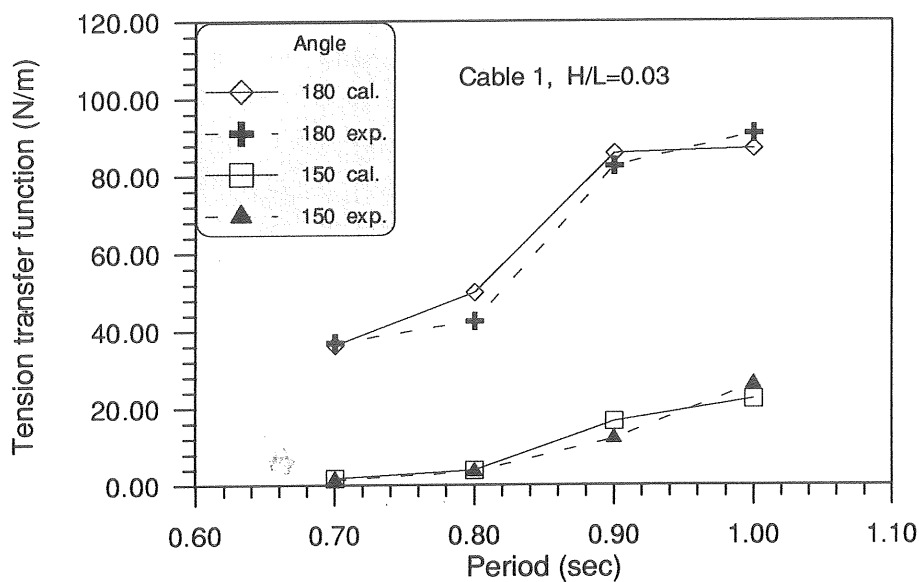tensions for oblique waves, θ =150°.

93

Fig. 5.44 Dynamic tensions of Cable 1 in response to the waves from 180°
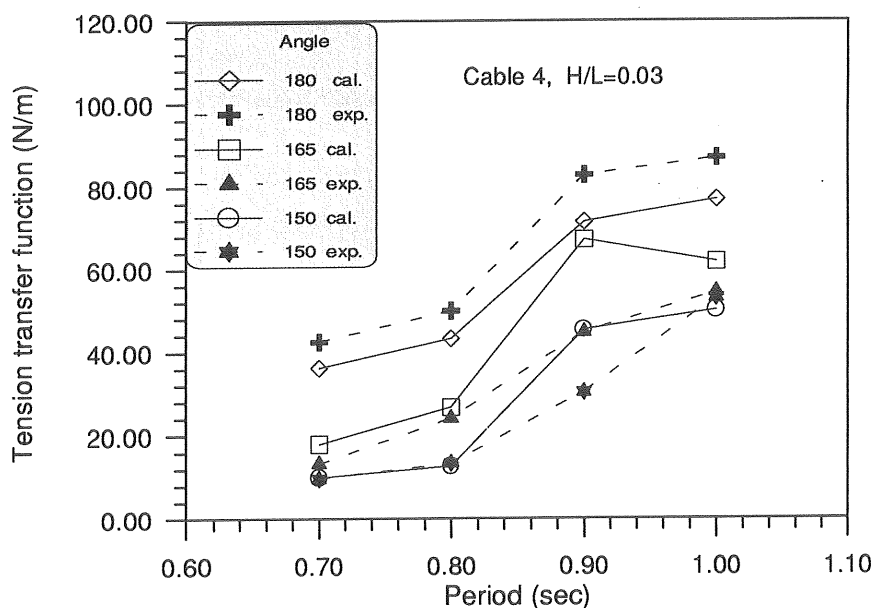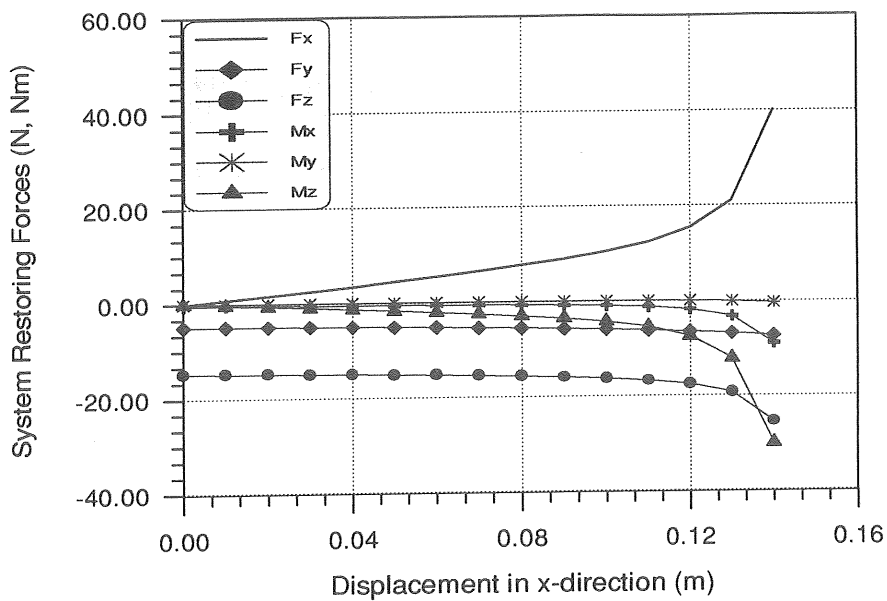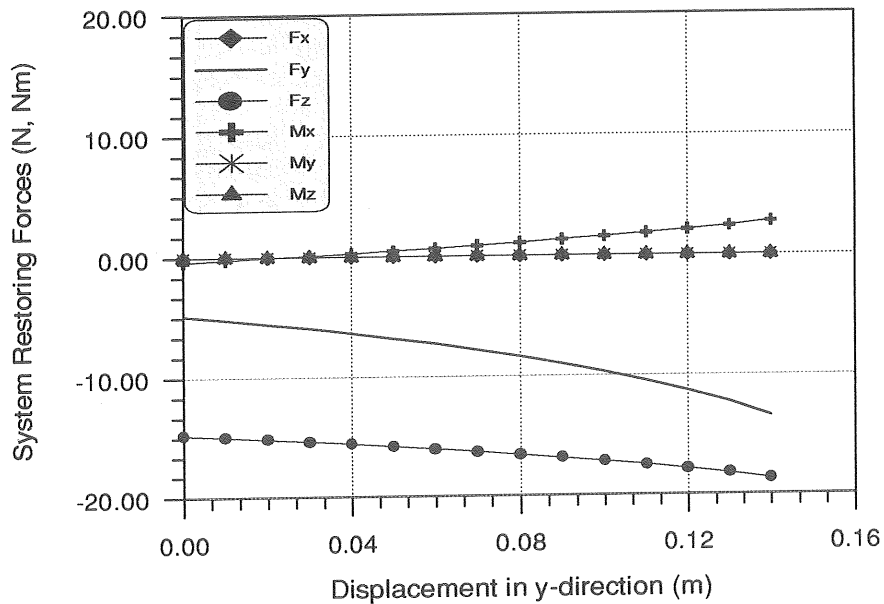and 150°.

Fig. 5.45 Dynamic tensions of Cable 4 in response to the waves from
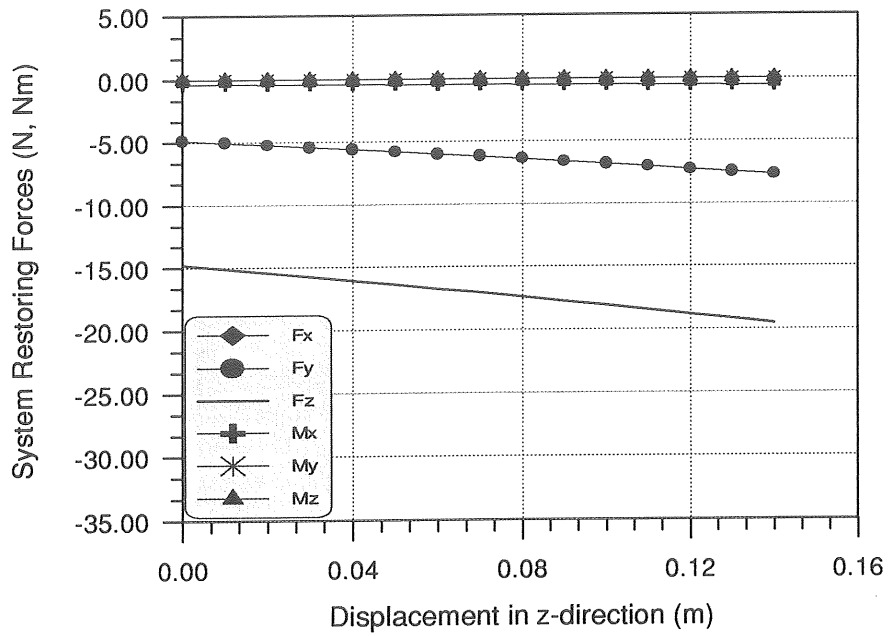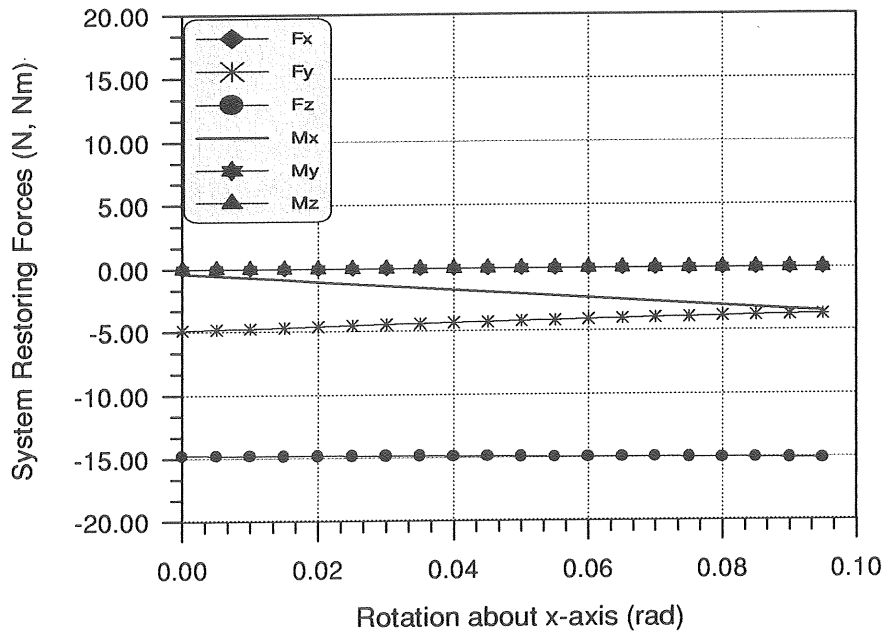180°, 165° and 150°.

(a) Sway

Fig. 5.46 System restoring forces versus breakwater offset in: a) Sway,
b) Surge, c) Heave, d) Pitch, e) Roll, f) Yaw.

(b) Surge

(c) Heave

(d) Pitch

(e) Roll

(f) Yaw

(a) Sway

Fig. 5.47 Typical plots of cable properties, static tension for cables connected to Body I versus the breakwater offset in: a) Sway, b) Surge, c)Heave, d) Pitch, e) Roll, f) Yaw.
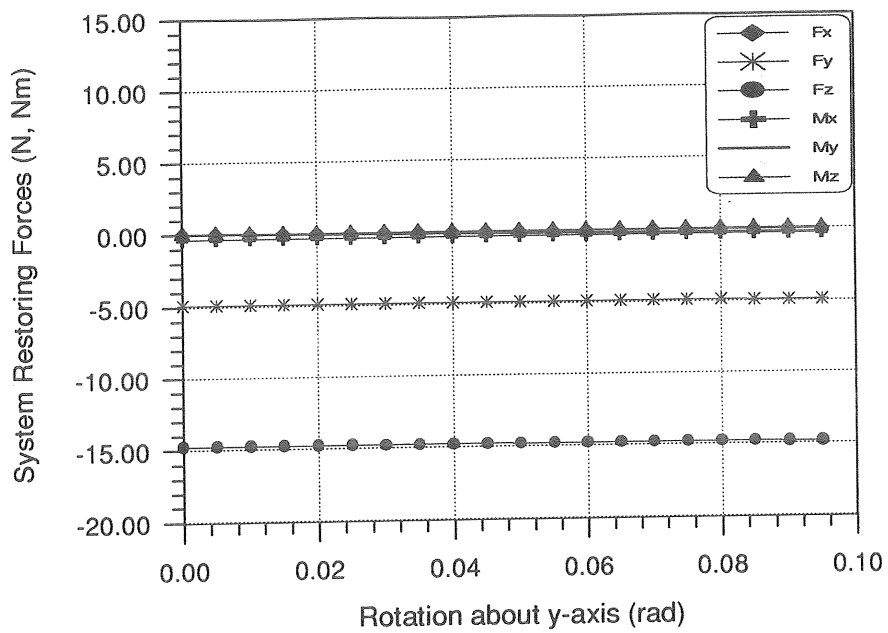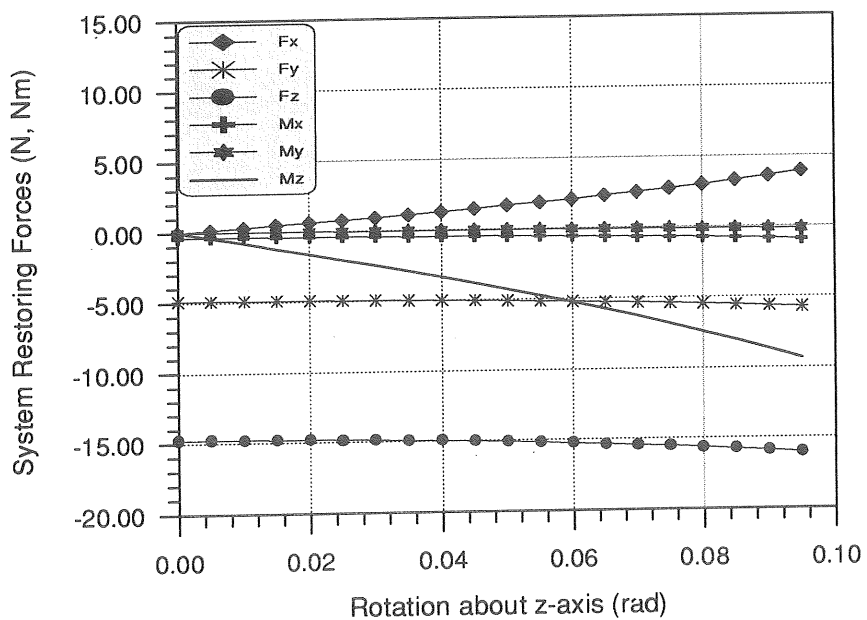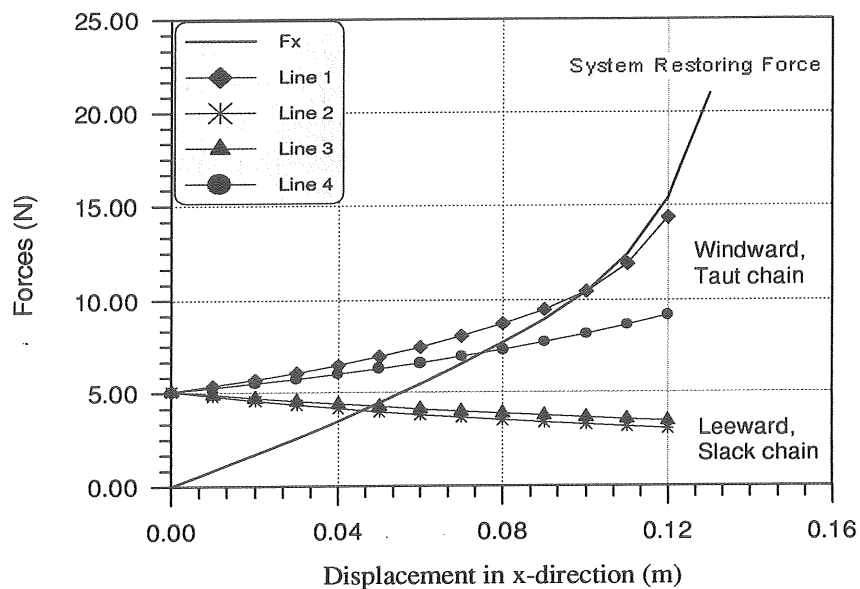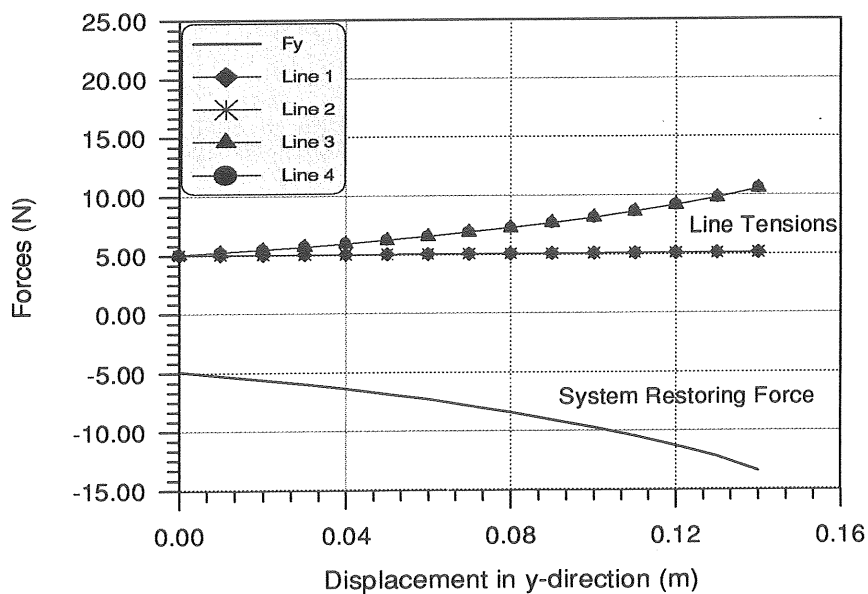

(b) Surge

(c) Heave

(d) Pitch

(e) Roll

(f) Yaw

100

HORIZONTAL DISPLACEMENT OF NODE 21

Case : Sea floor, static and dynamic.

File : cable4.INP - 23 DEC 1995
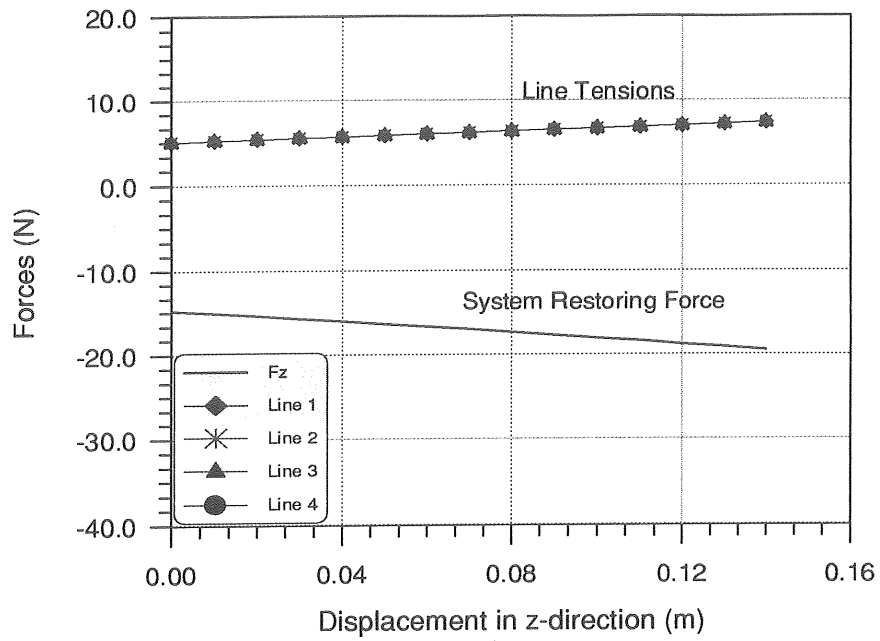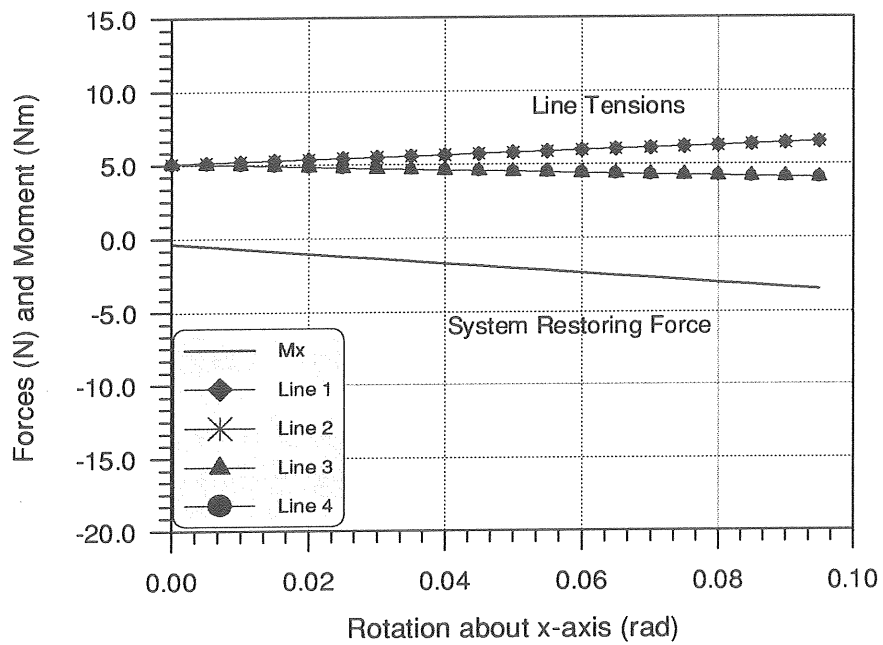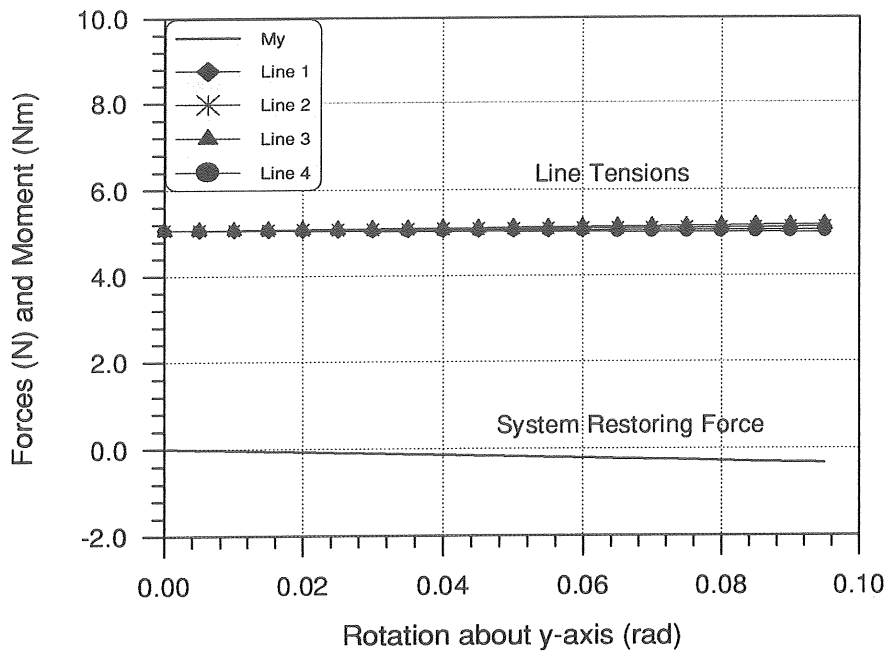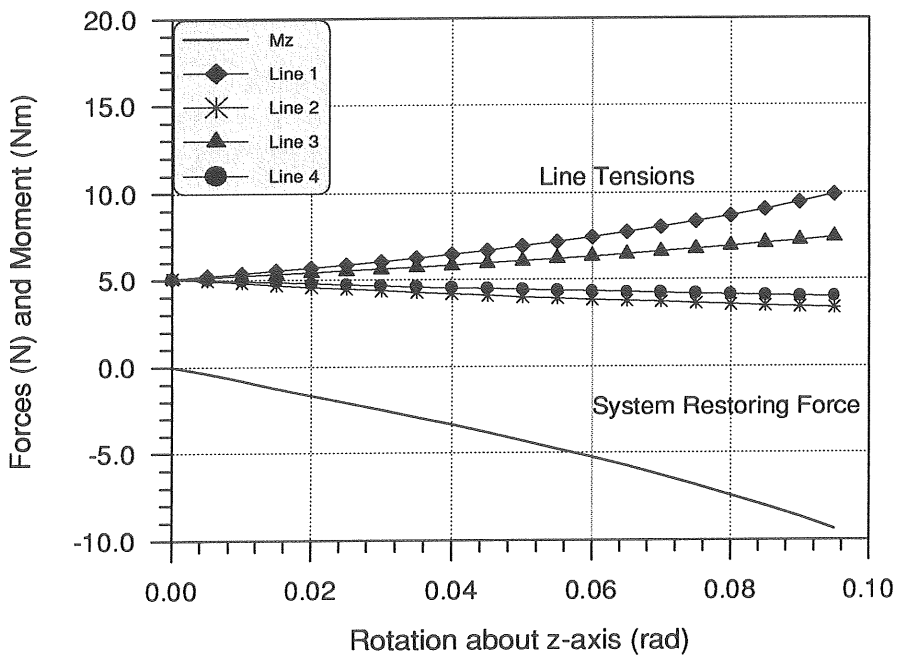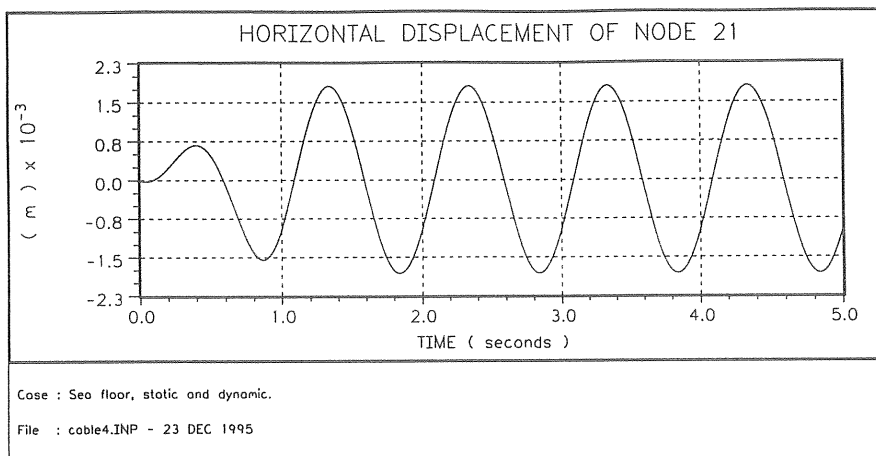
(a)

Fig. 5.48 Excitation of the displacement at the upper end of Cable 4 in
Model IV corresponding to a wave of H/L = 0.03 and T= 1.0sec.,
a) horizontal displacement, b) vertical displacement, and
c) displacement out of the equilibrium plane of the cable.

VERTICAL DISPLACEMENT OF NODE 21

Case : Sea floor, static and dynamic.

File : cable4.INP - 23 DEC 1995

(b)

101

DISPLACEMENT OUT OF PLANE OF CABLE, NODE 21

Case : Sea floor, static and dynamic.

File : cable4.INP - 23 DEC 1995

(c)

MAXIMUN   MINIMUN   MEAN DISPLACEMENT AND STANDARD DEVIATION   DIRECTION X

Case : Sea floor, static and dynamic.

File : cable4.INP - 23 DEC 1995

—————— Max
— — — Std+
— · — · — Mean
— — — — — Std-
· · · · · · · · · · Min
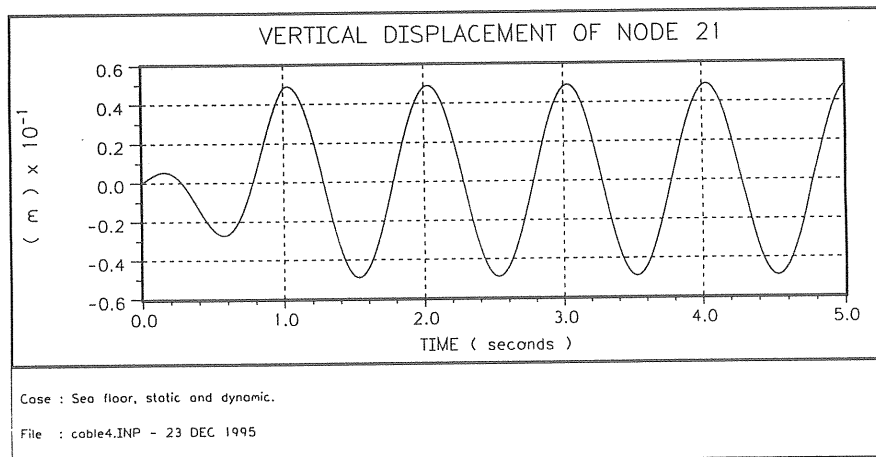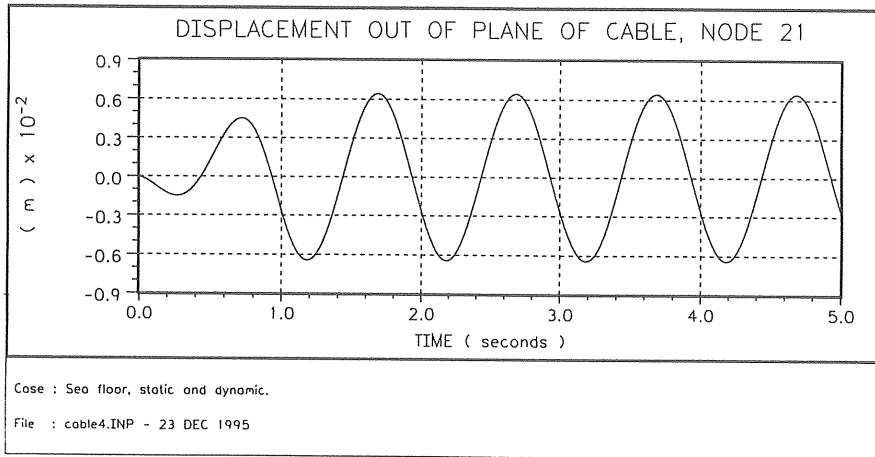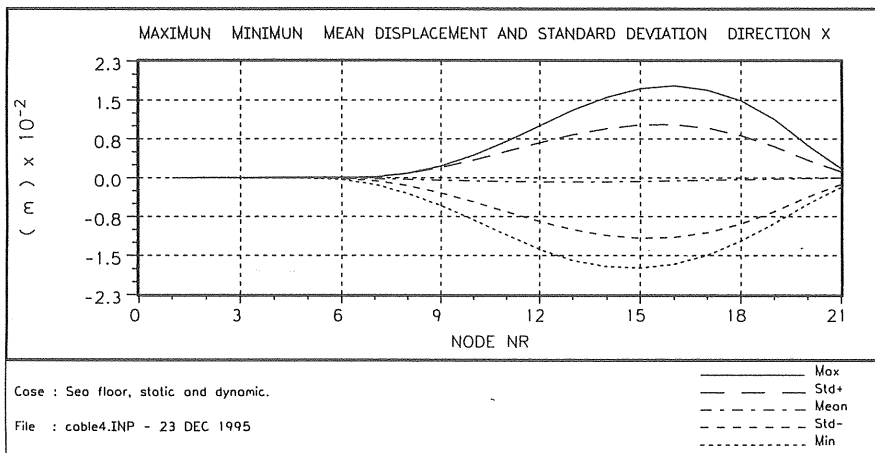
(a)

Fig. 5.49 Typical dynamic properties of Cable 4 in Model IV
corresponding to a wave of H/L=0.03 and T=1.0 sec.,
a) displacement in horizontal direction, b) displacement
in vertical direction, c) displacement out of the equilibrium
plane of the cable, and d) element tensions.

102

(b)

(c)

103

MAXIMUN MINIMUN MEAN TENSION AND STANDARD DEVIATION

Case : Sea floor, static and dynamic.

File : cable4.INP - 23 DEC 1995

Max
Std+
Mean
Std-
Min

(d)

CABLE POSITIONS PLANE X - Y

Case : Sea floor, static and dynamic.

File : cable4.INP - 23 DEC 1995
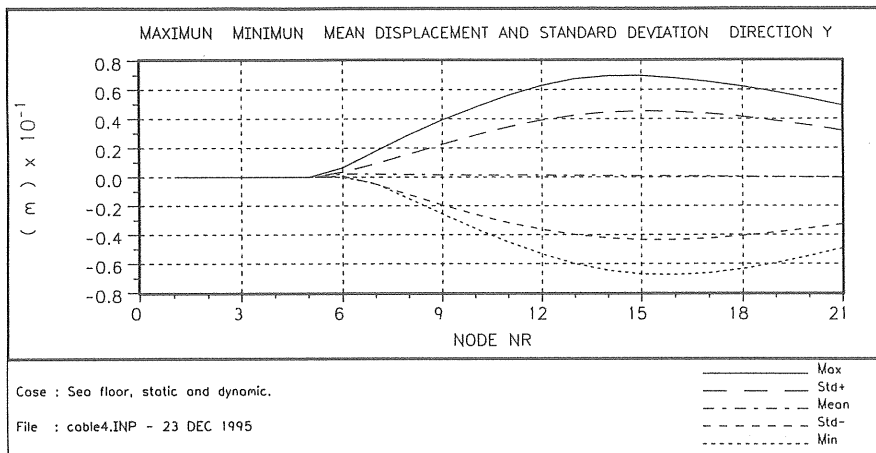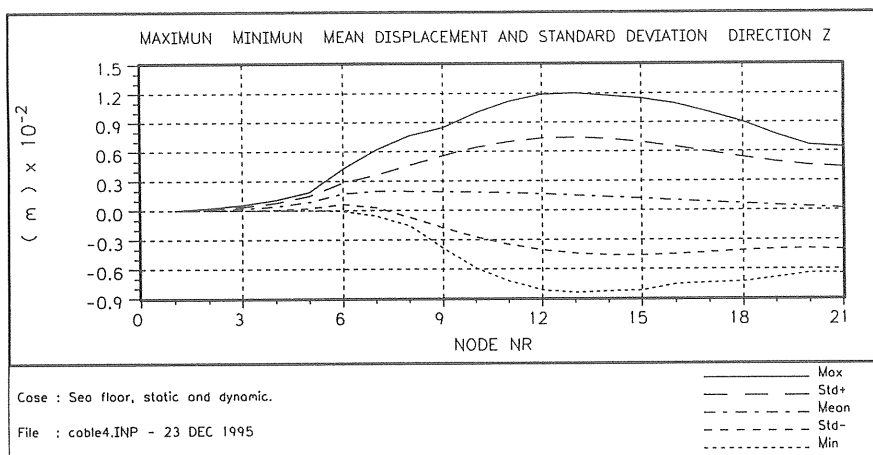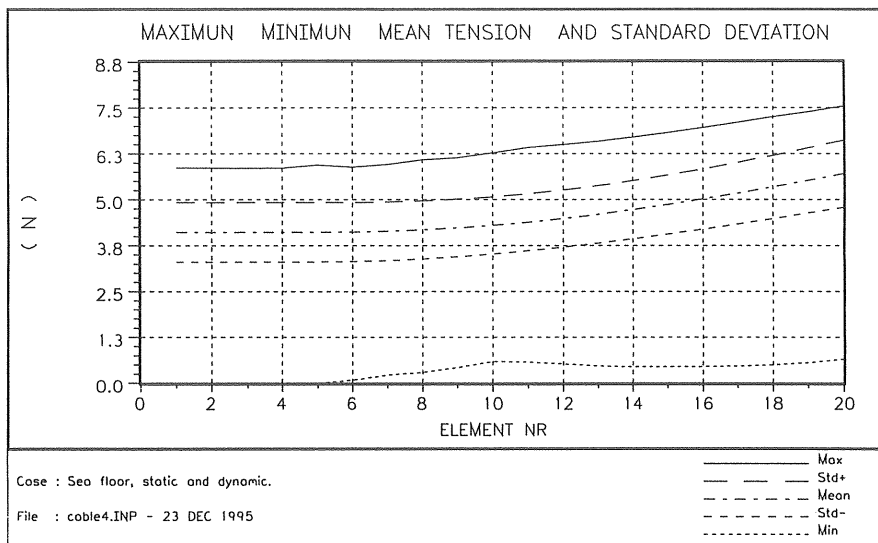
Fig. 5.50 Positions of Cable 4 in Model IV; at time = 4, 4.25, 4.5 and
4.75 sec.; for an incident wave of H/L = 0.03 and T = 1.0 sec.

104

6. Conclusions

A computational model has been developed which is capable of simulating the dynamic performance of a group of interconnected, moored floating structures subjected to harmonic wave action. In addition to the elasticity and damping of the mooring system and the constraints of the interconnections, linearized viscous damping, especially roll damping, was taken into account. Results from the computation and the model tests have been compared. The model tests confirm the general validity of the assumptions used in the modelling of the wave forces and the mooring line forces.

The following conclusions are derived from the results.
- The 3-D panel method implemented is a useful tool for estimating the wave-induced motion of multiple interconnected structures.
- The program MODEX, which is based on the finite element method, yields reliable results in the prediction of line tension and line deformation.
- The model developed simulates satisfactorily the structural motion, as well as the generated and diffracted waves. Hence, it can be 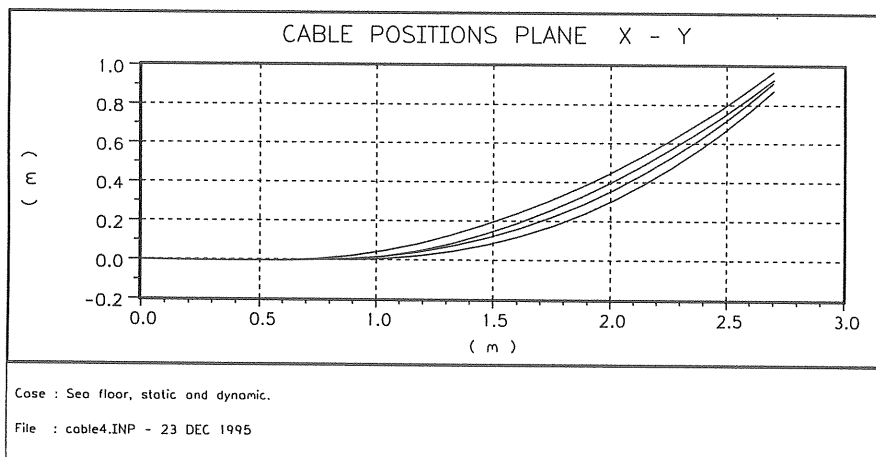stated that the model can be used to evaluate the efficiency of proposed floating breakwaters or used in the design of such breakwaters.

As shown in both the computations and the experiments, a compliant mooring system has little influence, compared to free floating structures, on structural motions of a frequency corresponding to the incident wave, or on the wave pattern around the structures, while it strongly influences the slowly varying motions induced by wind and waves. Due to the small damping in sway and surge, the drift motion can be greater than the wave frequency motion. In connection with the effect of the wave direction on structural motion, it has also been found that for high frequency waves the beam wave could be the most critical sea state for a system with long slender structures. Both the wave-induced motion and the slow drift motion exhibit large responses in beam waves, which in turn cause large tension in mooring cables.

Further improvement of the theoretical model is needed, however, for example damping simulation near the resonant motion in roll. Detailed hydrodynamic modelling, such as the discrete vortex method, may be required for structures with sharp-cornered sections. Furthermore, it is necessary, for a moored structural system exposed to a real sea state, to take into consideration not only the 1st-order wave-frequency forces but also the second-order dynamic forces. The motion of a certain specified point on the

structure, for example the connecting point between the structure and the mooring cable, is caused by various combinations of the components of structural motion, such as sway, surge, heave, pitch, roll and yaw. The amplitude of the combined motions is affected by the phases of the components. In addition to the combination of components of the same frequency (wave frequency or slowly-varying frequency), the motion associated with the wave frequency should be combined with different components of the slow drift motion in order to obtain a reliable prediction of the extreme load in the mooring cables.

REFERENCES

Bai, K. J. and **Yeung, R. W., 1974**, "Numerical Solution to Free Surface Flow Problems", Proceedings, Tenth Naval Hydrodynamics Symposium, Cambridge, Mass., U. S. A.

Bergdahl, L. and **Rask, I., 1987**, "Dynamic vs. Quasi-Static Design of Catenary Mooring System", Prec. Offshore Technology Conference, Paper No. OTC5530.

Berggren, L. and **Bergdahl, L. 1991**, "Forces on a Wave Energy Module", The Third Symposium on Ocean Wave Energy Utilization, Tokyo, Japan.

Berggren, L. and **Johansson , M., 1992**, "Hydrodynamic Coefficients of a Wave Energy Device Consisting of a Buoy and a Submerged Plate", Applied Ocean Research, Vol. 14, No. 1.

Bettess, P. and **Zienkiewicz, O. C., 1977**, "Diffraction and Refraction of Surface Waves Using Finite and Infinite Elements", International Journal for Numerical Methods in Engineering, Vol. 11, pp. 1271-1290.

Bishop, C. T., Donelan, M. A. and **Kahma, K. K., 1992**, "Shore Protection Manual's Wave Prediction Reviewed", Coastal Engineering, No. 17, pp. 25-48

Black, J. L., Mei, C. C. and Bary, C. G., 1971, "Radiation and Scattering of Water Waves by Rigid Bodies", J. of Fluid Mechanics, Vol. 46, Part I, pp. 151-164.

Bretschneider, C. L., 1958, "Revisions in Wave Forecasting: Deep and Shallow water", Proc. 6th Coastal Eng. Conf., Miami, pp. 30-67.

Bretschneider, C. L., 1970, "Forecasting Relations for Wave Generation", Look Lab/Hawaii, Vol. 1, No. 3, Univ. of Hawaii.

Bretschneider, C. L., 1973, "Prediction of Waves and Currents", Look Lab/Hawaii, Vol. 3, No. 1, Univ. of Hawaii.

McCartney, B. L., 1985, "Floating Breakwater Design", J. of Waterway, Port, Coastal and Ocean Engineering, Vol. IV, No. 2.

Calisal, S. M. and **Sabuncu, T., 1984**, "Hydrodynamic Coefficients for vertical Composite cylinders", Ocean Eng., Vol. 11, No. 5, 529-542.

Chakrabarti, S. K., 1978, "Wave Forces on Multiple Vertical Cylinders", J. of Waterway, Port, Coastal and Ocean Division, ASCE, Vol. 104, No. WW2, Proc. Paper 13727, pp. 147-161.

Chakrabarti, S. K., 1980, "Impact of Analytical, Model and Field Studies on the Design of Offshore Structures", International Symp. Ocean Engineering and Ship Handling, SSPA, Göteborg, Sweden.

Chakrabarti, S. K. and Cotter, D. C., 1983, "Interaction of Waves with a Moored Semisubmersible". Third International Offshore Mechanics and Arctic Engineering Symp., ASME, New Orleans.

Chen, H. S. and **Mei, C. C., 1974**, "Oscillations and Wave Forces in an Offshore Harbour", Ralph M. Parsons, Laboratory for Water Resources and Hydrodynamics, MIT, Report No. 190.

Chen, H. S. and **Mei, C. C., 1975**, "Hybrid-Element Method for Water Waves", Proceedings of the Modelling Techniques Conference (Modelling 1975), San Francisco.

Eatock Taylor, R. and **Zietsman J., 1982**, "Hydrodynamic loading on Multi-component Bodies", Proc. 3rd Int. BOSS Conference, MIT,
pp. 424-446.

Eatock Taylor, R. and **Zietsman J., 1981a**, "A Comparison of Localised Finite Element Formulations for Two Dimensional Wave Diffraction and Radiation Problem", International Journal for Numerical Methods in Engineering, Vol. 17, pp. 1355-1384.

Eatock Taylor, R. and **Zietsman J., 1981b**, "Implementation of Coupled Element Formulations for Hydrodynamic Analysis in Three Dimensions", in Numerical Method for Coupled Problems, Ed. by Hinton, E., Bettess, P. and Lewis, R. W., Swansea, U.K.: Pineridge Press, pp. 281-290.

Faltinsen, O. M. and **Michelsen, F. C., 1974**, "Motions of Large Structures in Waves at Zero Froude Numbers", Proc. Int. Symp. Dyn. Mar. Vehicles and Structures in waves", Inst. Mech. Engrs., London, pp. 91-106.

Garrett, C. J., 1970, "Wave Forces on A Circular Dock", J. Fluid Mech. 46(1), pp. 129-139.

Garrison, C. J. and **Chow, P. Y., 1972**, "Wave Forces on Submerged Bodies", Journal of the Waterways, Harbors and Coastal Engineering Division, Proc. of the ASCE, Vol. 98 No. WW3, pp. 375-392.

Garrison, C. J., 1974, "Dynamic Response of Floating Bodies", Prec. Offshore Technology Conference, Paper No. OTC2067.

Garrison, C. J., 1974, "Hydrodynamics of Large Objects in the Sea, Part I-Hydrodynamic analysis", Journal of Hydrodynamics, No. 8, pp. 5-12.

Garrison, C. J., 1975, "Hydrodynamics of Large Objects in the Sea, Part II-Motion of Free-Foating Bodies", Journal of Hydrodynamics, No. 9
pp. 58-63

Garrison, C. J., Rao, V. S., and **Snider, R. H., 1970**, "Wave interaction with large submerged objects", Proc. Offshore Technology Conference, Paper OTC1278.

Hasselman, K., *et al.*, **1973**, "Measurement of Wind-Wave Growth and Swell Decay During the Joint North Sea Wave Project (JONSWAP)", Deutschen Hydrographischen Zeitschrift, Erganzunscheft, 13, No. A.

Haug, E. J., 1989, "Computer Aided Kinematics and Dynamics of Mechanical Systems", Volume I, Ed. by Edward J. Haug.

Herfjord, K. and **Nielsen, F. G., 1988**, "Low Frequency Motion of a Deep Draft Column Stabilized Platform", BOSS' 88 Conference, Trondheim, Norway.

Hess, J. L. and **Smith, A. M. O., 1962**, "Calculation of Nonlifting potential Flow about Arbitrary Three-Dimensional Bodies", Douglas Aircraft Co. Report No. E.S. 40622. (Also in abbreviated form in J. Ship. Res. No. 8.)

Hogben, N. and **Standing, R. G., 1975**, "Wave Loads on Large Bodies", The dynamics of Marine Vehicles and Structures in Waves Ed. by R. E. D. Bishop and W.G. Price, pp. 258-277.

Huang, M. C., 1983, "Finite Element Analysis of Wave Interference Effects Between Large Structures", thesis presented to the Oregon State University, at Corvallis, Oregon.

John, F., 1949, "On the Motion of Floating Bodies I", Communications in Pure and Applied Math., Vol. 2.

John, F., 1950, "On the Motion of Floating Bodies II", Communications. in Pure and Applied Math., Vol. 3.

Kinoshita, T., et al., 1986, "Performance of Multi-Body-Type Floating Breakwater", Proceedings of the International of Offshore Mechanics and Arctic Engineering Symp. 5th v 1. Publ. by ASME, New York, NY, USA, pp. 410-416.

Korsmeyer, F. T., Lee, C. H., Newman, J. N. and **Sclavounos, P. D., 1988**, "The Analysis of Wave Effects on Tension-Leg Platforms",
OMAE' 88 Conference, Houston.

Kwan, C. T. and **Bruen, F. J., 1991**, "Mooring Line Dynamics: Comparison of Time Domain, Frequency Domain, and Quasi-Static Analyses", Prec. Offshore Technology Conference, Paper No. OTC6657.

Larsen, K. and **Sandvik, P. C., 1990**, "Efficient Methods for the Calculation of Dynamic Mooring Line Tension", Proc. of the First European Offshore Mechanics Symp., Trondheim, Norway.

Lindahl, J., 1983, "Manual för MODEX-MODIM", Department of Hydraulics, Chalmers University of Technology, Report Series B:43.

Lindahl, J. and **Sjöberg, A., 1983**, "Dynamic Analysis of Mooring Cables", Licentiate Thesis, Department of Hydraulics, Chalmers University of Technology, Report Series A:9.

Lindahl, J., 1984, "Implicit Numerisk Lösning av Rörelseekvationerna för En Förankringskabel", (Implicit Numerical Solution of the Equations of Motion of a Mooring Cable, in Swedish), Department of Hydraulics, Chalmers University of Technology, Report Series A:11.

Lindahl, J., 1985, "Modellförsök med en Förankringskabel", Department of Hydraulics, Chalmers University of Technology, Report Series A:12.

Lindahl, J. and **Bergdahl, L., 1987**, "MODEX-MODIM User's Manual", Department of Hydraulics, Chalmers University of Technology, Report Series B:49.

Lindgren, M. and **Björkenstam, U., 1989**, " Wave Interaction between Two Floating Bodies", The Tenth International Conference on Port and Ocean Engineering under Arctic Conditions, Luleå. Sweden.

Lysmer, J. and **Kuhlemeyer, R. L., 1969**, "Finite Dynamic Model for Infinite Media", Journal of the Engineering Mechanics Division, Proceedings of the American Society of Civil Engineers, EM4, pp. 859-877.

MacCamy, R. C. and Fuchs, R. A., 1954, "Wave Force on Piles. A Diffraction Theory", Beach Erosion Board Tech. Mem. No. 69.

McIver, P., 1986, "Wave Forces on Adjacent Floating Bridges", J. Applied Ocean Research, Vol. 8, No. 2, pp. 67-75.

Mei, C. C., 1978, "Numerical Methods in Water-Wave Diffraction and Radiation", Annual Review Fluid Mechanics, Vol. 10, pp. 393-416.

Miao, G. P. and Liu, Y. Z., 1984, "Hydrodynamic Coefficients of a Column with Footing in Finite-Depth Waters", Proceeding of the 3rd International Offshore Mechanics and Arctic Engineering Symposium, Vol. I, 199-205.

Mårtensson, N. and Bergdahl, L., 1987, "On the Wave Climate of the Southern Baltic", Licentiate Thesis, Department of Hydraulics, Chalmers University of Technology, Report Series A:15.

Newman, J. N., 1985a, "Algorithms for the free-surface Green Function", J. Eng. Maths., No. 19, pp. 57-67.

Newman, J. N., 1985b, "Transient axisymmetric Motion of a Floating Cylinder", J. Fluid Mech. No. 157, pp. 17-33.

Newman, J. N., 1985c, "The evaluation of free-surface Green Functions", Fourth International Conference on Numerical Ship Hydrodynamics, Washington D. C., pp. 4-19.

Newman, J. N., 1986, "Distributions of Sources and Normal Dipoles over a Quadrilateral Panel", J. Eng. Maths. No. 20, pp. 113-126.

Newman, J. N. and Sclavounos, P. D., 1988, "The computation of Wave Loads on Large Offshore Structures", BOSS' 88 Conference, Trondheim, Norway.

Newton, R. E., 1975, "Finite Element Analysis of Two-Dimensional Added Mass and Damping", Finite Elements in Fluids, Vol. 1, Wiley, 1975, Gallagher, R. H. et at. eds., pp. 219-232.

Nielsen, F. G., et al., 1994, "Dynamic Characteristics of a Large Catenary Moored Production Platform", BOSS' 94 Conference, MIT, Vol. 2, pp. 113-131.

Olsson, G. 1990, "Hybridelementmetoden, En Metod för Beräkning av Ett Flytande Föremåls rörelse" (The Hybrid Element Method, A method for the Calculation of the Motion of a Floating Object, in Swedish), Licentiate Thesis, Department of Hydraulics, Chalmers University of Technology, Report Series A:19.

Pierson, W. J., and Moskowitz, L., 1964, " A Proposed Spectral Form for Fully Developed Wind Seas Based on the Similarity Theory of S. A. Kitaigorodskii", J. of Geophysical Research, 69(24), pp. 5181-5203.

Sclavounos, P. D. and Lee, C. H., 1985, "Topics on Boundary -Element Solutions of Wave Radiation-Diffraction Problems", Fourth International Conference on Numerical Ship Hydrodynamics, Washington D. C., pp. 175-184.

Shore Protection Manual, 1984, U.S. Army Engineer Waterways Experiment Station, Vicksburg, MS, 2 Volumes, 4th edition.

Standing, R. G. and **Jackson, G. E., 1992**, "Experimental and Theoretical Investigation into the Roll Damping of a Systematic Series of Two-Dimensional Barge Sections", BOSS' 92 Conference, London.

Takaki, M. and **Tango, Y., 1994**, "Wave Drifting Force on Multiple Connected Floating Structures", Hydroelasticity in Marine Technology, Eds. Faltinsen *et al.*

Wehausen, J. V. and **Laitone, E. V., 1960**, "Surface Waves, Encyclopaedia of Physics", Fluid Dynamics III, Vol. 9, Ed. by S. Flugge, Springer-Verlag, Berlin, pp. 478

Wiegel, R. L., 1964, "Oceangraphical Engineering", Prentice-Hall, Englewood Cliffs, N.J.

Yeung, R. W., 1981, "Added Mass and Damping of A Vertical Cylinder in Finite-Depth Waters", Applied Ocean Research, Vol. 3, No. 3.

Yue, D.K.P., Chen, H. S. and **Mei, C. C., 1978**, "A Hybrid Element Method for Diffraction of Water Waves by Three-Dimensional Bodies", International Journal for Numerical Methods in Engineering, Vol. 12, pp. 245-266.

Zienkiewicz, O. C., Bettess, P. and **Kelly, D. W., 1978**, "The Finite Element Method for Determining Fluid Loading on Rigid Structures, Two- and Three-Dimensional Formulations", in Numerical Methods in Offshore Engineering, O. C. Zienkiewicz, et al., eds., Wiley, Chichester, England, pp. 141-183.

Zienkiewicz, O. C., Kelly, D. W. and **Bettess, P., 1977**, "The Coupling of the Finite Element Method and Boundary Solution Procedures", International Journal for Numerical Methods in Engineering, Vol. 11, pp. 355-375.

Zienkiewicz, O. C. and **Bettess, P., 1975**, "Infinite Elements in the Study of Fluid-Structure Interaction Problems", 2nd International Symposium on Computing Methods in Applied Science and Engineering, Versailles, France.